8-2011

OXYGENATE SYNTHESIS DURING CO HYDROGENATION ON CoCuZnO- BASED CATALYSTS

Yu-tung Tsai
Clemson University, oceandeep0122@gmail.com

OXYGENATE SYNTHESIS DURING CO HYDROGENATION ON CoCuZnO- BASED CATALYSTS

A Dissertation
Presented to
the Graduate School of
Clemson University

In Partial Fulfillment
of the Requirements for the Degree
Doctor of Philosophy
Chemical Engineering

---

by
Yu-Tung Tsai
August 2011

Accepted by:
Dr. James G. Goodwin, Jr., Committee Chair
Dr. David A. Bruce
Dr. Christopher L. Kitchens
Dr. Shiou-Jyh Hwu

ABSTRACT

The research of catalytic synthesis of methanol and other higher alcohols from CO hydrogenation has received great attention since 1980s. The focus of this research is to establish a better fundamental insight into heterogeneous metal catalysts for oxygenate (especially alcohol) synthesis by CO hydrogenation.

Co-based catalysts have been reported widely as the high-performance Fischer-Tropsch Synthesis (FTS) catalysts. The solid base, hydrotalcite (HT), using as a support for Co catalysts resulted in higher activity for CO hydrogenation comparing to other supports (pre-calcined hydrotalcite, MgO and Al_2O_3). The activities of Co/HT reduced at different reduction temperatures (300-600^{o}C) were also compared. Reduction at 500^{o}C resulted in the highest activity. However, CH_4 selectivity also enhanced. It was found that the thermal stability properties of hydrotalcite, BET surface area, particle size of Co, the interaction between Co and the support, and the reducibility of Co were all important in governing the catalytic performance of the Co catalysts for CO hydrogenation.

A comparison of the relationship of H_2 or CO chemisorption measurements at 25–100^{o}C to similar results measured under CO hydrogenation conditions by steady-state isotopic transient kinetic analysis (SSITKA) is made for a wide variety of Group VIII metal catalysts. The ratio N_T^*/N_{chem} (amount of chemisorption by SSITKA vs. by static chemisorptions) was found to be close to unity for most Co catalysts. SSITKA can, thus, be applied as a complementary technique to static chemisorption, TEM and XRD for better understanding of metal dispersion and the availability of metal surface active sites for Co catalysts with wide variety of promoters/supports. However, the application of

SSITKA for characterizing metal dispersion for the other metal is limited at this time.

The effects of individual components and an Al_2O_3 support on CuZnO for methanol (MeOH) synthesis were investigated at a site level using SSITKA for the first time. Surface reaction parameters for MeOH and dimethyl-ether (DME) were corrected for readsorption effects. SSITKA results suggested that CuZnO-based catalysts exhibited higher MeOH formation rates due to both higher intrinsic site activities and higher concentrations of active surface intermediates. The presence of ZnO seems to decrease the hydrocarbon formation ability of Cu. The synergy between Cu and ZnO was surprisingly less than an order-of-magnitude improvement based on MeOH TOF_{ITK} (a measure of site activity for MeOH formaiton).

The addition of Co into CuZnO has been investigated for the effect of component interaction on the synthesis of hydrocarbons and oxygenates during CO hydrogenation. The relationships between the surface kinetics of formation of the various products were investigated for the first time using multiproduct SSITKA. CO hydrogenation and SSITKA were carried out in a fixed-bed differential reactor at 250^{o}C and 1.8 atm. The SSITKA results showed that Cu can decrease the activity for all products probably due to blockage by Cu of the Co surface. ZnO appears to serve as a support/dispersion agent for Co, keeping Co highly dispersed and active for hydrocarbon and higher oxygenate synthesis. However, the effects for Cu and ZnO with Co were not additive. The Co-Cu-ZnO combination resulted in a synergy that maintain the oxygenate synthesis ability of highly dispersed Co (such as Co/Al_2O_3) while decreasing the ability to make hydrocarbons by loss of hydrocarbon sites. Interestingly, the rate of synthesis for C_2

oxygenates on Co/CuZnO was the essentially the same to that on Co/Al_2O_3- but without the high production/rate of hydrocarbons. Co/CuZnO is thus a selective but not an active catalyst for higher oxygenate synthesis.

DEDICATION

I would like to dedicate my dissertation to my beloved parents and sister, Yi-Hao Tsai, Li-Mei Hsieh and Yu-Chen Tsai, whose constant support and patience encouraged me all these years. Particularly, to my husband, Eric Fang, whose love has supported me throughout the course of my doctoral career.

I would also like to dedicate this work to my previous advisor in National Taiwan University, Dr. Ben-Zu Wan, who initiated my research interest in catalysis and recommended me to have further education with my current advisor, Dr. James G. Goodwin, Jr., in Clemson.

ACKNOWLEDGMENTS

I would like to acknowledge and express my sincere gratitude to all the people who persistently supported and motivated me during the completion of my journey. My greatest thanks go to my advisor and mentor, Dr. James G. Goodwin, Jr., who guided me through hurdles, and provided constant support throughout the past 3 years. Without his invaluable expertise, guidance and patience, I would not have come this far. I also would like to thank Dr. Xunhua Mo, my academic mentor, who inspired the series of experiments described in this dissertation. Her creativity and wide-scope knowledgements directly contributed to many of my accomplishments. I also thank my committee members, Dr. David Bruce, Dr. Christopher Kitchens and Dr. Shiou-Jyh Hwu, who provided me valuable scientific discussion and comments for this work.

I would like to thank all the members in Dr. Goodwin's group, Jack, Jia and Pam, who provided helpful assistance and discussion for my work and made my PhD study more pleasant. My thanks also go to the numerous individuals in Chemical Engineering Department and Taiwan association (TSSA) in Clemson, for making Clemson to be such a wonderful place. I especially thank Wen-Sheng and Shu-Yi, who also are endeavoring to their PhD careers in U.S., for their considerate friendship more than 10 years.

Finally, I greatefully acknowledge financial support from U.S. Department of Energy (DOE), the support from the staff of the EM lab and Chemistry Department at Clemson University, and Dr. James Spivey at Louisiana State University for his contribution to this project.

TABLE OF CONTENTS

Table of Contents (Continued)

Page

LIST OF TABLES

List of Tables (Continued)

LIST OF FIGURES

List of Figures (Continued)

CHAPTER ONE

INTRODUCTION

Alternative fuels and chemicals are being sought to improve environmental quality and increase energy efficiency by the development of novel technologies for the production of synthetic fuels and chemicals using renewable energy sources such as biomass. Oxygenates, such as alcohols, are considered as potential gasoline alternatives and solutions to the energy crisis in the future due to their lower costs and low pollution emissions in use. Alcohols are, currently, produced mainly (> 90%) by the fermentation of biomass-derived sugars, which are not energy efficient nor environmentally friendly. The process of alcohol synthesis by syngas ($CO + H_2$) could produce in large scale. However, the improvement of catalytic conversion of syngas to alcohol is still challenging. No commercial process is developed nowadays although the research on this topic has been studied for more than 90 years.

Catalytic hydrogenation of carbon monoxides has been widely studied and is known as one of the direct routes for converting syngas to usefel chemicals such as hydrocarbons and oxygenates. In recent years, the availability of biomass and the great amount of research on Fischer-Tropsch synthesis (FTS) make it potentially to be employed to produce hydrocarbons (HCs) commercially. The development of FTS catalyst is unique in this field of heterogeneous catalysis due to the focus of avoiding undesirable by-products from the variation of the product distribution. An ultimate goal for the development of FTS is to design catalysts with both high reactivity and selectivity.

The heterogeneous catalysts employed for the synthesis of methanol or higher alcohols could be roughly classified into two categories: (1) noble metal-based and (2) non-noble metal based catalysts. The noble metal-based catalysts are primarily rhodium (Rh) supported catalysts while the non-noble metal based catalysts are usually further classified as modified methanol synthesis catalysts, modified FTS catalysts and MoS_2-based catalysts.

Rh-based catalysts have been shown to have high activity for the synthesis of C_{2+} oxygenates due to the unique carbon monoxide adsorption behavior on Rh. However, the industrial application of supported Rh catalysts was limited to the low conversion and high cost. CuZnO catalyst system is well established as the leading industrial for methanol synthesis. However, the production process still poses great challenges: the reaction conversion is seriously limited by the reaction thermodynamics. Cobalt, iron and ruthenium are considered as the most favorable metals for FTS due to their high activity, high selectivity to linear paraffins and low water-gas shift reaction (WGSR) activity. Among them, Co-based catalysts generally produce a relatively high yield in long chain HCs. This behavior could be attributed to the ability of the catalyst to readsorb the produced olefins in the metallic centers, and thus increasing the chain length.

The objective of this study was to develop CoCuZnO-based catalysts for selective oxygenate synthesis from synthesis gas. Based on the results of previous research, a number of supports were investigated for Co-based catalysts in this research and it was found that Hydrotalcite (HT) could lead to the highest activities for Co catalyst. However, the selectivities for oxygenates were still pretty low. CuZnO-based catalysts

have been investigated for the effects of component and support for methanol (MeOH) synthesis. Finally, the products, including HCs and oxygenates, were studied for catalysts combining all Co, Cu and ZnO components at the site level by the application of SSITKA (Steady State Isotopic Transient Analysis). The comparison of chemisorption close to ambient and reaction conditions were also made for typical chemisorption and SSITKA.

CHAPTER TWO

BACKGROUND

Increasing concerns for the depletion of fossil fuel resources, global climate change and the rising prices of crude oil have made energy one of the central problems. The use of oxygenates (such as ethers or alcohols) as major sources of gasoline additives or alternative fuels have attracted great attention recently.

2.1 Reasons for Oxygenates

The International Energy Administration estimated that the world energy consumption will increase from 447 quadrillion Btu in 2004 to 702 quadrillion Btu in 2030 [1]. The majority of energy will be expected to be produced from fossil fuels [1-3]. Consequently, the world oil consumption is estimated to increase from 80 million barrels per day in 2003 to 118 million barrels per day in 2030, as shown in Figure 2.1. However, crude oil concentrated only in very limited regions around the world and the amount of reserve is declining significantly. Therefore, the interests for the research of the alternative energy sources such as biomass have increasing recently [5-6].

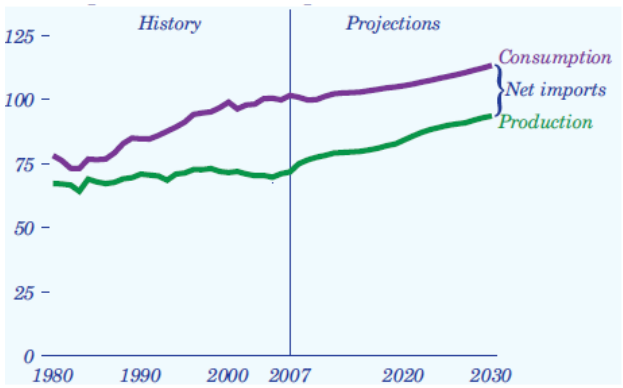

Figure 2.1 Total energy production and consumption, 1980-2030 (quadrillion Btu*)* [4]

Biomass feedstock, such as inexpensive forestry or agriculture residues, plays crucial role in developing alternatives for fossil fuels. There are several advantages for developing liquid biofuel based on these low-cost raw materials: (1) Reduce of the dependence for imported oil from using the renewable sources, such as agricultural crops; (2) oxygenated fuels, such as ethanol, burn more cleanly than fossil fuels, alleviating environmental concerns such as greenhouse effect and toxic NO_x emissions [7].

The use of oxygenates as gasoline additives are widely in the United States (U.S.) and some other countries. Fuel oxygenates can be divided into two chemical categories: ethers and alcohols. Ether oxygenates include methyl *tert*-butyl ether (MTBE), ethyl *tert*-butyl ether (ETBE), *tert*-amyl methyl ether (TAME), and diisopropyl ether (DIPE). Alcohol oxygenates include ethanol (EtOH), *tert*-butyl alcohol (TBA), and methanol (MeOH) [8].

Ethanol has been proposed to be one of the mostly used oxygenates in United States. It has been studied that the use of ethanol as a fuel in automobiles can provide the same

chemical energy as that of gasoline but with less environmental pollutants as well as less emissions of greenhouse gases, especially when ethanol is synthesized from cellulose rather than from cornstarch [9]. Ethanol is also being considered as a potential source of renewable hydrogen in fuel cell applications very recently [10-12]. Based on these facts, there is an increasing worldwide interest in the production of ethanol from biomass, and possibly from other available carbonaceous compounds such as coal without CO_2 emission. The use of ethanol could be potentially as an alternative fuel for transportation and as H_2 carrier in the future. The later on sections in this chapter will be particular focus on alcohol, especially ethanol, introduction.

2.2 Alcohol Production

2.2.1 Fermentation

Currently, alcohols are produced by two main processes: (1) fermentation of sugars derived from corn or sugar cane and (2) hydration of petroleum-based ethylene. Figure 2.2, for example, showed an overall picture for ethanol production [13]. Although the fermentation route is commercially applied for the production of the most of the alcohols today, the production of fuel-grade alcohols is still a high-cost and energy-efficient process because the process includes energy intensive distillation steps [14]. Besides, the fermentation process is not appropriate for sugar derived from forestry biomass or lignocelluloses because they have significant portion of 5-carbon pentose sugars which are not completely metabolized into alcohol [15]. In addition, despite the advantages of high selectivity and domestically available, fermentation processes are actually

characterized by low reaction rate, difficult product separation, and especially energetically inefficiency (For example, nearly 70% energy are required to produce ethanol than the energy actually in ethanol). Current fermentation process is limited in its application due to these constraints.

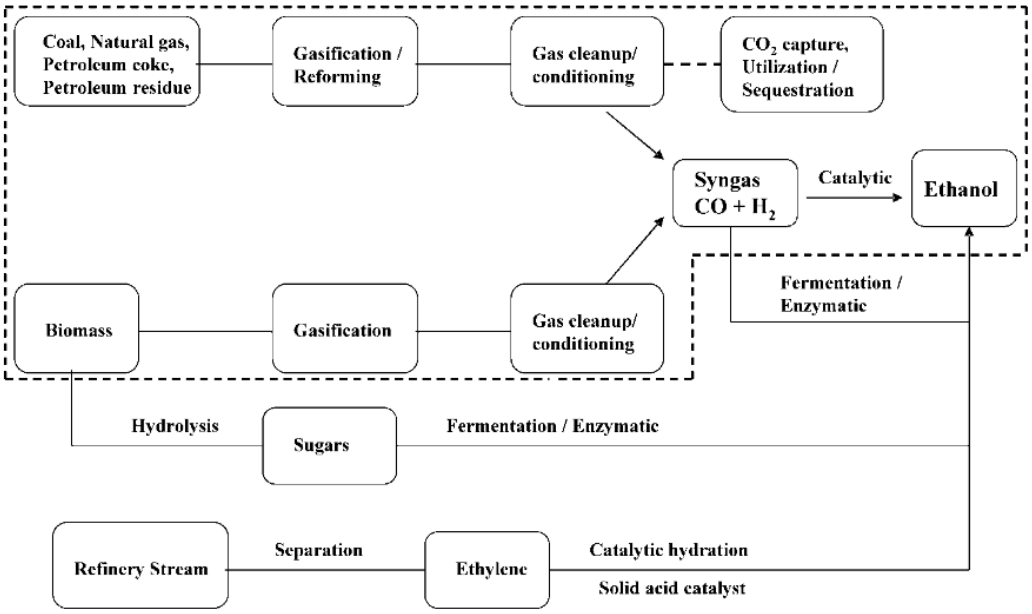

Figure 2.2 Synthesis of ethanol from various carbon-containing feedstocks [13].

The area of research of production of higher alcohols from syngas has received great attention for more than fifty years [16]. However, there are still many challenges for synthesizing alcohols from syngas.

2.2.2 Synthesis Gas Production for Alcohol Synthesis

Synthesis gas (or syngas) is given name for a gas mixture of various concentrations of carbon monoxide and hydrogen. Synthesis gas could be derived from natural gas, coal or biomass by gasification/reforming [17]. There are still many difficulties for directly converting syngas into alcohols. Methanol and higher alcohols can be simultaneously produced from syngas with many different types of catalysts. The catalysts for the production of ethanol from syngas can be classified into four categories: (1) Rh-based catalysts [18-20], (2) modified methanol synthesis [21], (3) modified Fischer-Tropsch catalysts [22-23], and (4) modified Mo-based catalysts [24-25]. However, the required catalysts are mostly utilized in severe conditions with complex compositions. The products are mixture of either branched or linear primary alcohols ranging from methanol to hexanol [26]. Types of catalysts that have been studied are summarized as follows.

(1) Rh-based catalysts

Rh appears to be the most adaptable element in terms of its properties for catalysis among the choice of supported transition metal catalysts, particularly for syngas conversion [27]. Rh-based catalysts tend to be the more selective for C_{2+} oxygenates [28-29]. The addition of suitable promoters can obviously enhance the activity and selectivity to C_{2+} oxygenates [30].

(2) Modified methanol synthesis catalysts

Modified methanol synthesis catalysts include high-temperature-pressure ZnCr-based catalysts and low-temperature-pressure CuZn-based catalysts [26]. The addition of alkali promoters to these catalysts can increase the selectivity toward

ethanol.

(3) Modified Fischer-Tropsch catalysts [26, 31-32]

Cobalt is the most well-known transition metals to be very active for FTS while copper has the ability to produce alcohols. This leads to the assumption that CoCu-based catalysts could be the promising catalysts for syngas conversion into alcohols. These catalysts show better selectivity to higher alcohol selectivities if suitable alkali promoters are introduced.

(4) Modified Mo-based catalysts [33-34]

Mo-based catalysts have good sulfur tolerance when promoted with proper alkali promoters. These kinds of catalysts are affected significantly by the composition, structures and reaction conditions. It required higher reaction pressures (>10 MPa) for ethanol synthesis compared with Cu-based catalysts. It should be also noted that CO hydrogenation activities of transition metal sulfides have not been investigated yet except W and Mo sulfides.

2.3 Catalyst Design for Alcohol Synthesis

2.3.1 CO Hydrogenation Mechanism

The possible products for CO hydrogenation are paraffins, olefins and oxygenates, which include alcohols, aldehydes, ketones, esters and acids. Extensively efforts have been focus on the mechanistic studies. By summarizing the published results, Chuang et al. [35] linked all possible pathways in a network as shown in Figure 2.3.

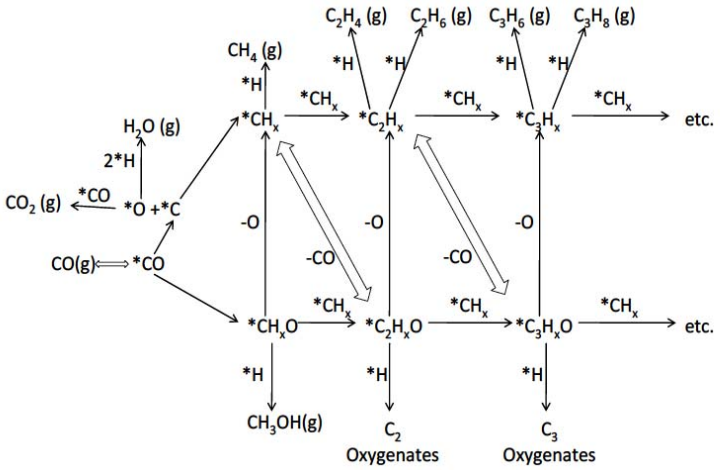

Figure 2.3 CO hydrogenation network [35].

The reaction on catalysts starts with the steps of CO dissociation and hydrogenation or hydrogen adsorption and splitting to produce CH_x species, then follow by the steps:

(a) CH_4 production via hydrogenation of CH_x species.

(b) Chain growth with another CH_x species to form C_2 hydrocarbons.

(c) CO insertion to form C_2 oxygenates.

Thus, a catalyst with the abilities of promoting the CO dissociation and insertion reaction would be more favorable for higher alcohol formation.

2.3.2 Criteria for Alcohol Synthesis Catalyst Design

Alcohol synthesis catalysts have to meet numerous requirements including non-chemical and chemical. The non-chemical requirements include the mechanical strength, the morphology or even the cost of the catalyst. The chemical requirements include three important issues:

(a) Activity- the ability of producing relatively larger amount of products.

(b) Selectivity- the ability to produce the desired products and avoid other products.

(c) Stability- the duration time of the catalyst to maintain activity before deactivated or poisoned.

Several factors could affect catalytic behaviors, such as the composition of the catalysts. In order to achieve the optimal dispersion as well as the stabilization against sintering effect, a support is necessary with properties such as chemical non-active and large surface area. The addition of suitable promoter(s) can also improve the activity or selectivity of the catalysts. In addition, the preparation methods, the pretreatments or reaction conditions could also affect the catalytic performance and selectivity.

2.4 Research Objective

The objective of this research was to develop CoCuZnO-based catalyst systems for oxygenate, especially ethanol, synthesis from synthesis gas with higher activity and selectivity. The research began with investigation of support effect for cobalt catalysts. CuZnO-based catalysts and CoCuZnO catalysts were studied for methanol synthesis and ethanol synthesis by SSITKA, respectively. The comparison of typical chemisorption and SSITKA was also made in this study.

2.5 References

[1] Energy Information Administration (EIA). International Energy Outlook; U.S. Department of Energy: Washington, DC, 2007.

[2] International Energy Agency. Global Energy Outlook: Issues and Challenges. 10th International Energy Forum, April 22–24, 2006.

[3] C. Song, Catal. Today 115 (2006) 2.

[4] EIA, Annual Energy Outlook 2009.

[5] B. Hahn-Hagerdal, M. Galbe, M.F. Gorwa-Grauslund, G. Liden, G. Zacchi, Trends Biotechnol. 24 (2006) 549.

[6] L. Petrus, M.A. Noordermeer, Green Chem. 8 (2006) 861.

[7] S. Rajagopalan, R.P. Datar, R.S. Lewis, Biomass Bioenerg. 23 (2002) 487.

[8] R.A. Deeb, K.-H Chu, T. Shih, S. Linder, I. Suffet, M.C. Kavanaugh, L. Alvarez-Cohen, Environ. Eng. Sci. 20 (2003) 433.

[9] A.E. Farrell, R.J. Plevin, B.T. Turner, A.D. Jones, M. O'Hare, D.M. Kammen, Science 311 (2006) 506.

[10] S. Velu, N. Satoh, C.S. Gopinath, K. Suzuki, Catal. Lett. 82 (2002) 145.

[11] D.A. Deluga, J.R. Salge, L.D. Schmidt, X.E. Verykios, Science 303 (2004) 993.

[12] S. Velu, C. Song, Advances in Catalysis and processes for hydrogen production from ethanol. In Catalysis; Spivey, J. J., Ed.; Royal Society of Chemistry: London, 20 (2007) 65.

[13] S. Velu, K.G. Santosh, Energ. Fuel 22 (2008) 814.

[14] C.M. Fougret, W.F. Holderich, Appl. Catal. A-Gen. 207 (2001) 295.

[15] K.A. Gray, L. Zhao, M. Emptage, Curr. Opin. Chem. Biol. 10 (2006) 141.

[16] G.W. Roberts, M.A. Márquez, M.S. McCutchen, Catal. Today 36 (1997) 255.

[17] J.J. Spivey, A. Egbebi, Chem Soc Rev 36 (2007) 1514.

[18] M.A. Haider, M.R. Gogate, R.J., Davis, J. Catal. 261 (2009) 9.

[19] A. Egbebi, V. Schwartz, S.H. Overbury, J.J. Spivey, Catal. Today 149 (2010) 91.

[20] J. Gao, X. Mo, J.G. Goodwin, Jr., Catal. Today 160 (2011) 44.

[21] X. Sun, G.W. Robert, Appl. Catal. A- Gen. 247 (2003) 133.

[22] K. Okabe, H. Yamada, T. Hanaoka, T. Matsuzaki, H. Arakawa, Y. Abe, Chem. Lett. 30 (2001) 904.

[23] M. Pijolat, V. Perrichon, Appl. Catal. 13 (1985) 321.

[24] G. Bian, L. Fan, Y. Fu, K. Fujimoto, Appl. Catal. A-Gen. 170 (1998) 255.

[25] J. Bao, Z. Sun, Y. Fu, G. Bian, Y. Zhang, N. Tsubaki, Top Catal. 52 (2009) 789.

[26] N. Tien-Thao, M.H. Zahedi-Niaki, H. Alamdari, S. Kaliaguine, J. Catal. 245 (2007) 348.

[27] J.L. Hu, Y. Wang, C.S. Cao, D.C. Elliott, D.J. Stevens, J.F. White, Catal. Today 120 (2007) 90.

[28] H.Y. Luo, W. Zhang, H.W. Zhou, S.Y. Huang, P.Z. Lin, Y.J. Ding, L.W. Lin, Appl. Catal. A- Gen. 214 (2001) 161.

[29] M. Ojeda, M.L. Granados, S. Rojas, P. Terreros, F.J. García-García, J.L.G. Fierro, Appl. Catal. A-Gen. 261(2004) 47.

[30] J. Gao, X. Mo, J.G. Goodwin, Jr., J. Catal. 268 (2009) 142.

[31] R. Kieffer, M. Fujiwara, L. Udron, Y. Souma, Catal. Today 36 (1997) 15.

[32] L. Nowicki, Chem. Eng. Process 44 (2005) 383.

[33] N. Koizumi, K. Murai, T. Ozaki, M. Yamada, Catal. Today 89 (2004) 465.

[34] J. Iranmahboob, H. Toghiani, D.O. Hill, Appl. Catal. A-Gen. 247(2003) 207.

[35] S.S.C. Chuang, R.W. Stevens, Jr., R. Khatri, Top. Catal. 32 (2005) 225.

CHAPTER THREE

HYDROTALCITE SUPPORTED Co CATALYSTS FOR CO HYDROGENATION

[As published in Applied Catalysis A-General, 396 (2011) 91-100]

It is well known that the catalytic performance of Co catalysts depends on supports and promoters. The focus of this work was to investigate the catalytic activities for CO hydrogenation of Co catalysts supported on the solid base, hydrotalcite (HT), and to probe the role of support in the reaction. A cobalt catalyst containing 10 wt% cobalt supported on HT was prepared using the incipient wetness impregnation method. Pre-calcined HT (CHT), alumina and magnesium oxide were also employed as supports for comparison purposes. Catalysts were characterized by surface area and porosity analysis, XRD, TEM/STEM/EDX, TPR and H_2 chemisorption. The catalytic activity was tested using a fixed-bed reactor at 230^{o}C, 1.8 atm, and $H_2/CO = 2$. It was found that the hydrotalcite supported catalyst showed the highest steady-state reaction rates. The activities of Co/HT reduced at different reduction temperatures (from 300 to 600^{o}C) were also compared. Reduction at 500^{o}C resulted in the highest activity; however, CH_4 selectivity was also enhanced as the reduction temperature increased. The product distributions for Co/HT obeyed an Anderson–Schulz–Flory distribution. The α values were not impacted by the different reduction temperatures for Co/HT. The characterization and reactivity results suggest that the thermal stability properties of hydrotalcite, BET surface area, particle size of Co, the interaction between Co and the support, and the reducibility of Co were all important in governing the catalytic

performance of the Co catalysts for CO hydrogenation. Our study suggests that HT is a promising support for Co for Fischer–Tropsch synthesis because it gives high activity (higher than Co/Al_2O_3) without the need for a reduction promoter.

3.1 Introduction

In order to meet the environmental, economic and social challenges associated with the energy supply-demand problem, the usage and research of alternative fuels have recently gained a lot of interest. Fischer–Tropsch synthesis (FTS) has attracted great attention as a solution for this problem by converting natural gas, coal, or biomass resources to liquid fuels through the generation and conversion of syngas ($CO + H_2$) [1]. The heavy paraffins formed from the synthesis can be further processed to produce a wide range of sulphur- and aromatic-free liquid hydrocarbon fuels.

Supported cobalt catalysts have long been used for FTS, especially when long catalyst life times and high selectivities for paraffins are required, because of their relatively low costs and low activity for the water–gas shift reaction [1,2]. The selection of the support for a cobalt catalyst can have a great influence on its physicochemical properties. For instance, the functional groups on the surface and the porosity of the support can alter the cobalt particle size, dispersion and reducibility, thus affecting the performance for CO hydrogenation [3,4]. A moderate interaction between Co and supports is beneficial to achieve a high selectivity and activity [5,6]. Even though many oxides have been studied as supports for cobalt for Fischer–Tropsch synthesis, such as Al_2O_3 [7–10], SiO_2 [11–14] and TiO_2 [4,15–20], the search for new supports continues in order to optimize the design of FTS catalysts to more easily commercialize FTS.

Hydrotalcite (HT)-like compounds have attracted attention in the field of catalysis either as base catalysts or as catalyst supports for a broad spectrum of catalytic organic reactions including steam conversion of methane, synthesis of alcohols, and many

aromatic organic reactions [21,22]. Belonging to the class of anionic clays, HT is easy and inexpensive to synthesize. A general form for HT is $[M^{2+}_{1-x}M^{3+}_{x}(OH)_2](A^{n-}_{x/n})^{x-} \cdot yH_2O$ where M^{2+} is a bivalent metal ion, M^{3+} is a trivalent metal ion and A^{n-} is the interlayer anion. Generally, M^{2+} and M^{3+} are Mg^{2+} and Al^{3+}, respectively. The HT structure consists of positively charged brucite, $Mg(OH)_2$-type MOH-layers in which M^{2+} is substituted by M^{3+}, and the excess positive charges are balanced by anions in the interlayer for charge compensation.

A transition metal of catalytic interest can be incorporated into HT-like structures by coprecipitation with Al and Mg during the preparation of HT [23–27], by ion-exchange as anionic species [28,29], by direct impregnation [30], and by impregnation on pre-calcined HT [31–34]. In general, these catalysts have high surface area, high metal dispersion, synergetic effects between the elements, and, in some cases, a memory effect which allows the reconstruction of the original structure when HT is decomposed at high temperature [21,22]. HT and calcined HT (CHT) containing transition metals have been used either as catalysts or supports for FTS [35–37]. For instance, Pinnavaia et al. [38] proposed that the mechanism for oxygenate formation on HT-supported Ru catalysts in CO hydrogenation arises from the decoration of the metal crystallites by base species of the support. Although a few cobalt containing HT-like compounds have been synthesized [26,39–43] and utilized for several reactions including CH_4 combustion [39] and CH_4 reforming [26,41], there is little information concerning HT-supported Co catalysts and their use in CO hydrogenation. Cavani et al. [44] reported that HT containing Co and Cu have good catalytic activities due to the high dispersion of metallic

copper. Krylova et al. [5] studied the activities for FTS of Co supported on as-prepared and calcined HT and found that the pretreatment of HT has marked effects on the activity and selectivity of the catalyst; however, no other characterization was carried out by this group in order to understand the differences in physicochemical properties of the catalysts.

The objective of the current work was to obtain more insight into the use of HT-supported Co catalysts for CO hydrogenation. A commercial HT material either without any pretreatment or with pre-calcination was used in this study as the support. Furthermore, MgO and Al_2O_3 were each used as Co supports as well for comparison purposes. The supported cobalt catalysts were characterized by BET, STEM, EDX, TEM, TPR, H_2 chemisorption and CO hydrogenation. The effect of reduction temperature on the HT-supported Co catalyst was also studied in detail.

3.2 Experimental

3.2.1 Catalyst preparation

Catalysts containing 10 wt% Co on various supports were prepared by the incipient wetness impregnation method. Cobalt nitrate hexahydrate (Acros, 99%) was used as the metal precursor, and commercially available HT (Aldrich, $Mg_6Al_2(CO_3)(OH)\cdot 16.4H_2O$), HT pre-calcined at 500°C in air for 4 h (referred to as CHT), Al_2O_3 (Alfa-Aesar, γ-phase/α-phase, 99.98%), and MgO (Spectrum, 96–100%) were employed as supports. A support was first impregnated with a 1:1 H_2O and acetone solution containing the cobalt precursor (2 mL solution/1 g support). After mixing and stirring, the mixture was dried

at 90°C for 4 h and then at 120°C overnight before being calcined in air at 300°C for 4 h (ramp rate to 300°C of 10°C/min) to remove nitrogen-containing species. The catalysts are represented by the notation Co/S, where Co represents cobalt and S, the support, which was either HT, CHT, Al_2O_3 or MgO. The as-prepared catalysts were stored in a desiccator until use in order to avoid rehydration.

3.2.2 Catalyst characterization

BET surface areas, pore volumes, and pore sizes were estimated from nitrogen adsorption and desorption data at −196°C in a Micromeritics ASAP-2020. The catalyst samples were degassed at different specific temperatures under a vacuum of 10^{-3} mmHg before measurements. Degassing temperatures of 150°C and 400°C were applied. In general, a degassing temperature of 150°C was used to remove physically adsorbed water. Due to the unique thermal stability of HT, a degassing temperature of 400°C was also used in order to be comparable to what was done in other studies in the literature [45,46].

A Scintag XDS 2000 θ/θ powder X-ray diffractometer (XRD) using Cu Kα1/Kα2 (λ = 1.540592Å and 1.544390Å, respectively) radiation and a step size of 0.03° was used to identify the phases and crystallinity of the Co catalysts.

HRTEM images for fresh Co catalysts were obtained using a Hitachi 9500 with an accelerating voltage of 300 kV to investigate the morphologies of the catalysts. The morphologies and the elemental concentrations of the catalyst surfaces, as well as the elemental distributions for Co/HT after being reduced at various reduction temperatures,

were studied using HRTEM, STEM and EDX, respectively. STEM was performed using a Hitachi HD2000 under Z-contrast (ZC) mode. The accelerating voltage was 200 kV.

Temperature programmed reduction (TPR) was carried out using an Altamira-200R-HP microreactor to determine the reducibility of the Co-based catalyst. The as-prepared catalysts (0.2 g) were pretreated at 300°C in He for 1 h prior to TPR measurement. During a TPR experiment, 10% H_2/Ar flow of 30 mL/min was used for reduction. The catalysts were heated with a ramp rate of 10°C/min from 35°C to 800°C. H_2 consumption was analyzed using a thermal conductivity detector (TCD). The reduction of Ag_2O (99.99% metals basis, Alfa-Aesar) was used to calibrate the TCD signal for H_2 consumption.

H_2 chemisorption isotherms were measured at 100°C in a Micromeritics ASAP-2010 system. Before measurements, the catalyst samples were reduced with a hydrogen flow for 2 h at 500°C following a temperature ramp of 10°C/min. The samples were then evacuated at 500°C and 10^{-6} mmHg for about 2 h before cooling to 100°C.

3.2.3 Reaction

CO hydrogenation was carried out in a differential fixed-bed reactor with a maximum conversion below 10% to minimize concentration and temperature gradients. A catalyst sample of 0.3 g was mixed with 3 g α-alumina to avoid channeling and hot spots. The catalyst was heated to a specific reduction temperature (500°C for Co/CHT, Co/Al_2O_3 and Co/MgO, or 300–600°C for Co/HT) with a ramp rate of 5°C/min and kept at that temperature for 1 h in a H_2 flow of 30 mL/min at 1 atm, then cooled down to the

reaction temperature of 230^{o}C. The reaction started as the gas flow was switched to a CO–H_2 mixture and the total pressure adjusted to 1.8 atm. The total flow rate of the reactants was kept constant at 45 mL/min which consisted of 30 mL/min of H_2 and 15 mL/min CO. The reaction effluent lines and the sampling valves were wrapped with heating tape to avoid condensation of H_2O and higher hydrocarbon products. The effluent products were analyzed on-line by a Varian 3380 GC with a flame ionization detector (FID) connected to a Restek RTQPLOT column (I.D. 0.53mmand length 30m) for hydrocarbon and oxygenates, and with a thermal conductivity detector (TCD) connected to a Restek HayeSep® Q column (I.D. 3.18mm and length 1.83m) for inorganic gases. The reaction reached a pseudo-steady state after 15 h TOS (time-on-stream).

The identification and the calibration of gas products were achieved using standard gases [alkanes (C_1–C_7), alkenes (C_2–C_7) and oxygenates (methanol, ethanol, 1-propanol, 1-butanol, acetaldehyde and acetone), Scott Specialty Gases]. The carbon selectivity (in C atom%) for a given product was calculated using the formula $n_iC_i/\sum n_iC_i$, where n_i and C_i represent the carbon number and molar concentration of the ith product, respectively.

3.3 Results and discussion

3.3.1 Catalyst characterization

3.3.1.1 BET surface area and porosity measurements

The BET surface areas, pore volumes and pore sizes for the as-prepared calcined (300 ◦C) cobalt catalysts are shown in Table 3.1. Two degassing temperatures (400^{o}C and 150^{o}C) were used.

Table 3.1 BET surface areas, pore volumes and average pore sizes of the Co-based catalysts (pre-calcined at 300^{o}C) with different degassing temperatures prior to BET measurements.

Catalyst[a]	Degassing temperature (^{o}C)	BET S.A.[b] (m^2/g)	Pore volume[b] (cm^3/g)	Average pore size[b] (nm)
Co/HT	400	265	0.21	3.2
	400 (500)[c]	265	0.21	3.1
	400 (600)[d]	268	0.21	3.3
	150	24	0.06	10.7
Co/CHT	400	271	0.37	5.5
	150	13	0.06	18.6
Co/MgO	400	90	0.37	16.5
	150	25	0.15	23.4
Co/Al_2O_3	400	93	0.60	25.8
	150	102	0.60	23.7

[a] All catalysts contained 10 wt% Co.
[b] Max error = ±5%.
[c] Co/HT was reduced ex-situ at 500^{o}C for 1 h before BET measurement.
[d] Co/HT was reduced ex-situ at 600^{o}C for 1 h before BET measurement.

It was found that, except for Co/Al_2O_3 which showed similar surface area and pore distribution regardless of the degassing temperature, all the other catalysts exhibited significant changes in BET surface area and average pore size with a change in the

degassing temperature. For a degassing temperature of 400°C, the BET surface area decreased in the order of Co/CHT ≈ Co/HT > Co/Al_2O_3 ≈ Co/MgO, while the pore volume and average pore size were found to be the largest for Co/Al_2O_3. It appears that the calcination temperature of 300°C during catalyst preparation was not sufficient to open up the structure of the HT, or even MgO, since the degassing temperature of 150°C before BET measurements was lower than the calcination temperature of 300°C and would not change the surface areas. Previous studies [47] have reported that the surface area of Co/MgO decreased significantly due to the formation of bulk cobalt oxide or composite oxides while cobalt loading was relatively large (≥10%), which is consistent with the trend in this study. The increase of surface area and pore volume at higher degassing temperature for Co/MgO can be partly due to decomposition of carbonates. The change in surface area with degassing temperature for the HT-based catalysts is likely due mainly to the decomposition of hydrated HT phases [48–50] and to a lesser extent the decomposition of carbonates. It has been reported that the thermal decomposition for Mg–Al hydrotalcite generally starts with the loss of the interlayer water molecules at 150–200°C, followed by the collapse of the layered hydroxide structure in the temperature range of 300–400°C and the complete loss of the layered structure after 500°C [48,51]. Although there are controversies regarding the detailed thermal decomposition mechanisms of HT [24,43,51–54], there is agreement that the surface area and pore volume of HT increase with the calcination temperature up to 400–500°C depending on the composition of HT, then the surface area decreases with further increase in temperature [54,55]. The restructuring of the support should affect the local

chemical environment of Co and may cause the migration of Co. In order to determine further the effect of temperature on the surface area and pore properties of Co/HT, it would be meaningful to measure the BET surface area using a degassing temperature higher than 400°C. However, due to the limitation of the BET instrument, higher pretreatment temperatures before the BET surface area measurement could only be reached ex-situ. Thus, as shown in Table 3.1, two more BET measurements with a degassing temperature of 400°C were carried out for the Co/HT catalyst pre-reduced at 500°C and 600°C, respectively. The results showed that, in the temperature range of 400–600°C, neither calcination nor reduction influenced the BET properties of the Co/HT catalyst and that heating in this temperature range gave high total surface areas and pore volumes.

3.3.1.2 XRD

XRD was used to study the crystalline phases of the calcined catalysts. As can be seen in Figure 3.1, the XRD patterns show that the Co/HT, Co/CHT and Co/Al_2O_3 catalysts exhibited only a few weak and broad diffraction peaks, indicating nearly X-ray amorphous powders. The weak peaks around 37° and 62° observed for Co/HT and Co/CHT are characteristic for calcined HT [46,56], indicating the formation of the Mg(Al)O mixed oxide after calcination for both catalysts. No discernible peaks for any Co oxide phases could be identified for these two catalysts at this Co loading of 10 wt%, suggesting high Co dispersions. Characteristic peaks at 46° and 67°, ascribed to the γ-Al_2O_3 phase [57], were found in the XRD pattern of Co/Al_2O_3, but no Co-related peaks

could be observed. The XRD pattern of Co/MgO showed the typical features of MgO or (Co, Mg)O with peaks at 37°, 42° and 61° [47]. In addition, weak peaks at 36° and 59° could be assigned to Co_3O_4 [16,57,58]. Based on the XRD results, Co/MgO appeared to have the largest Co particles among these four catalysts.

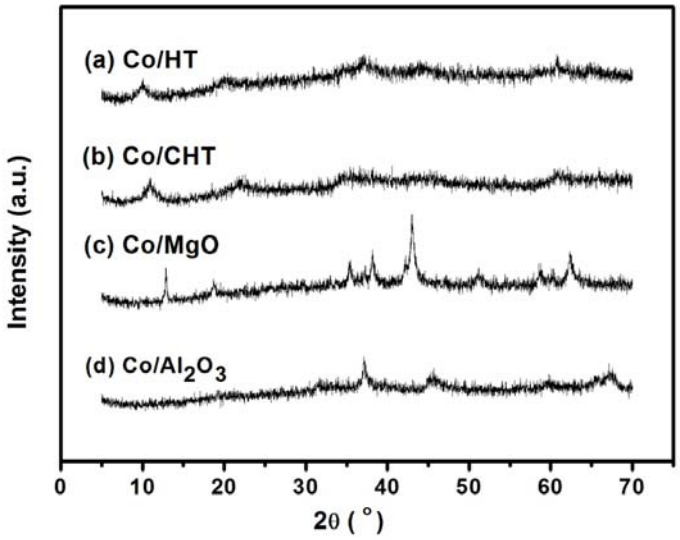

Figure 3.1 XRD patterns of the calcined Co catalysts: (a) Co/HT; (b) Co/CHT; (c) Co/MgO and (d) Co/Al_2O_3.

3.3.1.3 TEM, STEM and EDX

Representative HRTEM images of the as-prepared catalysts are shown in Figure 3.2. For Co/HT, multiple layers and many 5–10nm particles could be observed, which can be ascribed to amorphous HT and aggregated Co particles, respectively. Co particles are more dense and higher dispersed compared to the HT. Therefore it can appear to form a greater fraction of the catalyst in a resulting 2D TEM image of a 3D catalyst granule.

Reichle et al. [24] observed from TEM images that HT particle morphology and crystal thickness were retained after heating to 450^{o}C. After being heated at 500^{o}C, however, Stanimirova et al. [51] reported the existence of a significant change in the morphology of HT. The calcination temperature used in this study was 300^{o}C, thus, the observation of the layered structure for the support of Co/HT is in agreement with the literature. The HRTEM image for Co/CHT shows disordered structures [see Figure 3.2 (b)] consistent with previous results [24] for HT treated at 500^{o}C. Distinguishable from the support are some small particles with a size of 2–10 nm, which may have been Co particles.

(a) Co/HT

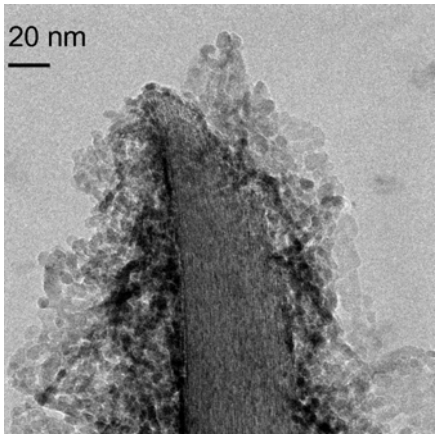

(b) Co/CHT

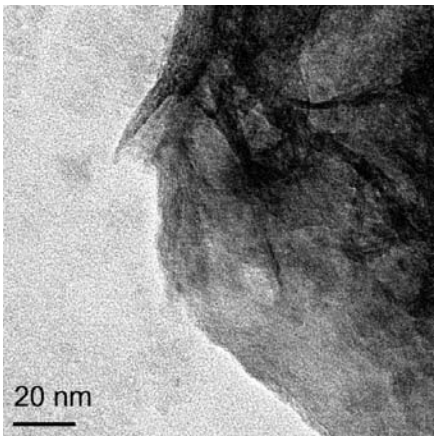

(c) Co/MgO

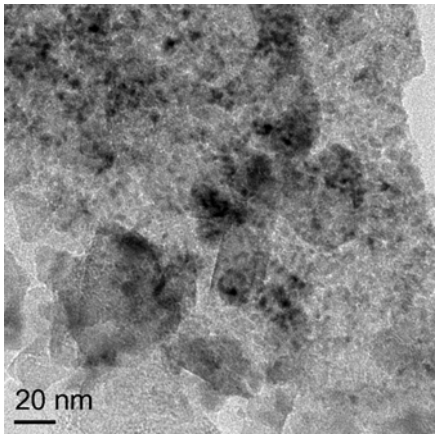

(d) Co/Al_2O_3

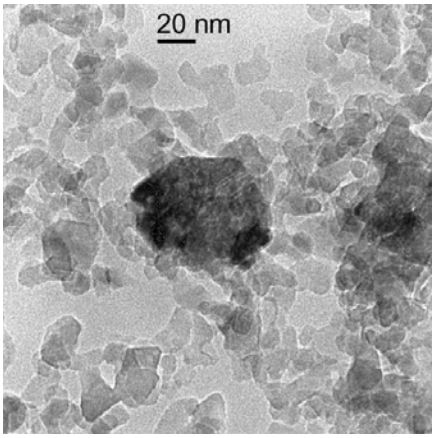

Figure 3.2 HRTEM micrographs after calcination at 300°C of (a) Co/HT; (b) Co/CHT; (c) Co/MgO and (d) Co/Al_2O_3.

For Co/MgO, MgO exhibited some irregular shaped support granules and larger Co particles could be identified, as shown in Figure 3.2 (c). Compared to the HRTEM image of Co/HT, no significant difference in particle size can be observed for discernable Co particles in Co/MgO. It is also noted that the Co particle size distribution was not homogeneous on the MgO surface. Co/Al_2O_3 exhibited structures with size of 15–25nm

[Figure 3.2 (d)]. These structures were not very distinct and were possibly aggregated particles of numerous small Co particles since no distinguishable Co peaks could be seen from XRD results.

Since HRTEM results were obtained for the catalysts after calcination at 300^{o}C, it is possible that the particle sizes of the catalysts may have changed somewhat after reduction. In order to determine this, STEM images were taken for both Co/HT and Co/Al_2O_3 after reduction at 500^{o}C. STEM was utilized since the distinct differences between particles and supports could be seen by Z-contrast. The location for the Co particles could also be confirmed by simultaneous EDX mapping. A relatively larger scale (lower resolution) and dark field had to be used to determine Co particle distribution and to better distinguish the Co particles from the supports. From Figure 3.3, it is clear that Co particles sintered to some extent during reduction at 500^{o}C for both catalysts (the brighter particles were verified to be Co by EDX mapping). Most Co particles were about 10–20nm for Co/HT while Co/Al_2O_3 had structures with dimensions ranging from 10nm to larger than 50 nm. However, since no significant difference was exhibited for the XRD pattern of reduced Co/Al_2O_3 compared to that of the as-prepared catalyst, it is unlikely for reduced Co/Al_2O_3 to have had Co particle sizes larger than 50 nm. A more likely explanation is that these seemingly large particles were aggregations of particles. Although it is hard to distinguish single particles from aggregation of particles by TEM, it is obvious that the average size of the Co particles for Co/HT was smaller than that for Co/Al_2O_3.

(a) Co/HT

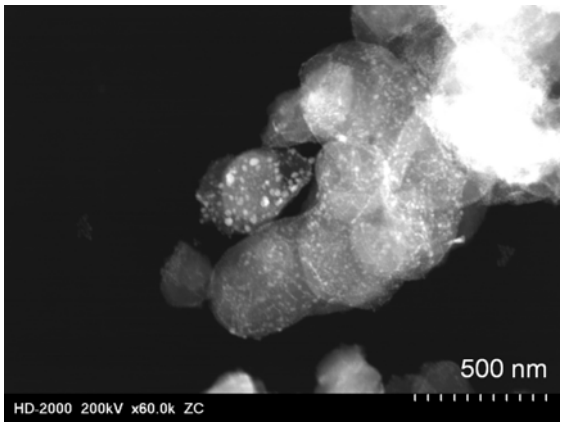

(b) Co/Al_2O_3

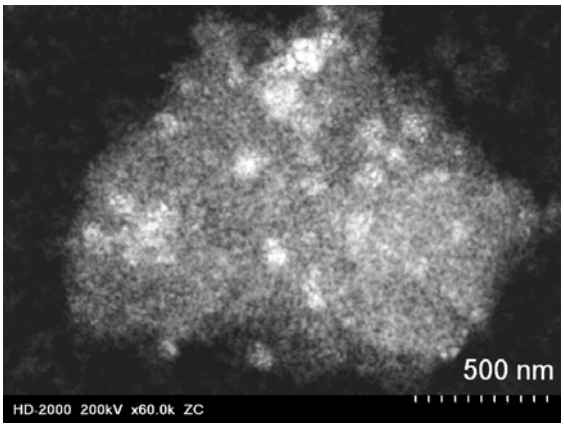

Figure 3.3 STEM micrographs after H_2 reduction for 1 h at 500°C of (a) Co/HT; (b) Co/Al_2O_3.

STEM (figures not shown) and HRTEM (Figure 3.4) were also carried out to determine the influence of the reduction temperature on the dispersion/particle size of Co supported on HT. The reduction temperatures were varied from 300 to 600°C. From the information provided by STEM and HRTEM, three interesting features can be observed. First, cobalt particles appeared mainly located on the external support surface after being

reduced at 300^{o}C; however, they showed a more uniform distribution on HT after reduction at 400^{o}, 500^{o} and 600^{o}C. Second, the Co particle sizes were smaller (≈ 10 nm, error = ±10% of the value measured) for reduction temperatures of 500^{o}C or lower. The existence of larger cobalt particles could be clearly seen for STEM images after the reduction temperature of 600^{o}C, which showed a unimodel particle size distribution with maximum frequency at 20nm in size (error = ±10% of the value measured). However, another possibility for the image could be overlapping of some particles with dimensions each less than 20 nm. Third, comparing the images for Co/HT after reduction at 500^{o}C [Figure 3.4 (c)] to those for the "as-prepared" Co/HT [Figure 3.2 (a)], except for small amounts of larger (10–20 nm) particles formed during reduction, not much difference in particle size could be observed.

(a) 300°C

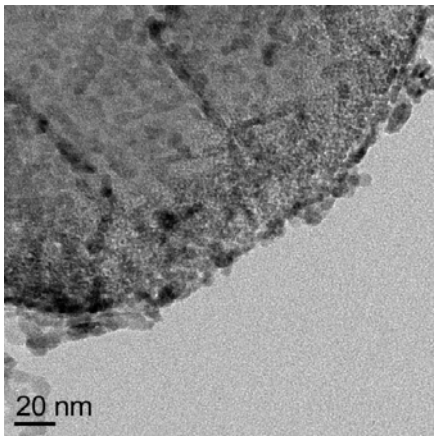

(b) 400°C

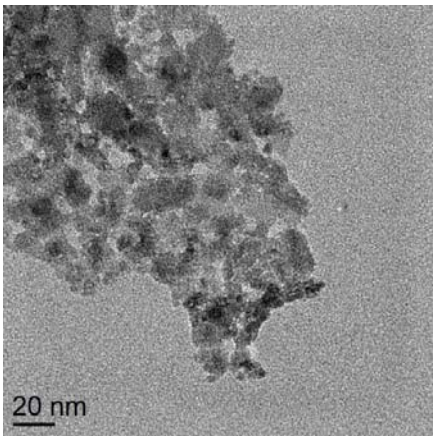

(c) 500°C

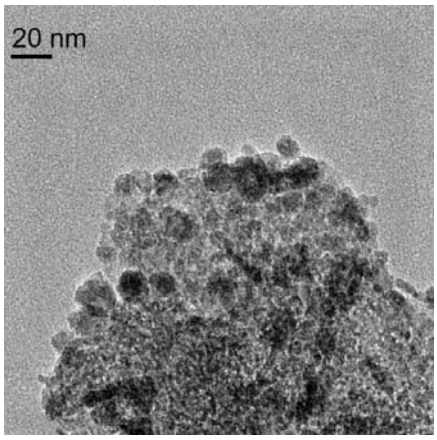

(d) 600°C

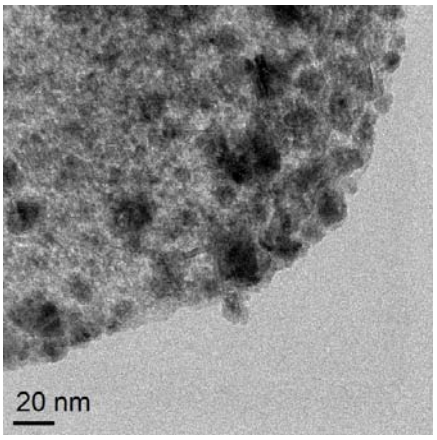

Figure 3.4 HRTEM micrographs of Co/HT for various reduction temperatures: (a) 300°C; (b) 400°C; (c) 500°C and (d) 600°C.

EDX (Energy-dispersive X-ray spectroscopy) mapping was also conducted in order to study the elemental distribution on the catalyst samples. EDX results, along with the information provided by other electron microscopy techniques, have been extensively used as a tool for surface composition investigation in recent Co catalysts studies [16,18,59,60]. Although EDX is not surface sensitive enough to obtain precise surface concentrations, the results are an indication as to the relative Co loading on the surface. In this study, EDX mapping results were collected and averaged over a number of locations on the sample surfaces. The results for the relative cobalt loading on the external surface of the Co/HT catalyst granules after being reduced using different reduction temperatures are shown in Figure 3.5. It is seen that the external surface cobalt composition for Co/HT reduced at various reduction temperatures was much higher than the loading values (10 wt% cobalt), which confirms that the cobalt particles formed to a greater extent on the external surfaces of the support particles. Up to 500^{o}C, the cobalt amounts gradually increased as the reduction temperature increased. Co/HT reduced at 500^{o}C showed the highest surface cobalt concentration, ca. equivalent to 30 wt%. However, when the reduction temperature was increased to 600^{o}C, cobalt external surface wt% dramatically decreased to half that for 500^{o}C. Note that due to instrumental limitation, in-situ EM and EDX were not available. The EM/EDX results obtained in this study may have some uncertainties due to the contact of the sample with air at room temperature, which could have led to some reconstruction of the support. However, the catalyst samples after reduction were passivated slowly so as to only oxidize the external

surface layers of the Co particles so that TEM images should be representative of the reduced Co catalysts.

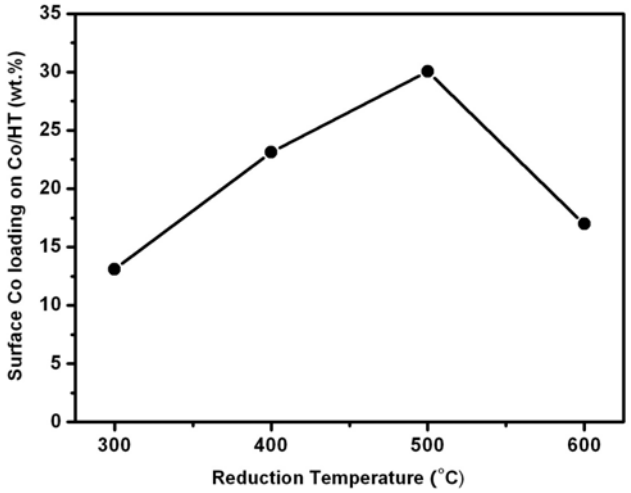

Figure 3.5 Effect of reduction temperature on Co loading amount on the external support surface of Co/HT.

3.3.1.4 TPR

TPR was carried out from room temperature to 800°C in a 10% H_2/Ar flow to obtain the reducibility of the cobalt catalysts. Figure 3.6 presents the TPR profiles of the calcined catalysts. Two overlapping peaks in the temperature range of 200–500°C were observed for all the catalysts. Since HT, MgO and Al_2O_3 cannot be reduced in that temperature range [61,62], the reduction peaks should only be related to the reduction of Co species. The low temperature peak can be ascribed to the reduction of Co_3O_4 to CoO and the higher-temperature one located between 300 and 500°C has been suggested to be related to the reduction of CoO to Co [63,64]. Regarding the peak temperatures for these

two reduction peaks, similar trends were found for the four catalysts prepared in this work: Co/Al_2O_3 < Co/HT < Co/MgO < Co/CHT. Except for Co/Al_2O_3, which had a degree of reduction ≈ 70%, all the other catalysts were fully reduced in the temperature range of 200–500°C based on the consumption of H_2. A broad peak located at ca. 500–750°C was also observed for Co/Al_2O_3, which can be ascribed to the reduction of Co strongly interacting with the support (Co_xO_y–Al_2O_3) [65]. The strong interaction of Co with Al_2O_3 that leads to the low reducibility of non-promoted Co supported on Al_2O_3 in the temperature range of 200–500°C has been reported by many researchers including our group [64–68]. The TPR profile for Co/MgO is in agreement with the literature [69,70]. It is interesting to note that the TPR profiles of Co/CHT and Co/MgO are similar.

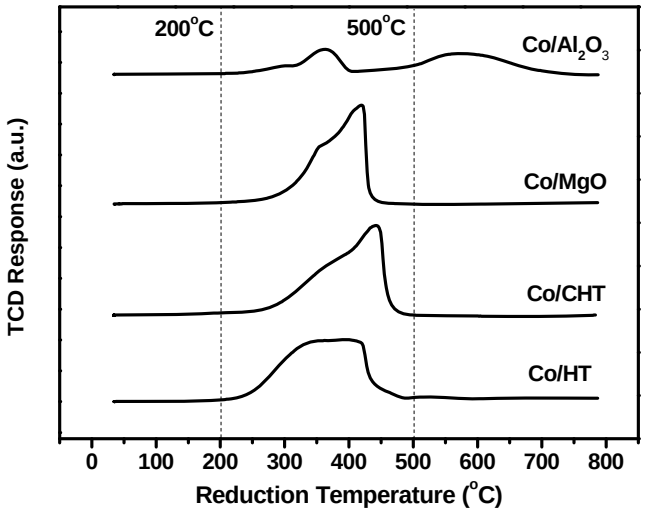

Figure 3.6 TPR profiles of the calcined Co-based catalysts.

3.3.1.5 H_2 chemisorption

Table 3.2 summarizes the results obtained from the volumetric H_2 chemisorption. The amount of adsorbed H_2 at 100°C decreased in the order of Co/HT > Co/Al_2O_3 > Co/CHT > Co/MgO. It is obvious that Co/HT had the greatest H_2 adsorption ability among all these four catalysts. Active Co metal dispersions were estimated ($\%D=Co_s/Co_T$) based on the assumption of a stoichiometry between hydrogen chemisorption uptake and surface metal atoms of 1:1 for H/Co_s (where Co_s is the number of estimated surface Co atoms per gram of catalyst and Co_T is the total number of Co atoms per gram of catalyst) [71]. Estimations of average Co metal particle sizes were made using the formula

$$d_p(Co^0, nm)=\frac{96}{\%D \times f_R},$$

where f_R represents the fraction of Co reduced to Co^0 [83].

Table 3.2 Results for hydrogen chemisorption on Co-based catalysts.

Catalyst[a]	Hydrogen chemisorption
	Total H atom uptake[b] (μmol/g)
Co/HT	121.4
Co/CHT	51.6
Co/Al_2O_3	89.0
Co/MgO	38.4

[a] All catalysts contained 10 wt% Co.
[b] Determined by extrapolating the total chemisorption isotherm to zero pressure. Max error = ± 3%.
[c] Based on total hydrogen chemisorption, H/Co_s = 1, % dispersion = total hydrogen atoms chemisorbed/total number of Co atoms. Max. error = ±5%.

3.3.1.6 Comparison of Co particle sizes obtained by different characterization techniques

Table 3.3 gives a comparison of average Co particle sizes estimated by H_2 chemisorption, XRD, or TEM. Larger Co particle sizes were calculated using the Co dispersion obtained from the results of H_2 chemisorption, suggesting perhaps that Co surfaces were partially blocked by support species and/or that H_2 chemisorption was partially suppressed (due to interactions between Co and the support). Representative Co particle size was also estimated by physical methods, XRD and TEM. Except for Co/MgO, XRD was not able to estimate any Co particle sizes due to Co being X-ray amorphous for these catalysts. Co particles were distinguishable by TEM only for Co/HT and Co/Al_2O_3. A relatively thin structure and aggregation of small Co particles for Co/HT and Co/Al_2O_3 could be possible explanations for these results. Despite the seemingly inconsistent particle size measurements obtained using different techniques, it would appear reasonable conclusive that Co/HT exhibited the smallest average Co particle size.

Table 3.3 Average Co particle sizes estimated by different techniques.

Catalyst	Average Co Particle Diameter (nm)		
	H_2 chemisorption[a]	XRD	TEM
Co/HT	13.4	n.a.[b]	5-10
Co/ CHT	31.6	n.a.[b]	n.d.
Co/Al_2O_3	18.3	n.a.[b]	15-25
Co/MgO	42.3	19.8	n.d.

[a] Average Co^0 particle size (nm) = $96/(\%D \times f_R)$, where f_R represents the fraction of Co reduced to Co^0 [83].
[b] X-ray amorphous.

3.3.2 Reaction activity for FTS

In order to investigate the role of the support in Co catalysis, the Co catalysts were studied under CO hydrogenation conditions. A negligible amount of CO_2 was formed during this reaction and was not taken into consideration for the calculation of selectivity and activity of the catalysts during reaction. In a previous study in our laboratory [64], the optimum reduction temperature for Co/Al_2O_3 catalysts was found to be ca. 350°C. Therefore, Co/Al_2O_3 reduced at 350°C was also evaluated in this study for comparison. Activities were compared on a per weight catalyst basis instead of using TOF due to the fact that the numbers of accessible surface metal atoms determined by chemisorption do not actually represent the number of catalytic sites for reaction [72]. Use of TOF in the case of a metal on a wide variety of supports can lead to misinterpretations because of the reason above and because of the difficulty in getting comparable chemisorption results for Co catalysts. Therefore, we prefer to report rate/g-cat since relative activity can be easily seen. However, we report all the data necessary for calculation of TOF or rate per surface area of exposed Co^0 if a reader finds it useful.

Table 3.4 shows the reaction results at steady state obtained for the catalysts with different supports. The steady-state rates were measured after 15 h TOS (time-on-stream). Co/HT exhibited a significantly higher steady-state CO hydrogenation rate than the other catalysts for the 10 wt% of Co used. Co/HT exhibited a rate that was almost 50 times higher than that of Co/CHT. Co/Al_2O_3 reduced at 500°C showed a moderate steady-state reaction rate in this study (1.73 μmol/g/s), which was very close to that found in a previous study in our laboratory under similar reaction conditions [73]. Co/Al_2O_3

reduced at 350°C showed a relatively higher reaction rate (2.34 μmol/g/s) compared to that with a reduction temperature of 500°C, as expected. Co/MgO exhibited the lowest reaction rate, which was very close to the detectability limitation. Thus, the calculation of exact product selectivities was not able to be done for this catalyst. However, there was no oxygenate formation.

Table 3.4 Catalytic activities and selectivities of Co-based catalysts.

Catalysts	SS rate[a] (μmol/g/s)	% Hydrocarbon selectivity[b] at SS						% olefins at SS (C_2-C_4)
		C_1	C_2	C_3	C_4	C_5-C_7	Total oxygenates	
Co/HT	3.1	26.8	7.1	13.1	11.6	38.7	2.8	12.1
Co/CHT	0.07	21.6	10.9	14.2	10.4	39.6	3.3	23.0
Co/MgO	0.02	-	-	-	-	-	-	-
Co/Al_2O_3	1.73	44.4	11.0	15.2	10.5	16.2	2.7	4.3
Co/Al_2O_3(350°C)[c]	2.34	47.1	9.8	16.4	11.2	13.1	2.4	13.1

[a] Catalyst: 0.3 g, Inert: 3 g α-alumina; Reduction: 500°C for 1h; Reaction conditions: T = 230°C, P = 1.8 atm, Flow rate = 45 mL/min (H_2/CO =2); Data taken at 15 h after steady state had been reached. Experimental error = ±5%.
[b] Carbon selectivity = $nC_n / \sum nC_n$.
[c] The reaction conditions were the same as [a], except that reduction was at 350°C for 1h.

Similar hydrocarbon distributions were observed for Co/HT and Co/CHT. About 20–25% of the hydrocarbon product was CH_4, and the rest of the products were mostly higher hydrocarbons with a small amount of oxygenates (< 5%). The production distribution in this study is similar to what has been reported by Pinnavaia et al. [38] for their investigation of CO hydrogenation on HT-supported Ru catalysts at a relatively low pressure, ca. 101 kPa. It is noteworthy that the C_2–C_4 olefin selectivity was double for Co/CHT compared to Co/HT, possibly due to the low conversion level. The product distributions for Co/Al_2O_3 reduced at 350° and 500°C were very similar, however, the %

C_2–C_4 olefin selectivity was greater for the lower reduction temperature. Co/Al_2O_3 showed a poorer product selectivity than Co/HT or Co/CHT, with higher CH_4 and lower C_5–C_7 selectivities. The amount of oxygenate formation was small and comparable to that of Co/HT.

Figure 3.7 shows the TOS behavior of the overall reaction rate of CO hydrogenation for the Co-based catalysts of this study. The higher activities of Co/HT and Co/Al_2O_3 decreased slightly during the first 6 h and then remained steady. The activities of Co/CHT and Co/MgO were low and relatively constant, which might be within experimental error. The rate drop from the initial value was similar for Co/HT and for Co/Al_2O_3 in these investigations, which was about 10–12%. The deactivation behavior was similar to that found in the previous studies in our laboratory for Co/Al_2O_3, which might be due to Co aluminate formation, sintering, and/or coke deposition [73,74].

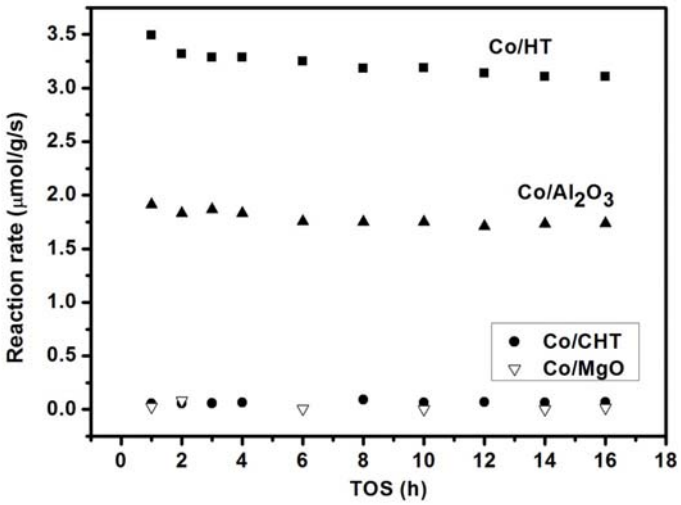

Figure 3.7 Time-on-stream behavior of the overall rate of CO hydrogenation for the catalyst with various supports.

Pronounced differences were observed in this study in the activities and selectivities of the Co catalysts supported on different supports. Al_2O_3 is a well-known excellent support for cobalt FTS catalysts and has been widely applied for CO hydrogenation. Often, in order to modify the surface characteristics for the purpose of improving the catalytic performance, some noble (or near-noble) metals, such as Ru [57,73,74] or Re [71] have been used as reduction promoters. However, HT as a support for cobalt catalysts was found in this study to have the ability to increase the reaction rate without the need for a second metal as a reduction promoter. Co_3O_4 existed initially on all the catalysts. Based on TPR results, it reduced essentially completely for Co/HT, the most FTS active of the catalysts, in the range 200–300^{o}C. However, the almost equally active FTS catalyst Co/Al_2O_3 showed lower reducibility in the same range, demonstrating that

the reducibility degree for cobalt can only be one of the parameters leading to higher activity. In fact, the higher FTS activity for Co/HT was also due to the higher Co metal dispersion and related smaller average Co metal particle size, resulting in part probably because of the relatively higher BET surface area of the HT support.

Based on the results, Co/HT reduced at 500^{o}C provided the most active catalyst, even compared to what has usually been found to be one of the best and most active Co FTS catalysts, namely Co/Al_2O_3. In addition to a high reducibility of the cobalt and a higher activity for CO hydrogenation, use of the HT support also led to better selectivities for higher hydrocarbons.

As evidenced from XRD, BET surface analysis and TEM results, Co supported on HT had a higher total surface area and smaller Co particle size compared to Co supported on Al_2O_3. In addition, use of the HT support obviously enhanced the reducibility of Co. Thus, it is not surprising that Co/HT had better H_2 chemisorption ability and activity for CO hydrogenation. Another possible factor that may have affected the activity of the catalysts was the support basicity. It has been reported that the surface basicity of HT increases with the pretreatment temperature until 500^{o}C [55,75]. After calcination at 300^{o}C and reduction at 500^{o}C, Co/HT may have had optimum basicity, which might have influenced the activity and selectivity.

However, the much decreased activities for Co supported on MgO and pre-calcined HT cannot be explained by total surface area, average Co particle size, or Co reducibility. Compared to Co/Al_2O_3, Co/MgO had a similar BET surface area, a similar average Co particle size, and a much higher reducibility, but the activity of Co/Al_2O_3 was about 100

times higher than that of Co/MgO. Extremely low activities of Co-based catalysts supported on MgO compared to other supports have been reported in the literature for CO hydrogenation (compared to Al_2O_3, SiO_2, TiO_2 and C [70,76]; compared to ZrO_2, CeO_2 and Nb_2O_5 [77]; compared to ZnO and La_2O_3 [78]), for hydroformylation of ethylene (compared to ZnO and La_2O_3 [78]) and for methanol decomposition (compared to ZrO_2 and CeO_2 [79]). The possible reasons for the low activity of Co/MgO proposed in the literature can be summarized as (1) suppression of H_2 adsorption [80]; (2) formation of an inactive Mg–Co mixed oxide after pretreatment at a temperature higher than 400–500^oC [69,76,79] due to the strong basicity of MgO. Low H_2 chemisorption was also observed for Co/MgO in this study. The shift of reduction peaks to higher temperature also indicated some interaction of Co with MgO. Thus, the low activity of MgO observed in this study may be ascribed to the presence of fewer Co active sites due to the interaction of Co with MgO.

The low activity of Co/CHT found in this study seems to be at variance with results in the literature. Yuan et al. [32] found that Pt supported on calcined HT had the greatest activity for the hydrogenolysis of glycerol compared to Pt supported on other supports including HZSM-5, C, Al_2O_3 and MgO. Hsiao and Lin [35] showed that Cu/CHT had comparable activity with that of Cu/Al_2O_3 for methanol conversion to make higher oxygenates. A possible explanation for the differences seen might be in the differences in main catalyst metal used and the different reactions used to test the catalysts.

Taking into account that Co/CHT had dramatically decreased H_2 chemisorption, it can be speculated that Co had a strong interaction with the support, perhaps with the Co

heavily decorated by support species and not accessible to reactants, leading to a significant decrease in available active sites. The differences in the TPR profiles for Co/HT and Co/CHT also validate this speculation. It is worth noting that the only difference in the preparation of Co/HT and Co/CHT was the pre-calcination in air of the HT before being used as a support for Co/CHT. After calcination at 500 ◦C, the layered structure of HT should have changed with the formation of Mg(Al) mixed oxide, which affects the surface basicity of the resulting CHT [22,24,46]. This has been shown for various physicochemical characterizations of CHT materials [45,56,75]. Thus, it is possible that the much stronger interaction of Mg(Al) oxide with Co resulted in the significantly decreased activity of Co/CHT. The similar behavior for Co/CHT and Co/MgO is interesting. However, since the focus of this paper was on the more active FTS catalysts, in-depth studies of these less active catalysts were not pursued.

The Anderson–Schulz–Flory (ASF) product distribution for hydrocarbon formation was also investigated in this study. Co/MgO and Co/CHT are not discussed here due to the very low activity and the resulting error in concentration estimations of individual products. C_1 (methane) was not included in the calculation of chain growth probability for any of the other catalysts due to the fact that it is often larger or smaller than what would be predicted by the polymerization probability based on the other products. The C_{2+} hydrocarbon distributions for the catalysts all followed an ASF distribution. However, the chain growth probability factors (α) varied significantly between Co/Al_2O_3 and Co/HT and even somewhat for different reduction temperatures of Co/HT as shown in Table 3.5.

The α values suggest that Co/Al_2O_3 has only half the chain growth probability compared to Co/HT for the reaction conditions used. The differences in chain growth probability for Co/HT and Co/Al_2O_3 could be a crucial indication of differences in the mechanism. Product distributions for Co catalysts with different α values have been suggested to be due to a superposition of two different mechanisms [81]. It has been suggested that the lower and higher α values are related to the CH_2 insertion and CO insertion, respectively.

Table 3.5 Chain growth probability (α) for Co-based catalysts.

Catalyst	Reduction temperatures(^{o}C)	Alpha values[a]
Co/Al_2O_3	500	0.29
Co/HT	300	0.65
Co/HT	400	0.68
Co/HT	500	0.57
Co/HT	600	0.53

[a] Max error = ±5%.

3.3.3 Effect of reduction temperature of Co/HT

Figure 3.8 shows the steady-state reaction results obtained for Co/HT reduced at various temperatures. The reduction temperature had a dramatic effect on the overall rate of CO hydrogenation. It can be seen that the rate increased as the reduction temperature increased, passing through a maximum at the reduction temperature of 500^{o}C before decreasing. The TOS behavior for Co/HT after being reduced at various reduction temperatures (data not shown) was very similar to what is shown in Figure 3.7. The

reaction rate slightly decreased and stablized after 6 h of reaction. However, the deactivation rate for reduction at 600°C was larger than for lower reduction temperatures.

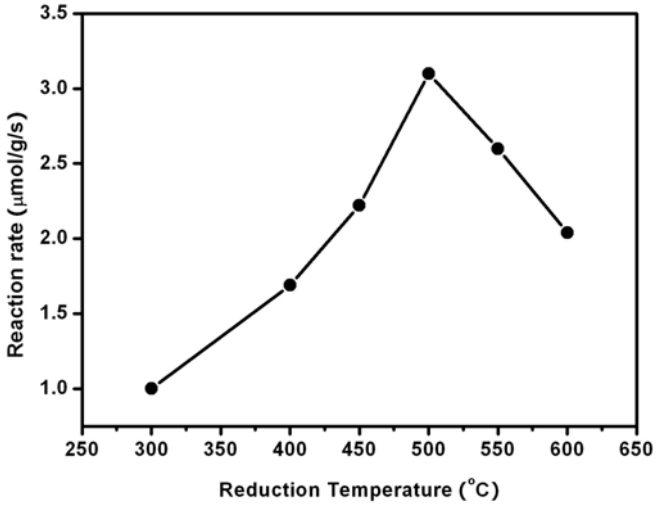

Figure 3.8 Effect of reduction temperature on overall catalyst activity of Co/HT.

Three complementary effects need to be addressed to explain the results in Figure 3.8: the thermal decomposition properties of HT, the reducibility of Co, and the sintering of Co particles. Our BET surface area analysis confirmed that a higher pretreatment temperature (400°C) increased the surface area. The TPR results indicated that the reduction of Co/HT was not fully completed when the temperature was much below 500°C. With respect to the sintering effect, serious sintering is known to occur for high reduction temperatures > 500°C for cobalt catalysts [57,64,82]. Thus, 500°C appears to be a critical temperature for the optimization of Co supported on HT. As evidenced by TEM and EDX, more Co particles appeared to migrate to the support surface as the reduction temperature increased from 300°C to 500°C. The trend of external support

surface Co loading (Figure 3.5) is identical to that for the reaction rate (Figure 3.8) for the various reduction temperatures, suggesting that reaction may have been facilitated when more cobalt sites were accessible on the external surface of the HT support. The similarity of external surface Co loading and reaction rate for various reduction temperatures is strong evidence for the existence of an optimum reduction temperature for HT as a support for Co catalysts and the manifest relationship between reaction rate and cobalt sites on the external surface of HT. Based on BET surface analysis results, the opening of the HT structure from 300^{o}C to 400^{o}C may have helped in increasing the reaction rates. However, the reaction rate differences seen after reduction in the temperature range from 400^{o} to 600^{o}C were not affected by any change in BET surface area or pore volume since these parameters remained constants.

Different reduction temperatures used for Co/HT also showed a significance influence on the value of α (Table 3.5). It can be seen that carbon chain growth ability decreased with increasing reduction temperature. The cause remains to be determined.

3.4 Conclusions

A series of 10 wt% cobalt supported catalysts was prepared using the incipient wetness impregnation method and evaluated by CO hydrogenation. The catalyst activity and selectivity were significantly influenced by the particular supports. The usage of HT as a support for cobalt resulted in the highest catalytic activity. Use of MgO or CHT (HT pre-calcined at 500^{o}C), however, led to low activity catalysts while the Al_2O_3-supported Co exhibited a moderate activity, somewhat lower than that of Co/HT. Co/Al_2O_3 was

compared in this study primarily due to two facts: (1) aluminum oxide is one of the constituents of HT; (2) Co/Al_2O_3 is one of the best Co FTS catalysts known in terms of activity and selectivity. Co/HT, however, showed an impressive higher activity comparing to that of Co/Al_2O_3 even without a reduction promoter. HRTEM results suggested that the Co were highly dispersed in the Co/HT catalyst with relatively small particles. Furthermore, H_2 chemisorption showed that Co/HT had significantly higher H_2 uptakes compared to other supported Co catalysts in this study. The high catalytic performance of Co/HT appeared to be due to the effects of relatively higher total surface area, high reducibility, and smaller cobalt particle size. Product distribution analysis showed that both Co/HT and Co/Al_2O_3 followed an Anderson–Schulz–Flory chain growth probability. A significantly higher chain growth probability was found for Co/HT compared to Co/Al_2O_3.

The effect of reduction temperature was also investigated for Co/HT. The reaction results showed that a relatively moderate reduction temperature (500^oC) led to the highest activity, probably due to the optimization of incomplete cobalt reducibility at lower temperatures and the sintering effect at higher reduction temperatures, respectively. Furthermore, the similar trend for the effect of reduction temperature on the reaction rates and the external surface Co loading (from EDX) also suggested a less obvious relationship.

Based on the reaction and characterization results given in this paper, important conclusions concerning the effects of the different supports on Co catalysis could be made. More detailed conclusions concerning how these effects are produced by the

different supports await further study.

3.5 Acknowledgements

We acknowledge financial support from Chevron and the Department of Energy. We thank Dr. Haijun Qian of the EM Lab at Clemson University for his help in HRTEM and STEM measurements.

3.6 References

[1] E. Iglesia, Appl. Catal., A – Gen. 161 (1997) 59.

[2] R.B. Anderson, Fischer–Tropsch Synthesis, Academic Press, Orlando, 1984.

[3] E. Iglesia, S.L. Soled, R.A. Fiato, J. Catal. 137 (1992) 212.

[4] J.-H. Oh, J.W. Bae, S.-J. Park, P.K. Khanna, K.-W. Jun, Catal. Lett. 130 (2009) 403–409.

[5] M.V. Krylova, A.B. Kulikov, M.I. Knyazeva, A.Y. Krylova, Chem. Technol. Fuels Oils 44 (2008) 339.

[6] J.W. Bae, S.-M. Kim, S.-J. Park, P.S. Sai Prasad, Y.-J. Lee, K.-W. Jun, Ind. Eng. Chem. Res. 48 (2009) 3228.

[7] B. Jongsomjit, J. Panpranot, J.G. Goodwin Jr., J. Catal. 215 (2003) 66.

[8] B. Jongsomjit, J.G. Goodwin Jr., Catal. Today 77 (2002) 191.

[9] W.-J. Wang, Y.-W. Chen, Appl. Catal. 77 (1991) 223.

[10] D. Schanke, A.M. Hilmen, E. Bergene, K. Kinnari, E. Rytter, E. Adnanes, A. Holmen, Catal. Lett. 34 (1995) 269.

[11] G.J. Haddad, B. Chen, J.G. Goodwin Jr., J. Catal. 161 (1996) 274.

[12] A.H. Kababji, B. Joseph, J.T. Wolan, Catal. Lett. 130 (2009) 72.

[13] M.P. Rosynek, C.A. Polansky, Appl. Catal. 73 (1991) 97.

[14] G.J. Haddad, J.G. Goodwin Jr., J. Catal. 157 (1995) 25.

[15] R. Oukaci, A.H. Singleton, J.G. Goodwin Jr., Appl. Catal., A – Gen. 186 (1999) 129.

[16] B. Jongsomjit, C. Sakdamnuson, J.G. Goodwin Jr., P. Praserthdam, Catal. Lett. 94 (2004) 209.

[17] D.J. Duvenhage, N.J. Coville, Appl. Catal., A – Gen. 153 (1997) 43.

[18] B. Jongsomjit, T. Wongsalee, P. Praserthdam, Catal. Commun. 6 (2005) 705.

[19] S. Storsæter, B. Tøtdal, J.C. Walmsley, B.S. Tanem, A. Holmen, J. Catal. 236 (2005) 139.

[20] K. Jalama, N.J. Coville, D. Hildebrandt, D. Glasser, L.L. Jewell, J.A. Anderson, S. Taylor, D. Enache, G.J. Hutchings, Top. Catal. 44 (2007) 129.

[21] A. Vaccari, Catal. Today 41 (1998) 53.

[22] B.F. Sels, D.E. De Vos, P.A. Jacobs, Catal. Rev. 43 (2001) 443.

[23] A. Olafsen, C. Daniel, Y. Schuurman, L.B. Raberg, U. Olsbye, C. Mirodatos, Catal. Today 115 (2006) 179.

[24] W.T. Reichle, S.Y. Kang, D.S. Everhardt, J. Catal. 101 (1986) 352.

[25] C.-X. Chen, C.-H. Xu, L.-R. Feng, F.-L. Qiu, J.-S. Suo, J. Mol. Catal. A – Chem. 252 (2006) 171.

[26] A.F. Lucredio, G.T. Filho, E.M. Assaf, Appl. Surf. Sci. 255 (2009) 5851.

[27] R. Shiozaki, T. Hayakawa, Y.-y. Liu, T. Ishii, M. Kumagai, S. Hamakawa, K. Suzuki, T. Itoh, T. Shishido, K. Takehira, Catal. Lett. 58 (1999) 131.

[28] Z. Kiraly, B. Veisz, A. Mastalir, G. Kofarago, Langmuir 17 (2001) 5381.

[29] S. Narayanan, K. Krishna, Appl. Catal., A – Gen. 174 (1998) 221.

[30] Y. Wang, J. Qu, H. Liu, C. Hu, Catal. Today 126 (2007) 476.

[31] Y.Z. Chen, C.M. Hwang, C.W. Liaw, Appl. Catal., A – Gen. 169 (1998) 207.

[32] Z. Yuan, P. Wu, J. Gao, X. Lu, Z. Hou, X. Zheng, Catal. Lett. 130 (2009) 261.

[33] V.B. Kazansky, V.Y. Borovkov, A.I. Serykh, F. Figueras, Catal. Lett. 49 (1997) 35.

[34] P. Seetharamulu, V. Siva Kumar, A.H. Padmasri, B. David Raju, K.S. Rama Rao, J. Mol. Catal. A – Chem. 263 (2007) 253.

[35] T.C. Hsiao, S.D. Lin, Catal. Lett. 119 (2007) 72.

[36] S. Narayanan, K. Krishna, Catal. Commun. 20 (1997) 1991.

[37] S. Narayanan, K. Krishna, Catal. Today 49 (1999) 57.

[38] T.J. Pinnavaia, M. Rameswaran, E.D. Dimotakis, E.P. Giannelis, E.G. Rightor, Faraday Discuss. Chem. Soc. 87 (1989) 227.

[39] J. Cheng, J. Yu, X. Wang, L. Li, J. Li, Z. Hao, Energy Fuels 22 (2008) 2131.

[40] R. Xu, H.C. Zeng, Chem. Mater. 13 (2001) 297.

[41] A.I. Tsyganok, M. Inaba, T. Tsunoda, K. Uchida, K. Suzuki, K. Takehira, T. Hayakawa, Appl. Catal., A – Gen. 292 (2005) 328.

[42] Y. Ding, L. Xu, C. Chen, X. Shen, S.L. Suib, J. Phys. Chem. C 112 (2008) 8177.

[43] J.T. Kloprogge, R.L. Frost, Appl. Catal., A – Gen. 184 (1999) 61.

[44] F. Cavani, F. Trifiro, A. Vaccari, Catal. Today 11 (1991) 173.

[45] J. Shen, M. Tu, C. Hu, J. Solid State Chem. 137 (1998) 295.

[46] Y. Liu, E. Lotero, J.G. Goodwin Jr., X. Mo, Appl. Catal., A – Gen. 331 (2007) 138.

[47] Q. Shen, L. Li, J. Li, H. Tian, Z. Hao, J. Hazard. Mater. 163 (2009) 1332.

[48] M. Bellotto, B. Rebours, O. Clause, J.L. Bazin, E. Elkaim, J. Phys. Chem. 100 (1996) 8535.

[49] T. Wongkerd, A. Luengnaruemitchai, S. Jitkarnka, Appl. Catal. B – Environ. 78 (2008) 101.

[50] D. Tichit, M.H. Lhouty, A. Guida, B.H. Chiche, F. Figueras, A. Auroux, D. Bartalini, E. Garrone, J. Catal. 151 (1995) 50.

[51] T.S. Stanimirova, N. Piperov, N. Petrova, G. Kirov, Clay Miner. 39 (2004) 177.

[52] Z.P. Xu, H.C. Zeng, Chem. Mater. 13 (2001) 4564.

[53] R.L. Frost, A.W. Musumeci, T. Bostrom, M.O. Adebajo, M.L. Weier, W. Martens, Thermochim. Acta 429 (2005) 179.

[54] S. Kannan, D. Kishore, K. Hadjiivanov, H. Knozinger, Langmuir 19 (2003) 5742.

[55] I. Kirm, F. Medina, X. Rodriguez, Y. Cesteros, P. Salagre, J. Sueiras, Appl. Catal., A – Gen. 272 (2004) 175.

[56] W. Xie, H. Peng, L. Chen, J. Mol. Catal. A – Chem. 246 (2006) 24.

[57] A. Tavasoli, R.M.M. Abbaslou, A.K. Ajay, K. Dalai, Appl. Catal., A – Gen. 346 (2008) 58.

[58] Y. Zhang, D. Wei, S. Hammache, J.G. Goodwin Jr., J. Catal. 188 (1999) 281.

[59] B. Jongsomjit, T. Wongsalee, P. Praserthdam, Mater. Chem. Phys. 97 (2006) 343.

[60] X. Li, J. He, M. Meng, Y. Yoneyama, N. Tsubaki, J. Catal. 265 (2009) 26.

[61] J.J. Yu, Z. Jiang, L. Zhu, Z.P. Hao, Z.P. Xu, J. Phys. Chem. B 110 (2006) 4291.

[62] F. Kovanda, K. Jiratova, J. Rymes, D. Kolousek, Appl. Clay Sci. 18 (2001) 71.

[63] A.A. Khassin, T.M. Yurieva, G.N. Kustova, I.S. Itenberg, M.P. Demeshkina, T.A. Krieger, L.M. Plyasova, G.K. Chermashentseva, V.N. Parmon, J. Mol. Catal. A – Chem. 168 (2001) 193.

[64] A. Sirijaruphan, A. Horvath, J.G. Goodwin Jr., R. Oukaci, Catal. Lett. 91 (2003) 89.

[65] B. Jongsomjit, J. Panpranot, J.G. Goodwin Jr., J. Catal. 204 (2001) 98.

[66] Y. Ji, Z. Zhao, A. Duan, G. Jiang, J. Liu, J. Phys. Chem. C 113 (2009) 7186.

[67] D. Xu, W. Li, H. Duan, Q. Ge, H. Xu, Catal. Lett. 102 (2005) 229.

[68] Ø. Borg, N. Hammer, S. Eri, O.A. Lindvag, R. Myrstad, E.A. Blekkan, M. Rønning, E. Rytter, A. Holmen, Catal. Today 142 (2009) 70.

[69] C.A. Querini, M.A. Ulla, F. Requejo, J. Soria, U.A. Sedran, E.E. Miro, Appl. Catal. B– Environ. 15 (1998) 5.

[70] C.H. Bartholomew, R.C. Reuel, Ind. Eng. Chem. Prod. Res. Dev. 24 (1985) 56.

[71] Ø. Borg, S. Eri, E.A. Blekkan, S. Storsæter, H. Wigum, E. Rytter, A. Holmen, J. Catal. 248 (2007) 89.

[72] J.G. Goodwin Jr., S. Kim,W.D. Rhodes, Catalysis 17 (2003) 1.

[73] A. Kogelbauer, J.G. Goodwin Jr., R. Oukaci, J. Catal. 160 (1996) 125.

[74] A.R. Belambe, R. Oukaci, J.G. Goodwin Jr., J. Catal. 166 (1997) 8.

[75] F. Prinetto, G. Ghiotti, R. Durand, D. Tichit, J. Phys. Chem. B 104 (2000) 11117.

[76] R.C. Reuel, C.H. Bartholomew, J. Catal. 85 (1984) 78.

[77] T. Ishihara, N. Horiuchi, K. Eguchi, H. Arai, Appl. Catal. 66 (1990) 267.

[78] J. Llorca, A. Barbier, G.A. Martin, J. Sales, P.R. de la Piscina, N. Homs, Catal. Lett. 42 (1996) 87.

[79] T. Tsoncheva, L. Ivanova, C. Minchev, M. Froba, J. Colloid Interface Sci. 333 (2009) 277.

[80] R.C. Reuel, C.H. Bartholomew, J. Catal. 85 (1984) 63.

[81] J. Gaube, H.-F. Klein, J. Mol. Catal. A – Chem. 283 (2008) 60.

[82] G. Jacobs, P.M. Patterson, Y. Zhang, T. Das, J. Li, B.H. Davis, Appl. Catal., A – Gen. 233 (2002) 215.

[83] R.D. Jones, C.H. Bartholomew, Appl. Catal. 39 (1988) 77.

CHAPTER FOUR

COMPARISON OF CHEMISORPTION CLOSE TO AMBIENT VS. UNDER REACTION CONDITIONS FOR GROUP VIII METAL CATALYSTS

[As published in Journal of Catalysis, 281 (2011) 128-136]

A comparison of the relationship of H_2 or CO chemisorption measurements at 25–100^{o}C to similar results obtained under CO hydrogenation conditions by steady-state isotopic transient kinetic analysis (SSITKA) is made for the first time for a wide variety of Group VIII metal catalysts. The ratio N_T^*/N_{chem} (amount of chemisorption by SSITKA vs. by static chemisorptions) was found to be almost always ca. unity for Co catalysts. SSITKA can, thus, be used as a complementary characterization technique to TEM, XRD, and static chemisorption for better understanding of Co metal catalyst dispersion and metal surface site availability for Co catalysts with a wide variety of promoters/supports. Unfortunately, application of SSITKA chemisorption measurements under reaction conditions for characterizing metal dispersion for the other metals is limited at this time. However, the results do suggest some possibilities for Ru and Rh.

4.1 Introduction

Metal catalysts comprised Fe, Co, Ni, Ru, Rh, or Pt are widely used in industrial applications. All are active to some degree for CO hydrogenation. The first five are also promising candidates for the production of alternative fuels by Fischer–Tropsch synthesis (FTS) [1–6]. Although much research has been undertaken in the past addressing their catalytic properties, the relationships of their metal surface structures to those properties are still not completely understood since measures of their adsorptive properties (used often to estimate metal surface areas, active site densities, and other surface properties) vary greatly with composition, conditions, and even the analysis method used.

H_2 or CO static chemisorption is used typically to estimate the number of surface metal atoms for most heterogeneous Group VIII metal catalysts [7–9]. Investigations have confirmed that such things as metal loading, nature of support, and the preparation method impact the stoichiometries for H_2 and CO adsorption on these metal catalysts. For example, Reuel and Bartholomew [10], in a systematic study of CO and H_2 adsorption on Co catalysts, showed that hydrogen adsorption is highly activated on cobalt, with the degree of activation dependent on the metal loading. In addition, other complications that may affect chemisorption data analysis on various metals are suppression of H_2 chemisorption, formation of carbides, H_2 spillover, carbon deposition, the strong interaction between metal and supports (SMSI), the nature of chemisorption at metal–support interfaces, and the presence of promoters/poisons (illustrated in Figure 4.1) [5,10–13]. Although the number of surface metal atoms and metal dispersion measured by chemisorption has been demonstrated to be related to the catalytic properties for many

heterogeneous metal catalysts, the accuracy of such measurements is complicated by some of the problems mentioned above which limit the usefulness of these estimations.

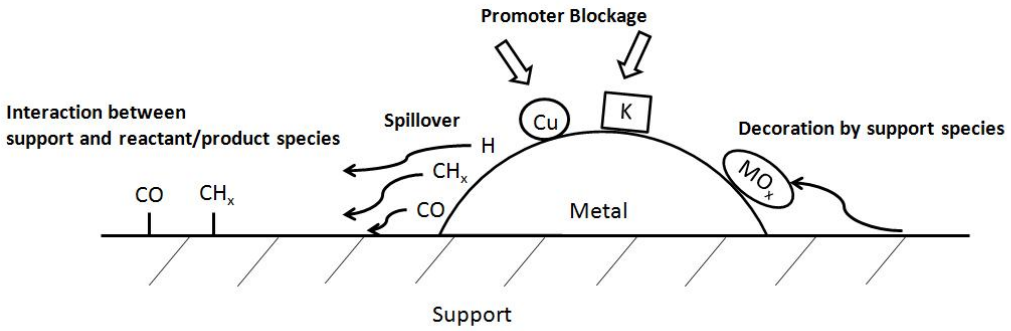

Figure 4.1 Factors that can affect surface coverage.

Steady-state isotopic transient kinetic analysis (SSITKA) is one of the most powerful tools to estimate the surface residence time, concentration of intermediates, intrinsic site activities, and surface reaction mechanism under reaction conditions. It has been widely applied since the early pioneering work of Happel, Bennett, Biloen and Bell [14–17]. SSITKA provides in-situ surface kinetic information based on tracing the isotopically labeled effluent species vs. time after switching the flow of a reactant in the reactor feed labeled with one isotope to that labeled with another. Reactant and product concentrations are not disturbed by the isotopic switch (for elements heavier than hydrogen) under isothermal and isobaric reaction conditions. SSITKA allows determination of the surface concentrations of the most active reaction intermediates and

reversibly adsorbed reactants, which provides an alternative way to obtain valuable information about chemisorption properties, especially at reaction conditions.

Significant transformations during reaction can affect not only the catalyst surface layer but also deeper structures by the formation of new microstructures or defects, which may be stabilized by various promoters. Such changes may only occur during reaction and may not exist during static chemisorption. In addition, rarely if ever, is the number of active sites on a catalyst equal to more than a small fraction of the number of available surface metal atoms, determined by static chemisorption [18]. Therefore, the estimation of active sites is more exact using SSITKA measurements. The surface concentration of CH_4 intermediates (N_M) is related to the number of reaction sites producing methane.

N_M, because it relates to the number of actual reaction intermediates, can be used to calculate a more true value of the TOF than that normally calculated using chemisorption. However, in this paper, since our interest is on comparing chemisorption at room temperature vs. reaction temperature, we will focus on N_T, the total concentration of adsorption species on the surface. The total amounts of chemisorption species under reaction (methanation) conditions (N_T) are the sum of N_M plus the surface concentration of CO reversibly adsorbing and desorbing (N_{CO}). It should be noted that SSITKA is performed at steady-state reaction conditions. However, static chemisorption is carried out usually for a metal catalyst after preparation and reduction. Therefore, one should keep in mind that the results from SSITKA measurements are after reaching steady-state reaction conditions, while the results for static chemisorption are for the catalyst in an initial state at 25–100^{o}C. This difference could affect the relationship between the

chemisorption results for SSITKA and for static chemisorption.

The purpose of this study was to compare a wide variety of results based on static chemisorption and SSITKA techniques for chemisorption uptakes close to room temperature (RT~100^{o}C) vs. at reaction temperatures, respectively. Use was made of results from the literature for Group VIII metal catalysts employed for CO hydrogenation where both adequate static chemisorption and SSITKA data were reported. The relationship of the results at static chemisorption and reaction conditions are completely discussed. It is shown how the use of SSITKA as a complementary characterization technique to static chemisorption, XRD, and TEM for Co catalysts can help in determining the availability of metal surface atoms in cases where SMSI, promoters, poisons, and surface blockage by carbon deposition may skew understanding.

4.2 Methodology

4.2.1 Catalysts

Although static chemisorption and SSITKA have been widely applied in methanation studies for Group VIII catalysts, their measurements can only be compared when the data from both techniques are available in a given study. Many previous reports would be appropriate to be listed in this study but for the lack of comparable data, due to missing static chemisorption data [6,19–22], different conditions for reaction and SSITKA measurements [23], an isotopic transient method being used that is somewhat different from SSITKA [24] or because of a different isotope being traced [25]. Surprisingly, Ni catalysts are not able to be discussed in this paper because of insufficient comparable data

[6,21,25]. A list of Co, Fe, Ru, Rh, and Pt catalyst studies in the literature containing sufficient chemisorption and SSITKA results for comparison is given in Table 4.1. All papers listed in Table 4.1 reported SSITKA studies under CO hydrogenation conditions and also provided H_2 and/or CO static chemisorption data. As shown in Table 4.1, the catalysts compared here utilized various supports (Al_2O_3, TiO_2, SiO_2, MCM-41, and carbon) and were often promoted with such species as Zr, Re, La, Ru, Cu, Mn, V, or alkali. All catalysts were prepared by incipient wetness impregnation except for the Fe catalysts, which were prepared by a pH precipitation method.

Table 4.1 Catalyst compositions and nomenclature.

Catalyst nomenclature for this paper	Original nomenclature	Primary metal (wt%)	Additive	Support	Reference
Co1	Co/Al	Co(20)	-	Al_2O_3	[30]
Co2	Co/Al-Zr-11	Co(20)	ZrO_2: 10.8 wt%	Al_2O_3	″
Co3	12Co/γ-Al_2O_3	Co(12)	-	γ-Al_2O_3	[31]
Co4	12Co0.5Re/γ-Al_2O_3	Co(12)	Re: 0.5 wt%	γ-Al_2O_3	″
Co5	20Co0.5Re/γ-Al_2O_3	Co(20)	Re: 0.5 wt%	γ-Al_2O_3	″
Co6	20Co0.5Re/α-Al_2O_3	Co(20)	Re: 0.5 wt%	α-Al_2O_3	″
Co7	12Co/TiO_2	Co(12)	-	TiO_2	″
Co8	12Co0.5Re/TiO_2	Co(12)	Re: 0.5 wt%	TiO_2	″
Co9	12Co/SiO_2	Co(12)	-	SiO_2	″
Co10	12Co0.5Re/SiO_2	Co(12)	Re: 0.5 wt%	SiO_2	″
Co11	B-La0	Co(20)	La/Co = 0 (atomic ratio)	SiO_2	[1]
Co12	B-La10	Co(20)	La/Co = 0.1	SiO_2	″
Co13	B-La30	Co(20)	La/Co = 0.3	SiO_2	″
Co14	B-La75	Co(20)	La/Co = 0.75	SiO_2	″
Co15 [a]	Ru-promoted Co/Al_2O_3	Co(20)	Ru: 0.5 wt%	γ-Al_2O_3	[2]
Co16 [a]	″	Co(20)	Ru: 0.5 wt%	γ-Al_2O_3	″
Co17 [a]	″	Co(20)	Ru: 0.5 wt%	γ-Al_2O_3	″
Co18	5CoRu/M1	Co(5)	Ru: 0.5 wt%	MCM-41 [b]	[36]
Co19	8CoRu/M1	Co(8)	Ru: 0.5 wt%	MCM-41 [b]	″
Co20	14CoRu/M1	Co(14)	Ru: 0.5 wt%	MCM-41 [b]	″
Co21	14CoRu/M2	Co(14)	Ru: 0.5 wt%	MCM-41 [c]	″
Co22	14CoRu/S	Co(14)	Ru: 0.5 wt%	SiO_2	″
Co23	5CoRu/S	Co(5)	Ru: 0.5 wt%	SiO_2	[5]
Co24	Co/Ru/TiO_2	Co(12.04)	Ru:0.18 wt%	TiO_2	[26]
Co25	Co/SiO_2	Co(23)	-	SiO_2	[27]
Co26	Co/Al	Co(20)	-	γ-Al_2O_3	[28]
Co27	Co/Ru/Al	Co(20)	Ru: 0.5 wt%	γ-Al_2O_3	″
Fe1	P9	Fe(20)	Cu: 5 wt%, K: 4.2 wt%	SiO_2	[33]
Fe2	100Fe	Fe(100)	-	-	[4]
Fe3	95Fe5Cr	Fe(95)	Cr: 5 wt%	-	″
Fe4	80Fe20Mn	Fe(80)	Mn: 20wt %	-	″
Fe5	90Fe10Zr	Fe(90)	Zr: 10wt %	-	″
Fe6	100Fe2.5K	-	K/Fe = 0.015 (atomic ratio)	-	[3]
Fe7	FeMn	-	Mn/Fe = 0.20	-	″
Fe8	FeMn4K	-	Mn/Fe = 0.20, K/FeMn = 4	-	″
Fe9	10wt%Fe/γ-Al_2O_3	Fe(10)	-	γ-Al_2O_3	[32]
Ru1	RuSCu00	Ru(3)	Cu/Ru = 0 (atomic ratio)	SiO_2	[11, 34]
Ru2	RuSCu05	Ru(3)	Cu/Ru = 0.05	SiO_2	[34]
Ru3	RuSCu10	Ru(3)	Cu/Ru = 0.10	SiO_2	″
Ru4	RuSCu20	Ru(3)	Cu/Ru = 0.20	SiO_2	″
Ru5	RuSCu50	Ru(3)	Cu/Ru = 0.50	SiO_2	″
Pt1	K Pt.0	Pt(4.5)	K^+/Pt = 0.1(atomic ratio)	SiO_2	[35]
Pt2	K Pt.1	Pt(4.5)	K^+/Pt = 0.2	SiO_2	″
Pt3	00K/Pt	Pt(20)	K^+/Pt = 0	C	[12]
Pt4	20K/Pt	Pt(20)	K^+/Pt = 0.2	C	″
Pt5	40K/Pt	Pt(20)	K^+/Pt = 0.4	C	″
Pt6	80K/Pt	Pt(20)	K^+/Pt = 0.8	C	″
Rh1	Rh/SiO_2	Rh(1.5)	-	SiO_2	[13]
Rh2	Rh/V/SiO_2	Rh(1.5)	V: 1.5 wt%	SiO_2	″
Rh3	Rh/Al_2O_3	Rh(5.2)	-	γ-Al_2O_3	[37-38]
Rh4	Rh/MgO	Rh(2.5)	-	MgO	[39]

[a] Co15: calcined at 300°C; Co16: calcined at 350°C; Co17: calcined at 400°C

[b] MCM-41 with small pores.

[c] MCM-41 with large pores.

4.2.2 SSITKA measurement during methanation

The FTS catalysts are usually investigated by SSITKA under methanation conditions (high H_2/CO ratios, > 2) due to simplicity of product analysis and less deactivation with TOS (time-on-stream). Methanation on Co, Ru, Fe, Rh, and Pt catalysts has been extensively studied by SSITKA [1–5,11–13,26–39].

SSITKA systems utilized to carry out reaction and isotopic analyses typically consist of a plug flow reactor (PFR) using small amounts of catalysts under differential conditions (i.e., for conversions often lower than 5–10%) to minimize the effects of heat and mass transfer and to simplify kinetic analysis. No significant readsorption occurs for methanation, suggesting that there is no effect of conversion, provided it is kept in the differential range. The general procedure for isotopic transient measurements of methane and CO during reaction involves a switch between input flows of ^{12}CO/Ar and ^{13}CO without disturbing the stability of the reaction. The purpose of adding a trace of Ar (5%) to CO is to determine the gas phase holdup time innate to the experimental system. The pressure on both feed streams is maintained by back-pressure regulators to a constant value in order to minimize disturbances during switching of the feed streams. The effluent gas is monitored online by GC, for reaction rate and product distribution, and a mass spectrometer (MS) with a high-speed acquisition system for the isotopic transients. Information about the calculation of the surface residence times and the concentration of active surface intermediates has been given in detail elsewhere [18,29,40].

The methanation conditions applied in SSITKA are typically the same as for CO hydrogenation in general except that the ratio of H_2 to CO and the temperature are

usually higher. This shifts the product distribution to CH_4 as the primary product, which simplifies the mass spectrometric (MS) online isotopic analysis during SSITKA. Table 4.2 summarizes the methanation conditions utilized by the studies discussed in this paper. Except for the Pt catalysts, most catalysts were investigated under a total pressure of 1.0–1.8 atm and for a temperature range of 180–300^{o}C, with a H_2/CO ratio of 2–20. Methanation on Pt was studied at 2.56 atm and 392^{o}C with H_2/CO = 20. Such a high temperature is required due to the low activity of Pt for CO hydrogenation.

Table 4.2 Methanation conditions for SSITKA measurements on the catalysts reported in this paper.

FTS catalysts	Reaction temp. (^{o}C)	Pressure (atm)	H_2/CO ratio	References
Co	202-225	1.18-1.82	2-15	[1-2, 5, 26-28, 30-31, 36]
Fe	265-280	1.00-1.80	9-20	[3-4, 32-33]
Ru	240-270	1.80	5-20	[11, 34]
Pt	392	2.56	12	[12, 35]
Rh	180-300	1.00-1.80	9-20	[13, 37-39]

4.2.3 Static chemisorption measurements at 25–100^{o}C

H_2 or CO static chemisorption was performed typically at 25 or 100^{o}C. The catalysts were generally reduced in a hydrogen flow at a specific temperature (usually the same as the reduction temperature applied in the reaction study) prior to chemisorption measurements. Particle sizes and active metal dispersion were calculated based on the assumption of a stoichiometry between chemisorbed gas molecules and surface metal atoms, typically 1:1 for both CO/M_s and H/M_s when M_s is a surface metal atom. The representative static chemisorption quantity used (total vs. irreversible) varied with

different metals, depending on what has been established in the literature by the best correlation with physical techniques, such as TEM. For example, total chemisorption uptake is employed for the estimations of metal dispersion for Co, Fe, Pt, and Rh catalysts. Valid estimations for Ru catalysts, however, can only be obtained by using irreversible chemisorption uptake.

4.2.4 Nomenclature

The nomenclature for the static chemisorption and SSITKA parameters in this study is as follows. N_{CO}^{*} and N_{M}^{*} represent the concentration of adsorbed CO and methane intermediates, respectively, on the surface under reaction conditions as measured by SSITKA (identified by "*"). Note that the concentration of hydrogen atoms on the surface during reaction, unlike C-containing species, cannot be measured by SSITKA accurately due to the isotope effect. However, it is well known that during CO hydrogenation, most of the metal surface is covered by CO and CH_x species since little free hydrogen exists in the presence of CO due to competitive adsorption by CO [10], although it is possible that for some catalyst systems or at very particular reaction conditions, this may not be true. N_{T}^{*} represents the total amount of species adsorbed on the surface in terms of carbon atoms from SSITKA measurements ($N_{T}^{*} = N_{CO}^{*} + N_{M}^{*}$). N_H and N_{CO} give the amounts of uptake from static H_2 and CO chemisorption, respectively. N_{chem} is a general term for the uptake from chemisorption and can stand for either N_H or N_{CO} depending on whether H_2 or CO chemisorption was measured.

The nomenclature for the catalysts has been changed from the original references for

an easier comparison in this paper. All catalysts are renamed in Table 4.1 in the form of ‘‘main metal + number’’. For example, Co1 represents a Co catalyst, the first in the list of Co based catalysts, consisting of 20 wt% Co/Al_2O_3 which had an original nomenclature of Co/Al, reported in Ref. [30].

4.3 Results and discussion

4.3.1 General

The adsorption of CO and H_2 on several metal catalysts during CO hydrogenation has been widely investigated [41,42]. It was found that at FTS conditions, most hydrogen chemisorption is reversible. The rate of hydrogen desorption is relatively faster than the rate of hydrogen adsorption. Chemisorption of CO is much stronger than that of hydrogen at FTS conditions [10], and thus, the surface is primarily covered by CO and hydrocarbon intermediates, and the coverage by hydrogen is very low as indicated in the previous section.

Thermodynamics, kinetics of the given reaction, and reaction/chemisorption conditions determine whether the amount of chemisorbed species measured by static chemisorption is similar to that detected by SSITKA. Thus, it has to be anticipated that measurements could be different from static chemisorption for SSITKA of a particular reaction or at particular reaction conditions. Surface coverage of adsorbed species calculated from static chemisorption results could possibly be different from that determined by SSITKA simply due to differences in the temperature of measurement. Several major factors affecting surface coverage on metals will be discussed later.

The ratio N_T^*/N_{chem} can be an indication of any such differences in the measurements. Before discussion of the results for the various metal catalysts, it is useful to list the possibilities for the ratio and the corresponding implications. These possibilities are as follows:

(a) $N_T^*/N_{chem} \approx 1$

When N_{chem} has a similar value as N_T^*, there is a good possibility that:

- There is full surface coverage for T_{chem} - T_{SSITKA}.
- $N_{chem} \approx N_T^* \approx \Sigma N_i^* \approx N_{metal,s}$

where $N_{metal,s}$ = the number of exposed surface metal atoms. A valid calculation of metal dispersion and particle size can be obtained from either N_T^* or N_{chem}, provided there is no decoration of the metal surface by support/promoter species.

(b) $N_T^*/N_{chem} > 1$

A significantly smaller value of N_{chem} than N_T^* for a specific metal catalyst would most likely indicate difficulty in getting full surface metal atom coverage during chemisorption measurements, probably due to the temperature of chemisorption being too low for adequate kinetics of adsorption, especially with the use of automated chemisorption systems. The effect is particularly evident for catalysts with low metal loadings, low reducibilities, or strong metal–support interactions which can affect the chemisorption kinetics [10,43]. Much previous literature has focused on the fact that chemisorption properties of Group VIII metals can be dramatically altered by reducible

metal oxide supports, such as TiO_2 [9,44]. For example, the suppression of H_2 and CO chemisorption in metal/TiO_2 systems is typically caused by site blockage due to the TiO_x overlayers formed during high-temperature reduction [45]. The dispersed metal particles may also agglomerate or sinter at higher reduction temperatures resulting in a decreased chemisorption [46], although this should be the case for both static chemisorption and SSITKA measurements, provided the same catalyst reduction temperature is used.

(c) $N_T^*/N_{chem} < 1$

When $N_{chem} > N_T^*$, there could be a number of possible reasons. The first relates to the phenomenon of H_2 spillover. The term spillover, in heterogeneous catalysis, is used to describe the transport of chemisorption species from the primary adsorption sites on one phase to those on another of the catalyst which essentially do not adsorb these species directly at the given conditions [47]. It is known that the contribution of H2 spillover is hard to quantify and can be altered markedly in the presence of impurities, especially water and carbon-containing species [48]. H_2 spillover is more likely to happen at a higher H_2 pressure or a higher temperature. The simplest way to determine the existence of H_2 spillover is to calculate the hydrogen-to-metal surface atom ratio ($N_H/N_{metal,s}$), where $N_{metal,s}$ is determined by a physical method like TEM or XRD. The $N_H/N_{metal,s}$ ratio should be larger than unity when spillover occurs [49].

A second explanation for $N_{chem} > N_T^*$ could be the effect of chemisorption equilibrium resulting in lower surface coverage ($\theta < 1$) of adsorbed species at the higher temperature used for reaction.

A third possibility could be that the number of active sites of the catalyst is reduced by carbon deposition/coke formation under reaction conditions. Carbonaceous deposits may accumulate significantly (e.g., in the order of 15 wt% of the catalyst) and accordingly deactivate the catalyst either by blocking pores or by covering active reaction/adsorption sites [50,51]. For instance, Ni catalysts have been found to be very active for dry reforming of methane with CO_2 [52,53] and for direct cracking of methane to hydrogen [54]. However, Ni catalysts deactivate quickly due to coking. Mechanisms of carbon deposition and coke formation on metal catalysts have been studied extensively [55,56].

Finally, changes in the physical/chemical makeup of the catalyst could occur at reaction conditions resulting in a loss of active metal sites. Some changes include sintering and solid-state transformation. Sintering causes the loss of active surface via structural modification or coalescence of small metal crystalline into larger ones. Solid-state transformation at higher reaction temperatures results in the formation of different crystalline phases which may result in significant changes in chemisorption and catalytic activity. Experimental observations have shown that sintering and solid-state transformation rates of supported metal catalysts can be significantly affected by the temperature [50]. Obviously, some such changes could also occur during standard reduction in the catalyst. If so, the effect should be seen in both static chemisorption and SSITKA measurements.

(d) Other issues

There are two more points that need to be addressed before any comparison. Firstly, the N_T^*/N_{chem} ratio would be affected by the stoichiometry of adsorption for the active reaction intermediates. For example, the assumption of H/M_s or CO/M_s = 1:1 is typical for H_2/CO chemisorption. However, the active intermediate, CH_x or CO, measured by SSITKA at reaction temperature may not occupy a single metal surface atom as a site. If so, then the ratio of N_T^*/N_{chem} would not be unity (i.e., N_T^* having a value very similar to that of N_{chem}) even if the surface was to be completely covered with adsorbed species.

Secondly, the comparison attempted in this study is also valid only if the active reaction intermediates are formed/adsorbed only on the metal surface, which is true for the methanation reaction discussed in this study. If readsorption of reaction intermediates/products can take place on non-metal sites, such readsorption must be accounted for before a comparison can be made [57,58]. If bifunctional catalysis takes place, a comparison with static chemisorption would not be correct.

4.3.2 Co catalysts

Table 4.3 gives the comparison of static chemisorption (H_2 chemisorption at 100°C) and SSITKA (at reaction temperature) results for Co catalysts [1,2,5,26–28,30,31,36]. The ratio N_T^*/N_{chem} for all these Co catalysts varied between 0.61 and 1.83. Most of the catalysts had values that fluctuated within the smaller range of 0.9–1.1. In other words, for most Co catalysts, the value of N_T^*/N_{chem} was close to unity. Let us now address why all Co catalysts do not give such an ideal result. Higher ratios were observed for some specific supports. For example, suppression of H_2 chemisorption due probably to strong

interaction of the metal with the support has been suggested to explain the low hydrogen uptakes for TiO_2-and small pore MCM-41-supported Co catalysts (Co7–Co8 and Co18–Co20) [31,36]. TiO_2 is a well-studied support where strong metal support interaction has been observed [45,59]. The migration of partially reduced TiO_2 species onto the metal surface has been proposed to cause the suppression of chemisorption in part by a physical blockage of active surface sites. This suppression/blockage would seem to cause also a decrease in the surface concentration of intermediates measured by SSITKA since Ti^{3+} cations can be produced by reduction as low as 200°C [45]. Therefore, ratios of N_T^*/N_{chem} having values of 1.2–1.3 for Co7 and Co8 are not surprising, although the reduction temperature was only 350°C. The effect was even more significant for small pore MCM-41-supported catalysts (Co18, Co19, and Co20), giving values of N_T^*/N_{chem} of 1.36–1.83.

The values of N_T^*/N_{chem} for Co catalysts appear to be able to be decreased by specific promoters. For example, the value gradually decreased as the amount of La promotion increased (Co11–Co14) for La/Co = 0–0.75. However, the ratios still remained relatively close to unity (0.75–1.25). Co15–17 and Co27 were all $Co/Ru/Al_2O_3$ with the same amounts of components (20 wt% Co and 0.5 wt% Ru). The effect of preparation could be a possible explanation for differences in the ratio seen because Co15–17 were calcined at 300, 350, and 400°C, respectively, while Co27 was calcined at 300°C. This might explain why Co15 had a closer value to Co27. The observed difference between these latter two catalysts may be explained by differences in reaction conditions (such as total flow rate).

Table 4.3 Chemisorption and SSITKA (methanation) results for Co catalysts.

Catalyst samples	Support	Additive	N_{chem} (μmol H/g cat.)	N_{CO}^{*}[e] (μmol/g cat.)	N_{M}^{*}[e] (μmol/g cat.)	N_{T}^{*}[e] (μmol/g cat.)	N_T^*/N_{chem}	References
Co1	Al_2O_3	-	59[a]	39	10	49	0.83	[30]
Co2	Al_2O_3	ZrO_2: 10.8 wt%	64[a]	41	17	58	0.91	″
Co3	γ-Al_2O_3	-	67[b]	32	9	41	0.61	[31]
Co4	γ-Al_2O_3	Re: 0.5 wt%	104[b]	67	20	87	0.84	″
Co5	γ-Al_2O_3	Re: 0.5 wt%	132[b]	79	30	109	0.83	″
Co6	α-Al_2O_3	Re: 0.5 wt%	63[b]	63	15	78	1.24	″
Co7	TiO_2	-	23[b]	22	8	30	1.30	″
Co8	TiO_2	Re: 0.5 wt%	24[b]	20	8	28	1.17	″
Co9	SiO_2	-	54[b]	31	10	41	0.76	″
Co10	SiO_2	Re: 0.5 wt%	59[b]	38	11	49	0.91	″
Co11	SiO_2	La/Co = 0 (atomic ratio)	225[c]	233	38	271	1.20	[1]
Co12	SiO_2	La/Co = 0.1	361[c]	292	119	411	1.14	″
Co13	SiO_2	La/Co = 0.3	450[c]	253	154	407	0.90	″
Co14	SiO_2	La/Co = 0.75	482[c]	214	153	367	0.76	″
Co15	γ-Al_2O_3	Ru: 0.5 wt%	330[c]	254	53	307	0.93	[2]
Co16	γ-Al_2O_3	Ru: 0.5 wt%	242[c]	227	41	268	1.11	″
Co17	γ-Al_2O_3	Ru: 0.5 wt%	176[c]	163	34	197	1.12	″
Co18	MCM-41	Ru: 0.5 wt%	49[a]	55	12	67	1.36	[36]
Co19	MCM-41	Ru: 0.5 wt%	55[a]	57	31	88	1.60	″
Co20	MCM-41	Ru: 0.5 wt%	59[a]	67	41	108	1.83	″
Co21	MCM-41	Ru: 0.5 wt%	116[a]	60	34	94	0.81	″
Co22	SiO_2	Ru: 0.5 wt%	93[a]	56	15	71	0.76	″
Co23	SiO_2	Ru: 0.5 wt%	36[a]	40	5	45	1.25	[5]
Co24	TiO_2	Ru: 0.18 wt%	61.8[a]	40	12	52	0.84	[26]
Co25	SiO_2	-	109[a]	60	18.5	78.5	0.72	[27]
Co26	γ-Al_2O_3	-	95[d]	49.2	10.4	59.6	0.63	[28]
Co27	γ-Al_2O_3	Ru: 0.5 wt%	285[d]	167	38	205	0.72	″

[a] Based on H_2 chemisorption at 100°C. Max error = ±5%.
[b] Based on H_2 chemisorption at 40°C. Max error = ±5%.
[c] Based on H_2 chemisorption at 40°C. Max error = ±10%.
[d] Based on H_2 chemisorption at ambient temperature. Max error = ±10%.
[e] $N_T^* = N_{CO}^* + N_M^*$. N_{CO}^* and N_M^* were the concentrations of adsorbed CO and surface intermediates, respectively, measured by SSITKA.

4.3.3 Fe catalysts

A number of SSITKA studies have addressed for bulk Fe-based FTS catalysts (Table 4.4) [3,4,32,33]. It can be seen from Table 4.4 that values of N_T^* were only a small fraction of N_{chem} for most of the Fe catalysts. The N_T^*/N_{chem} ratios varied from 0.05–0.86. A possible explanation for the small N_T^* for Fe1 could be due to not including N_{CO}^* since it was not reported in the study [33]. However, this does not explain the results for Fe2–Fe9 where N_{CO}^* was reported. The small N_T^* amounts for Fe2–Fe9 may be explained by site blockage following carbon deposition (mainly in the form of inactive coke) at reaction temperature [3,4]. A larger N_T^*/N_{chem} could be observed for K-promoted Fe or FeMn catalysts (Fe6 and Fe8) compared to that for unpromoted ones (Fe2 and Fe7), suggesting that (1) K species may have covered part of surface Fe atoms which results in lower CO chemisorption and (2) the amount of carbon deposition in the form of χ-Fe_2C_5, which has been suggested to be the major Fe active carbide phase for FTS [60], increased with increasing K content. The presence of Fe-carbide appears to significantly increase N_T^* at reaction temperature.

Table 4.4 Chemisorption and SSITKA (methanation) results for Fe catalysts.

Technique		Static chemisorption	Static chemisorption	SSITKA	N_T^*/N_{chem} (N_{chem} = N_H or N_{CO})	References
Catalyst samples	Additive[c]	N_H (μmol H/g cat.)	N_{CO} (μmol CO/g cat.)	N_T^* (μmol/g cat.)		
Fe1	Cu: 5; K: 4.2	41.2[d]	-	2.0[g]	0.05	[33]
Fe1	Cu: 5; K: 4.2	4.5[d]	-	1.3[g]	0.29	″
Fe2	-	-	119[e]	25[h]	0.21	[4]
Fe3	Cr: 5	-	232[e]	35[h]	0.15	″
Fe4	Mn: 20	-	140[e]	35[h]	0.25	″
Fe5	Zr: 10	-	191[e]	35[h]	0.18	″
Fe6	K/Fe=0.015	-	91[e]	40[h]	0.44	[3]
Fe7	Mn/Fe=0.20	-	141[e]	33[h]	0.23	″
Fe8	Mn/Fe=0.20	-	108[e]	93[h]	0.86	″
Fe9[a]	K/FeMn=4	-	63[f]	9	0.14	[32]
Fe9[b]	-	-	63[f]	11	0.17	″

[a] Reaction temperature: 280°C.
[b] Reaction temperature: 265°C.
[c] The additive of Fe1, Fe3-Fe5 were listed based on wt%. The additive of Fe6-Fe9 were listed based on atomic ratio.
[d] Based on H_2 chemisorption at 35°C. Max error = ±5%.
[e] Based on CO chemisorption at 35°C. Max error = ±5%.
[f] Based on CO chemisorption at -196°C. Max error = ±5%.
[g] N_{CO}^* was not available in this paper for Fe1, so $N_T^* = N_M^*$ only.
[h] $N_T^* = N_{CO}^* + N_M^*$.

4.3.4 Ru catalysts

Table 4.5 shows the results of two studies of Ru catalysts – one with only non-decorated Ru (Ru1) [11] and the other with Cu-decorated Ru catalysts (Ru2–Ru5) [34]. For the Ru catalyst without Cu decoration (Ru1), N_T^* remained pretty much constant with reaction temperature (in the range 240–270^{o}C) for a given H_2 partial pressure. A similar behavior could be observed also for the TOS study. N_T^*/N_{chem} ratios remained at about 2 (1.71–2.21) for Ru1, depending on P_{H2} and P_{CO} during reaction. It is noted that N_M^* decreased with increasing H_2 partial pressure at a specific reaction temperature.

For Cu-decorated Ru catalysts (Ru2–Ru5), as can be seen from Table 4.5, Cu significantly blocked hydrogen chemisorption sites. H_2 chemisorption in Ref. [34] was carried out at -196^{o}C in order to estimate the number of Ru surface atoms and to exclude hydrogen spillover onto Cu which can occur during chemisorption at room temperature and thus affect the results. N_M^* was relatively constant for different H_2/CO ratios. The results suggest that the surface carbon intermediate coverage is largely independent of H_2 partial pressure in this temperature range. SSITKA results showed that N_{CO}^* went through a maximum with moderate Cu/Ru loading (i.e., moderate Cu coverage). This may be explained by a change in Ru surface structure as a result of Cu decoration. A larger N_T^*/N_{chem} ratio (>2) for Cu decorated compared with Cu-free Ru catalysts can be observed in Table 4.5. This probably was due to the Ru surface being blocked by Cu adatoms. While the amount of chemisorption measured by both techniques decreased accordingly, the effect appeared to be less significant at reaction temperature, probably due to some spillover onto the Cu surface atoms.

Based on the limited number of Ru catalysts studied, there appears to be some possibility to use SSITKA chemisorption measurements at reaction temperature for characterization provided (1) a stoichiometry of $N_T^*/N_{metal,s} = 2$ (since $N_H/N_{metal,s} = 1$ for Ru) and (2) no second inactive component (like Cu) is present that can receive spillover species.

Table 4.5 Chemisorption and SSITKA (methanation) results for Ru/SiO_2 catalysts.

Catalyst samples	Cu/Ru ratio (atomic ratio)	T_{chem}[a] (^oC)	N_{chem} (μmol H/g cat.)	T_{rxn}[b] (^oC)	P_{H2}[b,c] (bar)	N_{CO}^* (μmol/ g cat.)	N_M^* (μmol/ g cat.)	N_T^*[g] (μmol/ g cat.)	N_T^*/N_{chem}	References
Ru1	0	25	110[d]	240	0.18	237	4.4	241	2.19	[11]
Ru1	0	25	110[d]	250	0.18	217	5.0	222	2.02	″
Ru1	0	25	110[d]	260	0.18	227	3.8	231	2.10	″
Ru1	0	25	110[d]	270	0.18	202	4.8	207	1.88	″
Ru1	0	25	110[d]	240	0.72	202	5.3	207	1.88	″
Ru1	0	25	110[d]	250	0.72	189	8.3	197	1.79	″
Ru1	0	25	110[d]	260	0.72	194	11.2	205	1.87	″
Ru1	0	25	110[d]	270	0.72	180	13.8	194	1.76	″
Ru1	0	25	110[d]	270[f]	0.45	205	11.6	217	1.97	″
Ru1	0	25	110[d]	270[f]	0.45	184	9.8	194	1.76	″
Ru1	0	25	110[d]	270[f]	0.45	195	8.9	204	1.85	″
Ru1	0	25	110[d]	270[f]	0.45	189	9.0	198	1.80	″
Ru1	0	-196	112.8[e]	240	0.18	241	7.9	249	2.21	[34]
Ru1	0	-196	112.8[e]	240	0.37	207	7.7	215	1.90	″
Ru1	0	-196	112.8[e]	240	0.55	183	9.8	193	1.71	″
Ru2	0.05	-196	96.4[e]	240	0.18	260	8.4	268	2.78	″
Ru3	0.10	-196	60.4[e]	240	0.18	293	7.8	301	4.98	″
Ru4	0.20	-196	39.0[e]	240	0.18	238	5.9	244	6.25	″
Ru5	0.50	-196	23.0[e]	240	0.18	198	3.6	202	8.77	″
Ru2	0.05	-196	96.4[e]	240	0.37	239	9.6	249	2.56	″
Ru3	0.10	-196	60.4[e]	240	0.37	245	7.2	252	4.18	″
Ru4	0.20	-196	39.0[e]	240	0.37	224	6.9	231	5.92	″
Ru5	0.50	-196	23.0[e]	240	0.37	198	3.8	202	8.77	″
Ru2	0.05	-196	96.4[e]	240	0.55	228	10.6	239	2.48	″
Ru3	0.10	-196	60.4[e]	240	0.55	250	8.5	259	4.28	″
Ru4	0.20	-196	39.0[e]	240	0.55	169	5.5	175	4.47	″
Ru5	0.50	-196	23.0[e]	240	0.55	188	2.4	190	8.28	″

[a] At chemisorption conditions.
[b] At reaction conditions.
[c] P_{CO} was fixed at 0.036 bar.
[d] Based on H_2 chemisorption at room temperature. Max error = ±5%.
[e] Based on H_2 chemisorption at -196^{o}C. Max error = ±5%.
[f] The results at 270^{o}C were obtained TOS (5, 25, 50, 77 min).
[g] $N_T^* = N_{CO}^* + N_M^*$.

4.3.5 Pt catalysts

Table 4.6 shows that N_T^*/N_{chem} ratios for unpromoted and K^+-promoted Pt catalysts were less than 1 regardless whether the support used was SiO_2 or C [12,35]. Catalysts containing K^+ would be expected to have some of their Pt surface atoms blocked by the promoter for both chemisorbing H_2/CO and reaction intermediates. Therefore, this is probably not the cause for the low N_T^*/N_{chem} ratios. Rather, it is likely that lower values of N_T^* at the very high reaction temperature (392°C) required for methanation on Pt due to lower coverage caused the N_T^*/N_{chem} ratio to be significantly < 1.

Table 4.6 Chemisorption and SSITKA (methanation) results for Pt catalysts.

Catalyst samples	K^+/Pt (atomic ratio)	Support	TOS (min)	N_{chem} (μmol / g cat.)	N_{CO}^{*c} (μmol/ g cat.)	N_M^{*c} (μmol/ g cat.)	N_T^{*c} (μmol/ g cat.)	N_T^*/N_{chem}	References
Pt1	0.1	SiO_2	5	55.4[a]	20	0.5	20.5	0.37	[35]
	″	″	90	55.4[a]	20	0.22	20.2	0.36	″
Pt2	0.2	SiO_2	5	55.4[a]	16	0.38	16.4	0.30	″
	″	″	90	55.4[a]	16	0.14	16.1	0.29	″
Pt3	0	C	5	278[b]	30	0.37	30.4	0.11	[12]
Pt4	0.2	C	5	264[b]	29	0.31	29.3	0.11	″
Pt5	0.4	C	5	252[b]	30	0.25	30.3	0.12	″
Pt6	0.8	C	5	177[b]	32	0.20	32.2	0.18	″

[a] Based on CO chemisorption at room temperature, in μmol CO/g cat. Max error = ±5%.
[b] Based on H_2 chemisorption at 35°C, in μmol H/g cat. Max error = ±5%.
[c] $N_T^* = N_{CO}^* + N_M^*$.

4.3.6 Rh catalysts

Rh/SiO_2 catalysts with and without V addition (Rh1 and Rh2) were investigated under methanation conditions by SSITKA [13]. It can be seen from Table 4.7 that the N_T^*/N_{chem} ratio was almost unity without V promotion (Rh1). However, with the addition of V (Rh2), the high values of N_T^*/N_{chem} (8–24.5) were due to the low H_2 chemisorption uptake at chemisorption conditions. The H_2 chemisorption results show clearly that H_2 adsorption was seriously suppressed at room temperature with the addition of V as has been shown [13,61]. For $Rh/V/SiO_2$ (Rh2), N_M^* and N_{CO}^* decreased as the reduction temperature increased, suggesting that the Rh surface as partially covered by VO_x species, which has been suggested to be a possible cause also for H2 chemisorption suppression.

Investigations of Rh/Al_2O_3 (Rh3) and Rh/MgO (Rh4) have also been carried out under methanation conditions by Efstathiou and Bennett [37,38] and Efstathiou [39]. Rh4 had values of N_T^*/N_{chem} similar to that for Rh/SiO_2 (Rh1), 1.1–1.2 compared to 1.0–1.1, respectively. Although Rh/Al_2O_3 (Rh3) had values of N_T^*/N_{chem} somewhat smaller than those of Rh/SiO_2 (Rh1) and Rh/MgO (Rh4), all of these non-promoted Rh catalysts had values in the range of ca. 0.6–1.2. It is possible that some of the differences in the ratios for Rh/Al_2O_3 (Rh3) were either due to (1) differences in the isotopic tracing procedures used and/or (2) a partial blockage of some Rh sites by additional spectator surface molecules (such as formates) formed on the acid sites of alumina.

Based on the limited Rh data available, there does appear to be a possibility to characterize simple Rh catalysts such as Rh on a non-SMSI-inducing support like SiO_2, Al_2O_3, and MgO using SSITKA chemisorption results (with $N_T^*/N_{metal,s} = 1$). However,

one would need to be careful when promoters or strong support interactions are present.

Table 4.7 Chemisorption and SSITKA (methanation) results for Rh catalysts.

Catalysts	Promoter	Support	Reduction Temp. (°C)	N_{chem} [a] (μmol H/g cat.)	Reaction Temp. (°C)	N_{CO}^{*} [b] (μmol/ g cat.)	N_{M}^{*} (μmol/ g cat.)	N_{T}^{*} [c] (μmol/ g cat.)	N_{T}^{*}/N_{chem}	Ref.
Rh1	-	SiO_2	300	31.1	280	31.2	0.39	31.6	1.0	[13]
	″	″	600	31.1	280	32.6	0.38	32.9	1.1	″
Rh2	V: 1.5%	SiO_2	300	1.2	280	18.5	0.25	18.8	15.6	″
	″	″	400	0.6	280	14.5	0.17	14.7	24.5	″
	″	″	500	0.4	280	9.0	0.07	9.1	22.7	″
	″	″	600	0.3	280	2.3	0.01	2.3	7.7	″
Rh3	-	γ-Al_2O_3	350	60	220	36.6	2.4	39.0	0.65	[37-38]
	″	″	350	60	260	29.4	3.24	32.6	0.54	″
Rh4	-	MgO	350	30	260	32.1	0.18	32.3	1.08	[39]
	″	″	350	30	300	34.8	0.30	35.1	1.17	″

[a] Based on H_2 chemisorption at 35°C (Rh1 and Rh2) or 25°C (Rh3 and Rh4). Max. error = ±5%

[b] The data in ref. [13] was corrected by multiplying by 2 due to a calculation mistake made in the original paper.

[c] $N_T^* = N_{CO}^* + N_M^*$.

4.4 Conclusions

The relationships of the total amounts of chemisorbed species on Group VIII metal catalysts at reaction temperature {measured during CO hydrogenation by SSITKA (N_T^*)} and at 25–100°C {measured by static H_2 or CO chemisorption (N_{chem})} was systematically presented in this paper for Co, Fe, Pt, Ru, and Rh. Ideally, the ratio of N_T^*/N_{chem} should be close to unity if there is full coverage of the metal surface at both static chemisorption and reaction temperatures. However, N_T^*/N_{chem} can deviate from unity due to H_2 spillover, carbon deposition, formation of metal carbides, SMSI or other mechanisms causing active site blockage.

It is concluded based on data that Co catalysts routinely have close-to-unity values for N_T^*/N_{chem} for a wide variety of supports and promoters. Larger N_T^*/N_{chem} ratios, however, are typical for Ru catalysts, even when supported on SiO_2 without promoters. N_T^*/N_{chem} ratios close to one were observed for Rh/SiO_2 and Rh/MgO, but V promotion on Rh/SiO_2 increased this significantly because of H_2 chemisorption suppression during static chemisorption. Values much smaller than unity can be observed for both Fe and Pt catalysts. Site blockage by carbon deposition at reaction temperatures may be a possible explanation for low N_T^*/N_{chem} values observed for Fe-based catalysts. The low values of N_T^*/N_{chem} (due to low N_T^*) for Pt catalysts are probably due to the lower coverage at the high reaction temperature (392°C), necessary for methanation on Pt. Thus, Co is the best candidate for using chemisorption measured at reaction temperature by SSITKA for characterization. Both Ru and Rh look also like possibilities, provided care is taken to

avoid catalysts containing certain components, and, in the case of Ru, a stoichiometry of $N_T^*/N_{metal,s} = 2$ is used.

It has been stated that static chemisorption measurements at standard temperatures (25–100^{o}C) may not be representative of real active site concentrations under reaction conditions [18, 29]. SSITKA has been shown to measure such concentrations. However, it can also provide an alternative means for better understanding causes of chemisorption disruption at even static chemisorption conditions. For Co catalysts, especially, SSITKA can be applied as a complementary technique to static chemisorption, XRD line broadening, and TEM for better characterizing metal dispersion (availability of surface metal atoms) and metal particle size. Table 4.8 gives a comparison for hypothetical particle size measurements based on TEM, static chemisorption and SSITKA results for the same samples. When the results are consistent {(a) and (g)}, SSITKA results just confirm the other measurements. However, when the results are inconsistent with each other, SSITKA results provide a means to better ascertain the cause for the inconsistency. However, currently, such an application is limited to Co catalysts. More data is required for the other metals addressed before SSITKA can be used with confidence for metal dispersion characterization.

Table 4.8 Hypothetical Co average particle size results from different characterization techniques.

Technique	TEM	Static chemisorption	SSITKA	Probable Conclusions
Case (a)	small	small	small	Confirmation.
Case (b)	small	small	large	Low θ at reaction conditions due to surface blockage by coking/poisons or due to adsorption equilibrium at higher temperature.
Case (c)	small	large	small	"Suppression" of chemisorption at 25^{o}-100^{o}C due to slow kinetics.
Case (d)	large	small	small	Incorrect interpretations of TEM results are due to clustering of small metal particles or overlapping of a lot of particles in 3D that may appear as large particles in 2D.
Case (e)	small	large	large	Metal particles are small, but a lot of chemisorption blocked by support or promoter species decoration.
Case (f)	large	small	large	Overestimation of metal dispersion due to hydrogen spillover during static chemisorption.
Case (g)	large	large	large	Confirmation.

4.5 Acknowledgements

We acknowledge financial support from the US Department of Energy (Award No. DE-PS26-06NT43024).

4.6 References

[1] G.J. Haddad, B. Chen, J.G. Goodwin Jr., J. Catal. 161 (1996) 274.

[2] A.R. Belambe, R. Oukaci, J.G. Goodwin Jr., J. Catal. 166 (1997) 8.

[3] N. Lohitharn, J.G. Goodwin Jr., J. Catal. 260 (2008) 7.

[4] N. Lohitharn, J.G. Goodwin Jr., J. Catal. 257 (2008) 142.

[5] J. Panpranot, J.G. Goodwin Jr., A. Sayari, J. Catal. 213 (2003) 78.

[6] M. Agnelli, H.M. Swaan, C. Marquez-Alvarez, G.A. Martin, C. Mirodatos, J. Catal. 175 (1998) 117.

[7] M.A. Vannice, R.L. Garten, J. Catal. 56 (1979) 236.

[8] C.H. Bartholomew, R.B. Pannell, J.L. Butler, J. Catal. 65 (1980) 335.

[9] S.J. Tauster, S.C. Fung, R.L. Garten, J. Am. Chem. Soc. 100 (1978) 170.

[10] R.C. Reuel, C.H. Bartholomew, J. Catal. 85 (1984) 63.

[11] I.-G. Bajusz, J.G. Goodwin Jr., J. Catal. 169 (1997) 157.

[12] J.Z. Zhang, Y.-T. Tsai, K.L. Sangkaewwattana, J.G. Goodwin Jr., J. Catal. 280 (2011) 89.

[13] J. Gao, X. Mo, J.G. Goodwin Jr., Catal. Today 160 (2011) 44.

[14] J. Happel, Chem. Eng. Sci. 33 (1978) 1567.

[15] C.O. Bennett, ACS Symp. Ser. 178 (1982) 1.

[16] P. Biloen, J. Mol. Catal. 21 (1983) 17.
[17] M. Depontes, G.H. Yokomizo, A.T. Bell, J. Catal. 104 (1987) 147.

[18] J.G. Goodwin Jr., S. Kim, W.D. Rhodes, Catalysis 17 (2003) 320.

[19] D.M. Stockwell, J.S. Chung, C.O. Bennett, J. Catal. 112 (1988) 135.

[20] P. Biloen, J.N. Helle, F.G.A. van den Berg, W.M.H. Sachtler, J. Catal. 81 (1983) 450.

[21] D.M. Stockwell, C.O. Bennett, J. Catal. 110 (1988) 354.

[22] M. de Pontes, G.H. Yokomizo, A.T. Bell, J. Catal. 104 (1987) 147.

[23] F. Rohr, O.A. Lindvag, A. Holmen, E.A. Blekkan, Catal. Today 58 (2000) 247.

[24] K.R. Krishna, A.T. Bell, J. Catal. 130 (1991) 597.

[25] J. Barrault, A. Alouche, Appl. Catal. 58 (1990) 255.

[26] H.A.J. van Dijk, The Fischer–Tropsch synthesis: a mechanistic study using transient isotopic tracing, Ph.D. dissertation (Eindhoven University Press, Eindhoven, 2001).

[27] C.A. Mims, L.E. McCandlish, J. Phys. Chem. 91 (1987) 929.

[28] A. Kogelbauer, J.G. Goodwin Jr., R. Oukaci, J. Catal. 160 (1996) 125.

[29] S.L. Shannon, J.G. Goodwin Jr., Chem. Rev. 95 (1995) 677.

[30] B. Jongsomjit, J. Panpranot, J.G. Goodwin Jr., J. Catal. 215 (2003) 66.

[31] V. Froseth, S. Storsater, O. Borg, E.A. Blekkan, M. Ronning, A. Holmen, Appl. Catal. A – Gen. 289 (2005) 10.

[32] D.M. Stockwell, D. Bianchi, C.O. Bennett, J. Catal. 113 (1988) 13.

[33] K. Sudsakorn, J.G. Goodwin Jr., A.A. Adeyiga, J. Catal. 213 (2003) 204.

[34] B. Chen, J.G. Goodwin Jr., J. Catal. 158 (1996) 511.

[35] I.-G. Bajusz, D.J. Kwik, J.G. Goodwin Jr., Catal. Lett. 48 (1997) 151.

[36] J. Panpranot, J.G. Goodwin Jr., A. Sayari, J. Catal. 211 (2002) 530.

[37] A.M. Efstathiou, C.O. Bennett, J. Catal. 120 (1989) 118.
[38] A.M. Efstathiou, C.O. Bennett, J. Catal. 120 (1989) 137.

[39] A.M. Efstathiou, J. Mol. Catal. 67 (1991) 229.

[40] A.M. Efstathiou, X.E. Verykios, Appl. Catal. A – Gen. 151 (1997) 109.

[41] A.Y. Khodakov, B. Peregryn, A.S. Lermontov, J.-S. Girardon, S. Pietrzyk, Catal. Today 106 (2005) 132.

[42] P. Winslow, A.T. Bell, J. Catal. 94 (1985) 385.

[43] J.M. Zowtiak, C.H. Bartholomew, J. Catal. 83 (1983) 107.

[44] S.J. Tauster, S.C. Fung, J. Catal. 55 (1978) 29.

[45] R.T.K. Baker, S.J. Tauster, J.A. Dumesic (Eds.), Strong Metal–Support Interactions, American Chemical Society, Washington, DC, 1986.

[46] C.-M. Lu, Y.-M. Lin, I. Wang, Appl. Catal. A – Gen. 198 (2000) 223.

[47] V.V. Rozanov, O.V. Krylov, Russ. Chem. Rev. 66 (1997) 107.

[48] P.A. Sermon, G.C. Bond, Catal. Rev. 8 (1974) 211.

[49] A.D. Lueking, R.T. Yang, Appl. Catal. A – Gen. 265 (2004) 259.

[50] P. Forzatti, L. Lietti, Catal. Today 52 (1999) 165.

[51] C.H. Bartholomew, Appl. Catal. A – Gen. 212 (2001) 17.

[52] H.M. Swaan, V.C.H. Kroll, G.A. Martin, C. Mirodatos, Catal. Today 21 (1994) 571.

[53] G.-J. Kim, D.-S. Cho, K.-H. Kim, J. Kim, Catal. Lett. 28 (1994) 41.

[54] T. Zhang, M.D. Amiridis, Appl. Catal. A – Gen. 167 (1998) 161.

[55] C.H. Bartholomew, Catal. Rev. – Sci. Eng. 24 (1982) 67.

[56] S.B. Wang, G.Q.M. Lu, J. Chem. Technol. Biotechnol. 75 (2000) 589.

[57] S.H. Ali, J.G. Goodwin Jr., J. Catal. 171 (1997) 333.

[58] S.H. Ali, J.G. Goodwin Jr., J. Catal. 171 (1997) 339.

[59] R. Riva, H. Miessner, R. Vitali, G. Del Piero, Appl. Catal. A – Gen. 196 (2000) 111.

[60] J.W. Niemantsverdriet, A.M. van der Kraan, W.L. van Dijk, H.S. van der Baan, J. Phys. Chem. 84 (1980) 3363.

[61] J. Gao, X. Mo, A.C. Chien, W. Torres, J.G. Goodwin Jr., J. Catal. 262 (2009) 119.

CHAPTER FIVE

SYNERGY OF COMPONENTS IN CuZnO AND CuZnO/Al_2O_3 ON METHANOL SYNTHESIS: ANALYSIS AT THE SITE LEVEL BY SSITKA

In the present study, the effects of the individual components and an Al_2O_3 support on CuZnO for methanol (MeOH) synthesis were investigated for the first time using steady-state isotopic transient kinetic analysis (SSITKA). A fix-bed differential reactor was used at 250^{o}C and 1.8 atm. Surface reaction times for MeOH and dimethyl ether (DME) were corrected for readsorption. The presence of ZnO was found to decrease the hydrocarbon formation ability of Cu. By comparing the surface reaction parameters, it can be suggested that Cu/Al_2O_3 and ZnO/Al_2O_3 catalysts exhibit lower MeOH formation rates compared to CuZnO or CuZnO/Al_2O_3 due to both lower intrinsic "site" activities and lower concentrations of active surface intermediates (related to active sites). The synergy between Cu and ZnO, however, based on MeOH TOF_{ITK} (a measure of site activity for MeOH formation) was surprisingly less than an order-of-magnitude improvement.

5.1 Introduction

Copper-based catalysts are extensively applied in industrial reactions such as water-gas shift reaction [1], methanol reforming [2-4] and methanol synthesis [5-7]. CuZnO based catalysts, owing to their high commercial relevance for methanol synthesis, have received much attention in the past three decades [8-10]. Burch and Golunski [9], based on a study of adding different metal oxides (Al_2O_3, ZrO_2, Ga_2O_3 or ZnO) to Cu/SiO_2, concluded that there is a definite increase in reaction rate for MeOH synthesis per unit area copper after adding some of these components. The most apparent is the synergy between ZnO and Cu as also found in other studies [11]. The binary catalysts have been found to lead to several orders of magnitude higher activity than that of metallic Cu or pure ZnO [10]. Moreover, several studies have reported that the specific rate for methanol synthesis on CuZnO catalysts was significantly affected by the use of different supports or additives, which suggested that there is a synergy between Cu and ZnO [12-13]. Despite the main components being the same, many researchers have found that the properties of CuZnO-based catalysts can be greatly altered by the modification of surface acidity on a solid acid support, such as by adding sulfate to γ-Al_2O_3 [14-15] and MgO to HZSM-5 [16].

Mechanisms for methanol synthesis from syngas on CuZnO based catalysts have been proposed with regards to the nature of active sites and the valence of copper using several different models, such as: (i) Cu^+ in ZnO or dispersed on ZnO, (ii) Cu^0 supported on ZnO, and (iii) Cu-Zn alloy. It has been proposed by several groups that the active phase for methanol synthesis is the Cu^+ species dissolved in or supported on ZnO [11, 17-

21]. The function of the zinc component was suggested either to stabilize Cu^+ species or to form Cu^+/ZnO along with oxygen vacancies. Other groups have found a direct proportionality between the catalytic activity for methanol synthesis and metallic Cu surface area [22-25]. Microkinetic modeling was applied to support this point by using surface science measurements for Cu single crystal surfaces [26]. This microkinetic model study suggested that metallic Cu may be the active site for methanol synthesis, and the interaction between Cu and ZnO is crucial to help dynamic spreading of the Cu particles on the support. The formation of Cu-Zn alloy during reduction has also been proposed to result in active sites for methanol synthesis based on an observed increase in TOF with higher reducing conditions [27-29]. The formation of the proposed resulting surface alloy has been suggested to be reversible. That is, the surface alloy is destroyed upon increasing the oxidation potential, and such a process may cause the unique transient behavior observed in CuZnO catalysts [29-30].

Part of the controversy as to the mechanism originates from issues concerning the role of ZnO and the active sites for CuZnO based catalysts. It has been widely accepted that ZnO as a support results in higher Cu dispersion. The contentious issue is the effects of ZnO other than as the support. ZnO may affect the particle morphology of Cu, which could play an important role in the specific activity for methanol synthesis due to the structure sensitive nature of the reaction [23, 26, 29]. On the contrary, it has been reported that a physical mixture of metallic Cu and ZnO during reduction formed active sites for methanol synthesis [27, 31]. ZnO can be regarded as a reservoir for spillover

hydrogen, which by reverse spillover may increase hydrogenation of adsorbed intermediates on Cu sites [9, 32].

The application of the CuZnO system is sometimes limited by the essentially low catalytic activity. Various modifications, therefore, have been proposed such as addition of a suitable promoter [33-34] or introduction of an effective additional support [35-36]. Currently, industrial methanol synthesis is conducted at relatively low pressures (35-55 bar) and 200°-300°C over $CuZnO/Al_2O_3$ [8]. A large number of studies have been carried out to investigate the catalytic structure, the oxidation state of Cu and ZnO, the reaction mechanisms and the synergetic effect for CuZnO based catalysts [12-13, 18, 22-23, 29-30, 37]. However, limited information has been obtained regarding the number and activity of active sites using an in-situ technique.

The focus of this paper was to study in detail, using SSITKA (steady-state isotopic transient kinetic analysis) and Al_2O_3-supported Cu and ZnO, the synergy between the different components and the impact of an Al_2O_3 support on CuZnO catalysis. SSITKA is one of the most powerful in-situ kinetic techniques for analyzing surface reactions. It permits the accurate measurement of surface reaction parameters under reaction conditions [38-39]. In this study, surface residence times and concentrations of intermediates leading to methane, methanol (MeOH) and dimethyl-ether (DME) during CO hydrogenation and the time-on-stream (TOS) behavior were measured and are discussed. Such measurements carried out under reaction conditions can help us to better understand the causes of differences observed in catalytic behavior. Two main issues are addressed, therefore, in this paper using SSITKA: (1) the synergy between Cu and ZnO

for MeOH synthesis on CuZnO or CuZnO/Al_2O_3; and (2) the change in the surface parameters for MeOH synthesis for CuZnO catalysts upon using an Al_2O_3 support.

5.2 Experimental

5.2.1 Catalyst preparation

Copper nitrate trihydrate (Acros, 99%), zinc nitrate hexahydrate (Alfa Aesar, 99.998%), and Al_2O_3 (Alfa-Aesar, γ-phase, 99.98%) were used without further purification. CuZnO (Cu:ZnO = 2:1, by mass) was prepared by a precipitation method. In general, the desired amounts of aqueous copper nitrate and zinc nitrate solutions were mixed to produce 6 g of CuZnO. The mixture was then precipitated by Na_2CO_3 solution (Na_2CO_3: H_2O = 1:3) at room temperature, and the resulting solution mixture was left in a fume hood overnight. The mixture was filtered, washed 6 times with 1 L of hot (ca. 100^oC) deionized water, dried at 120^oC for 12h, and calcined in an oven at 350^oC in air for 4h. CuZnO/Al_2O_3 (CuZnO content = 20 wt%, with 13.3 wt% Cu and 6.7 wt% ZnO) was prepared by the incipient wetness impregnation method. Al_2O_3 as a support was impregnated with an aqueous solution of copper and zinc nitrate. After mixing and stirring, the mixture was dried at 90^oC for 4 h and then at 120^oC overnight before being calcined in air at 350^oC for 4 h (ramp rate to 350^oC of 10^oC/min) to remove nitrogen-containing species. Cu/Al_2O_3 and ZnO/Al_2O_3 were also prepared by the incipient wetness impregnation method similar to the procedure for preparing CuZnO/Al_2O_3 using aqueous solutions of copper or zinc nitrate (resulting Cu contents = 13.3 and 20 wt%; resulting ZnO contents = 6.7 and 20 wt%). 13.3Cu/Al_2O_3 and 20Cu/Al_2O_3 represent 13.3

and 20 wt% Cu/Al_2O_3 while $6.7ZnO/Al_2O_3$ and $20ZnO/Al_2O_3$ represent 6.7 and 20 wt% ZnO/Al_2O_3, respectively. Catalyst characterization, CO hydrogenation, and SSITKA were compared mainly using 20 wt% Cu/Al_2O_3 and 20 wt% ZnO/Al_2O_3 due to their higher activities. The comparisons of ($13.3Cu/Al_2O_3$ vs. $20Cu/Al_2O_3$) and ($6.7ZnO/Al_2O_3$ vs. $20ZnO/Al_2O_3$) using CO hydrogenation and SSITKA measurements (section 3.2 and 3.3) were made to exclude any differences due to catalyst loading.

5.2.2 Catalyst characterization

BET surface areas, pore volumes, and pore sizes were estimated using nitrogen adsorption at -196^{o}C in a Micromeritics ASAP-2020. Prior to measurements, the catalyst samples were degassed under a vacuum of 10^{-3} mm Hg at 150℃.

A Scintag XDS 2000 θ/θ powder X-ray diffractometer (XRD) using Cu Kα1/Kα2 (λ = 1.540592Å and 1.544390Å, respectively) radiation and a step size of 0.03^{o} was used to identify the phases and crystallinity of the catalysts.

HRTEM images were obtained to investigate the morphology of the catalysts in this study using a Hitachi 9500 with an accelerating voltage of 300kV. However, due to the difficulty of distinguishing the Cu particles and ZnO from the Al_2O_3 support, no information was able to be obtained and, therefore, the images are not shown.

5.2.3 CO hydrogenation

CO hydrogenation was performed in a differential fixed-bed reactor. A catalyst sample (1 g) was diluted with 2 g of α-alumina for the purpose of minimizing channeling and hot spots. The samples were loaded between quartz wool plugs in the middle of the

reactor and the temperature was observed by positioning a thermalcouple internally close to the catalyst bed. The catalyst was heated from room temperature to 300^{o}C with a ramp rate of 5^{o}C /min, maintained at that temperature for 1 h in a H_2 flow (30 ml/min) at 1 atm for reduction, and then cooled down to the reaction temperature of 250^{o}C. After reduction, reaction was started by switching the gas flow to a CO-H_2-He mixture (CO: 3 mL/min, H_2: 24 mL/min and He: 3 mL/min) at a constant pressure of 1.8 atm. A ratio of H_2/CO = 8 was used to minimize deactivation [40]. The reaction system lines and the sampling valves were kept at 200^{o}C with heating tape to avoid condensation of products. Blank runs with an empty reactor indicated no activity of the reaction system without a catalyst presented. The effluent samples were analyzed on-line using a Varian 3380 GC equipped with a Restek RT-QPLOT column (I.D. 0.53 mm and length 30 m) connected to a flame ionization detector (FID) for hydrocarbons and oxygenates detection, and with a Restek HayeSep® Q column (I.D. 3.18 mm and length 1.83 m) connected to a thermal conductivity detector (TCD) for CO and CO_2 detection. The reaction reached a pseudo-steady state after 15 h TOS (time-on-stream).

The identification and calibration of the products were accomplished using standard gases [alkanes (C_1-C_7), alkenes (C_2-C_7) and oxygenates (methanol, ethanol, 1-propanol, 1-butanol, acetaldehyde and acetone); Scott Specialty Gases]. In all reaction studies, the maximum conversion was kept below 5% to minimize concentration and temperature gradients. The carbon selectivity (in C atom%) for a certain product was calculated based on carbon efficiency using the formula $n_iC_i/\Sigma n_iC_i$, where n_i and C_i represent the carbon number and molar concentration of the ith product, respectively.

5.2.4 SSITKA

Surface reaction measurements were carried out in the reaction system adapted for SSITKA (Figure 5.1). SSITKA measurements were made by switching between 95% ^{12}CO + 5% Ar (National Specialty Gases) and ^{13}CO (Isotec, 99%) using a Valco 2-position valve with an electric actuator without disturbing any other reaction conditions (i.e., the reaction total flow rate and the total pressure for the two gas feed streams were maintained at constant values during the switch). The gas phase hold-up time was determined using the 5% Ar in the unlabelled ^{12}CO stream as an inert tracer. The effluent gas was analyzed on-line by GC (as described for CO hydrogenation) and a Pfeiffer mass spectrometer (MS) with a high-speed data acquisition system. Two back pressure regulators in the system were used to ensure a constant reaction pressure and to minimize any pressure disturbance during the switch. The reaction conditions were the same as for the regular CO hydrogenation studies. SSITKA measurements were taken after 5, 25, 45, 60, 90, 120, 180, 240, 300, and 360 min of reaction for every catalyst.

Readsorption effects on the kinetics parameters were estimated after steady-state reaction was achieved at 250^{o}C and 1.8 atm. The total flow rate of reactants was varied from 10 to 45 mL/min for partial pressures of CO and H_2 of 0.2 and 1.6 atm, respectively, permitting SSITKA measurements for different space times.

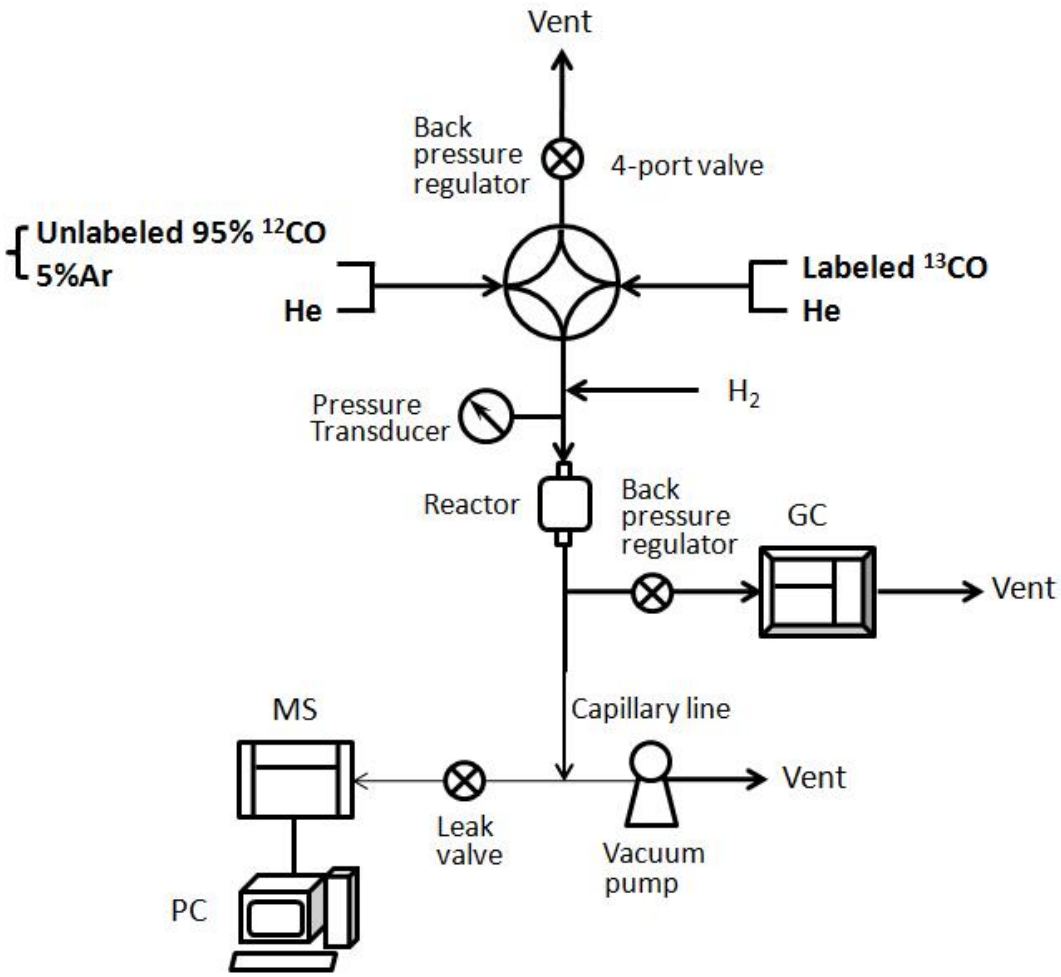

Figure 5.1 SSITKA reaction system for MeOH synthesis.

5.3 Results

5.3.1 Catalyst characterization

The BET surface areas, pore volumes and average pore sizes are shown in Table 5.1. Al_2O_3-supported catalysts exhibited a marked higher BET surface area as well as pore volume compared to unsupported CuZnO, as expected. The specific surface area and pore volume of $CuZnO/Al_2O_3$ were between those of $20Cu/Al_2O_3$ and $20ZnO/Al_2O_3$. It should be noted that the pore sizes for all catalysts were very similar.

Figure 5.2 shows the XRD patterns of the calcined catalysts. The diffraction peaks of CuO could be observed at $2\theta = 35.6^o$, 38.8^o and 48.9^o (JCPDS 80-1268) for all Cu containing catalysts. However, no discernible Cu metal or Cu_2O diffraction peak at $2\theta = 43.3^o$ and 41^o, respectively, could be observed for the calcined catalysts. The results are in agreement with those reported in the recent literature [41] that no Cu^+ or Cu^0 could be observed for CuZnO calcined at a relatively low temperature, ca. 500^oC. The diffraction peaks for CuO were larger for $20Cu/Al_2O_3$ and $CuZnO/Al_2O_3$ than for CuZnO, indicating a higher degree of crystallinity for CuO on the former two catalysts, even though the amount of Cu in CuZnO was greater. The average crystalline sizes of CuO in the calcined catalysts estimated by the Scherrer equation are shown in Table 5.1. CuO crystalline size was essentially the same for $CuZnO/Al_2O_3$ and CuZnO (within ± 10% experimental error). For catalysts containing ZnO, very weak diffraction peaks at $2\theta = 34.5^o$, 36.3^o could be observed, which can be assigned to ZnO. The crystalline size for ZnO could not be determined due to the weak diffraction peaks. This may be explained by high dispersion and the existence of X-ray amorphous ZnO (in the form of thin rafts or

small particles) in ZnO containing catalysts. There were also small and broad peaks visible at $2\theta = 31.3^{o}$, 36.9^{o}, 59.4^{o}, which could be due to the spinel $ZnAl_2O_4$. However, the compounds $CuAl_2O_4$ and $ZnAl_2O_4$ display nearly identical diffraction patterns, resulting in difficulty in identifying the XRD patterns for these individual compounds. Previous studies [41-42] have reported that the peaks should correspond to zinc aluminate due to bulk $CuAl_2O_4$ being thermodynamically unstable below $600^{o}C$ [41, 43] and the fact that copper aluminate forms above $900^{o}C$ [44]. However, the existence of some sort of meta-stable surface $CuAl_2O_4$ cannot be ruled out due to the presence of copper in these catalysts.

Table 5.1 Physicochemical properties of the various catalysts.

Catalyst[a]	BET S.A.[b] (m^2/g)	Pore volume[b] (cm^3/g)	Average pore size[b] (nm)	CuO crystallite size[c] (nm)
CuZnO	17.1	0.10	25.3	5.8
$CuZnO/Al_2O_3$	72.6	0.39	21.3	6.3
Cu/Al_2O_3	54.5	0.30	25.6	7.0
ZnO/Al_2O_3	88.4	0.48	21.8	-

[a] Al_2O_3-supported catalysts contained 20 wt% of Cu, ZnO or CuZnO (13.3 wt% Cu and 6.7 wt% ZnO).
[b] Max. error = ±5%.
[c] Non-reduced catalysts. Max. error = ±10%.

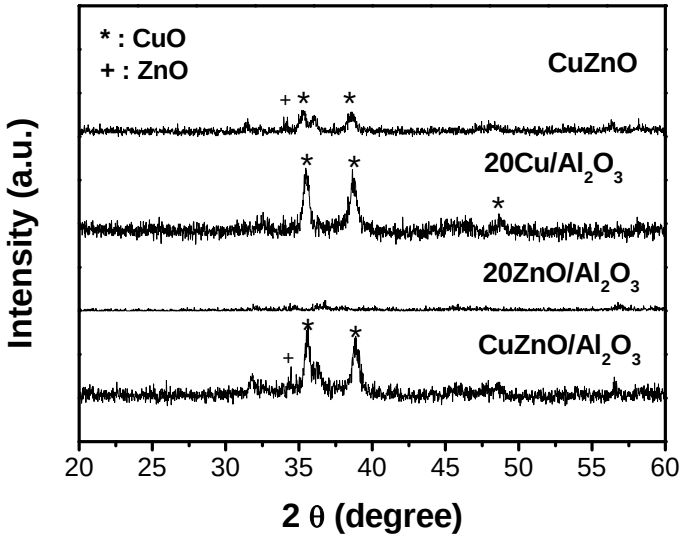

Figure 5.2 XRD patterns of the calcined catalysts.

5.3.2 CO hydrogenation

Figure 5.3 shows the time-on-stream behavior for the overall reaction rate for CO hydrogenation on the various catalysts. All the catalysts exhibited induction periods, reaching steady-state reaction after ca. 250 min except for the CuZnO catalyst which was essentially at steady-state after only 50 min of reaction. Similar induction behaviors for MeOH synthesis on CuZnO and Cu supported catalysts have been previously reported [45-46]. $CuZnO/Al_2O_3$ gave the highest overall steady-state reaction rate while ZnO/Al_2O_3 had the lowest. CuZnO had a much higher initial rate comparing to that of $CuZnO/Al_2O_3$; however, its rate steadily increased to a slightly higher value than that of CuZnO after about 200 min. It is noteworthy that $CuZnO/Al_2O_3$ contained only 20 wt% CuZnO. Therefore, if reactivity is compared on a CuZnO weight basis, the difference in

catalytic performance for the two catalysts would be even more significant. A comparison on CuZnO weight basis for these two catalysts will be discussed in a later section.

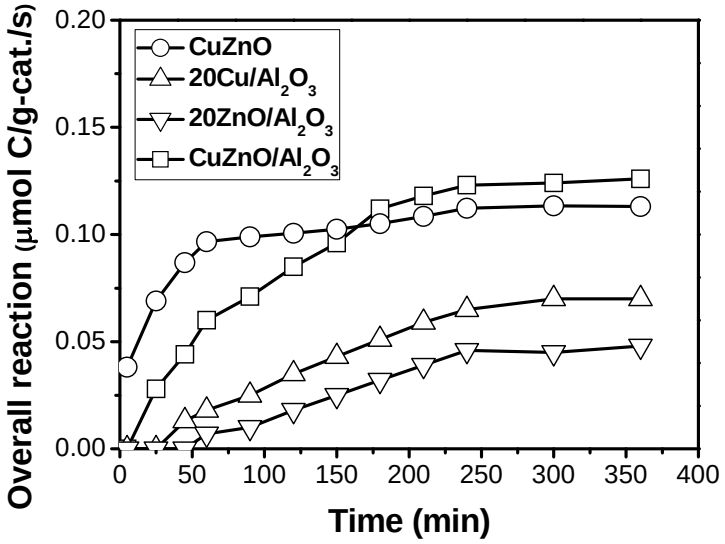

Figure 5.3 Overall reaction rate for CO hydrogenation vs. TOS.

Figure 5.4 and Figure 5.5 display the TOS behavior for the formation of MeOH and DME on the various catalysts. The formation of DME has been reported to occur due to dehydration of MeOH on acid sites on the Al_2O_3 support [47-48]. Therefore, the formation of MeOH and DME should be considered together for MeOH activity evaluation when the synthesis of MeOH occurs on catalysts with acidic supports, such as Al_2O_3 or SiO_2-Al_2O_3. It can be seen that obvious induction periods occurred for both MeOH and DME formation. CuZnO exhibited the highest rate for MeOH (as an effluent)

all the time since it formed no DME, as expected. $20Cu/Al_2O_3$ and $20ZnO/Al_2O_3$ had low but steadily increasing rates for both MeOH and DME formation but with different selectivities. The induction periods for $CuZnO/Al_2O_3$ were different for MeOH and DME. The formation rate of MeOH increased markedly and reached the highest value fast (less than 240 min). However, the formation rate of DME increased slowly and only reached steady-state after 300 min TOS.

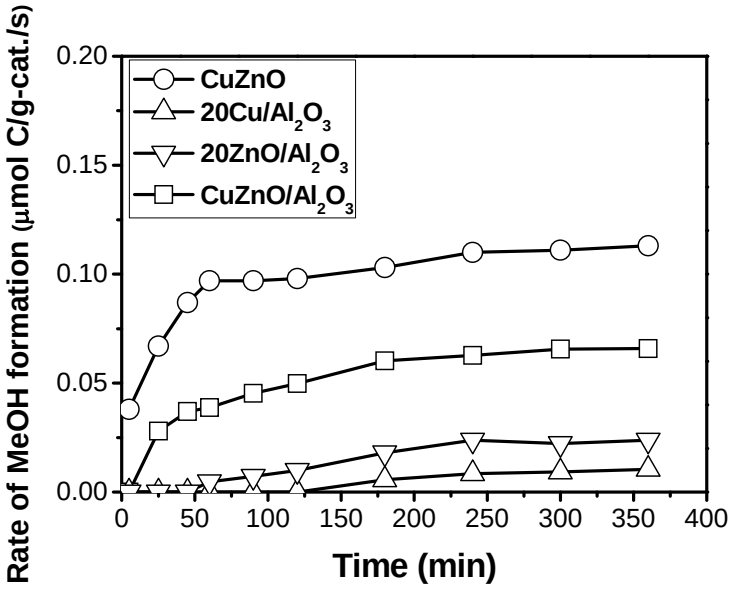

Figure 5.4 Rate of MeOH formation vs. TOS during CO hydrogenation.

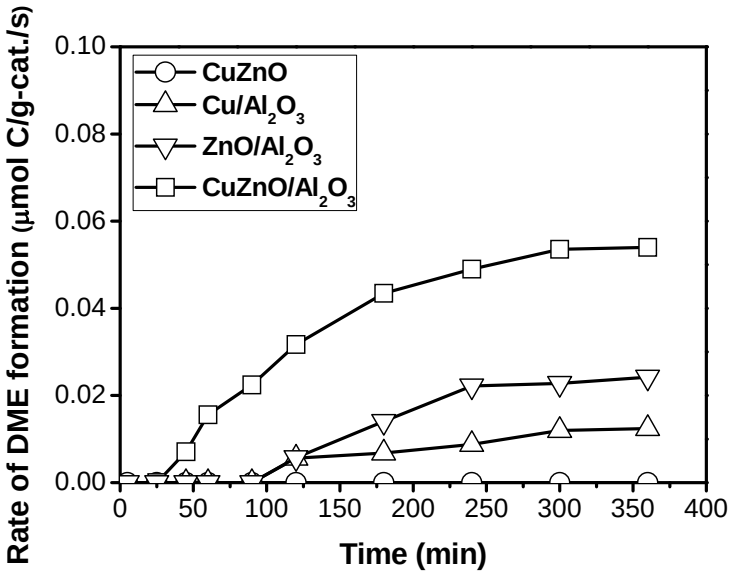

Figure 5.5 Rate of DME formation vs. TOS during CO hydrogenation.

Table 5.2 summarizes the results for CO hydrogenation on the catalysts at steady-state reaction conditions. The product for CuZnO was totally MeOH all the time while half of the MeOH produced was converted to DME on $CuZnO/Al_2O_3$ at steady-state. Both $20Cu/Al_2O_3$ and $20ZnO/Al_2O_3$ had relatively high selectivities for CH_4 during initial reaction (data not shown)- 100% and 32.8% for $20Cu/Al_2O_3$ and $20ZnO/Al_2O_3$, respectively. An induction period could be observed for CH_4 on $20Cu/Al_2O_3$ but not on $20ZnO/Al_2O_3$. At steady-state, there were still significant amounts of CH_4 formed (68.4%) on $20Cu/Al_2O_3$ but none on $20ZnO/Al_2O_3$. Therefore, the overall steady-state rate included CH_4 formation only for Cu/Al_2O_3. Only oxygenates were produced at steady state for all the catalysts except Cu/Al_2O_3. This increase in rate of the formation of oxygenates with TOS was not simply due to the conversion of the active sites which

produced methane to ones producing MeOH (and DME) since the overall CO hydrogenation rate increased at the same time. It should be noted that MeOH synthesis for 13.3Cu/Al_2O_3 and 6.7ZnO/Al_2O_3 were also carried out for the purpose of comparison to CuZnO/Al_2O_3, which contained 13.3 wt% Cu and 6.7 wt% ZnO. The product distributions for 13.3Cu/Al_2O_3 and 6.7ZnO/Al_2O_3 were very similar to those for 20Cu/Al_2O_3 and 20ZnO/Al_2O_3. The reaction rates of course were lower for 13.3Cu/Al_2O_3 and 6.7ZnO/Al_2O_3, but the lower rates were not proportional to the lower in loadings. This is not surprising because lower loadings usually lead to increased dispersions.

Table 5.2 Steady-state catalytic properties of the various catalysts for CO hydrogenation[a,b].

Catalyst	CO conversion (%)	Total steady -state rate (μmol C/g-cat./s)	Steady-state rate of specific products (μmol C/g-cat./s)			Steady-state selectivity of specific products (%C)[c]		
			CH_4	MeOH	DME	CH_4	MeOH	DME
CuZnO	0.59	0.113	-	0.113	-	-	100	-
CuZnO/Al_2O_3[d]	0.61	0.126	-	0.066	0.057	-	52.3	44.9
13.3Cu/Al_2O_3	0.30	0.059	0.042	0.007	0.010	71.1	12.4	16.5
20Cu/Al_2O_3	0.35	0.070	0.048	0.010	0.012	68.4	14.0	17.5
6.7ZnO/Al_2O_3	0.13	0.025	-	0.012	0.013		47.7	52.3
20ZnO/Al_2O_3	0.24	0.048	-	0.024	0.024	-	49.6	50.4

[a] Catalyst: 1g, inert (α-Al_2O_3): 2g. Reaction was carried out at 250°C; P_T = 1.8 atm, flow rate = 30 mL/min (H_2: He: CO = 8:1:1.). All reactions were carried out at differential conversions with % CO conversion < 5%. Max. error = ±5%.
[b] At steady-state (after 6 h reaction).
[c] Carbon selectivity = $n_iC_i/\Sigma n_iC_i$.
[d] 13.3 wt % Cu, 6.7 wt % ZnO.

5.3.3 SSITKA measurements

SSITKA was used to determine the surface concentrations and average reaction residence times of the active methane, MeOH and DME intermediates. Figure 5.6 shows a typical set of normalized transients obtained by switching from ^{12}CO to ^{13}CO for $CuZnO/Al_2O_3$ at steady-state. No methane transient is present since no CH_4 formation was detected (even by GC) for this catalyst. Transients for DME with one ^{12}C and one ^{13}C (DME') or with two ^{12}C (DME") are also shown in Fig. 6. It can be seen that the transient behavior of DME" is similar to the products with a single ^{12}C like MeOH. However, the transient for DME', formed only later after ^{12}CO switching to ^{13}CO when ^{13}C was able to be included in DME synthesis, went through a maximum. The average surface residence times of the reactive species (τ_i) except $\tau_{DME'}$ are equal to the area between the normalized transients of the corresponding species and the inert tracer Ar. $\tau_{DME'}$ was calculated by subtracting the area below the Ar normalized transient curve from that of DME'.

Table 5.3 shows the surface parameters (τ_i and N_i) for various catalysts at steady-state on various catalysts for methane, MeOH and DME. τ_{CH4} could not be estimated for CuZnO, $CuZnO/Al_2O_3$, $6.7ZnO/Al_2O_3$, and $20ZnO/Al_2O_3$ at steady-state due to their low activities for methane formation. τ_{DME} was calculated by combining the residence times obtained from both DME' and DME" according to the proportion of ^{12}C distribution ($\tau_{DME} = 1/3*\tau_{DME'} + 2/3*\tau_{DME"}$). Since the formation of DME occurred by the dehydration of MeOH on the acid sites of Al_2O_3 as a secondary reaction [47], the value of τ_{DME} should be always larger than τ_{MeOH}, as was found here. Figure 5.7 and Figure 5.8

show the time-on-stream behavior of τ_{MeOH} and τ_{DME}, respectively, for the various catalysts. τ_{MeOH} for CuZnO and for $CuZnO/Al_2O_3$ were similar and decreased slightly as time proceeded, reaching a constant value after ca. 120 min. However, τ_{MeOH} for $20ZnO/Al_2O_3$ increased significantly while that of $20Cu/Al_2O_3$ stayed at a fairly fixed value within experimental error, or only slightly decreased. τ_{DME} decreased somewhat over time for catalysts that produced DME. Plots of τ_i vs. TOS were similar for $13.3Cu/Al_2O_3$ and $20Cu/Al_2O_3$ and for $6.7ZnO/Al_2O_3$ and $20ZnO/Al_2O_3$ (not shown).

The concentration of active surface intermediates for a specific product can be determined by $N_i = Rate_i * \tau_i$ [38-39]. The units of rate in this paper are based on carbon atom amount; therefore the value for N_{DME} (units: μmol of product/g) was calculated by multiplying the rate by 0.5. That relationship is represented by the following equation:

$$N_{DME} = 0.5*[Rate_{DME}]*[\ \tau_{DME}]$$

$$= 0.5*[Rate_{DME}]*[\ 1/3*\tau_{DME'} + 2/3*\tau_{DME''}]$$

The factor of 0.5 was required to correct the rate from "carbon amount basis" to "product basis" because DME contains two carbons. N_i and τ_i at steady-state (Table 3) were very similar for ($13.3Cu/Al_2O_3$ vs. $20Cu/Al_2O_3$) and ($6.7ZnO/Al_2O_3$ vs. $20ZnO/Al_2O_3$), suggesting that the intrinsic activity and surface parameters were not affected by the amount of Cu or ZnO on Al_2O_3 in this range.

The surface concentration of the intermediates (N_i) is the most precise parameter obtained by SSITKA since the calculation is based only on a mass balance. However, one needs to be careful in interpreting both τ_i and N_i due to the fact that MeOH can easily readsorb and that the intermediates leading to DME consist of MeOH produced on

CuZnO sites and further reacted on acid sites of the Al_2O_3. Before the results can be analyzed, these values must be corrected for readsorption. This will be shown and discussed in the next section.

Table 5.3 Uncorrected steady-state surface reaction parameters for MeOH synthesis on the various catalysts measured by SSITKA[a,b].

Catalyst	τ_i (s)[c]			N_i (μmol of product/g)[e]			
	CH_4	MeOH	DME[d]	CH_4	MeOH	DME[f]	CO
CuZnO	-	2.9	-	-	0.33	-	4.0
$CuZnO/Al_2O_3$	-	3.1	7.4	-	0.20	0.21	3.1
$13.3Cu/Al_2O_3$	2.4	6.9	8.9	0.097	0.03	0.06	2.6
$20Cu/Al_2O_3$	2.3	7.5	9.2	0.110	0.03	0.08	2.5
$6.7ZnO/Al_2O_3$	-	8.4	13.0	-	0.10	0.08	3.2
$20ZnO/Al_2O_3$	-	8.1	12.6	-	0.19	0.15	3.1

[a] Catalyst: 1g, inert (α-Al_2O_3): 2g. SSITKA measurements were carried out at 250°C; P_T = 1.8 atm, flow rate = 30 mL/min (H_2: He: CO = 8:1:1). Max. error = ±10%.
[b] At steady-state (after 6 h reaction).
[c] Surface residence time of intermediates.
[d] $\tau_{DME} = 1/3^* \tau_{DME'} + 2/3^* \tau_{DME''}$, where DME' = DME with one ^{12}C and one ^{13}C and DME'' = DME with two ^{12}C.
[e] $N_i = Rate_i * \tau_i$, except for DME.
[f] $N_{DME} = 0.5*Rate_{DME}*\tau_{DME} = 0.5*Rate_{DME}*(1/3^* \tau_{DME'} + 2/3^* \tau_{DME''})$.

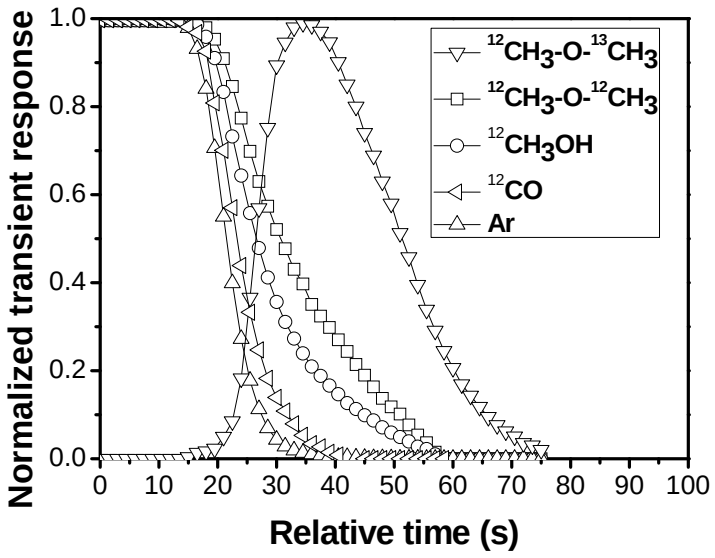

Figure 5.6 Typical normalized transient responses for MeOH, DME and Ar following a (^{12}CO + Ar)//(^{13}CO) switch for $CuZnO/Al_2O_3$. (no detectable CH_4 was produced)

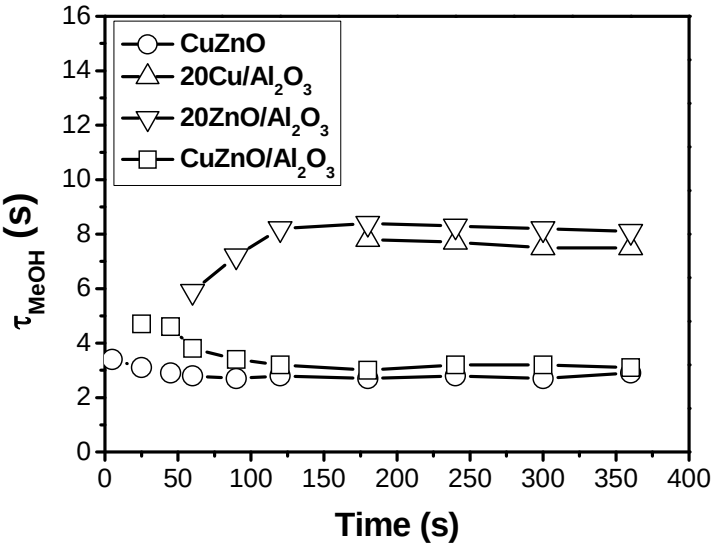

Figure 5.7 Surface reaction residence times for MeOH (τ_{MeOH}) vs. TOS.

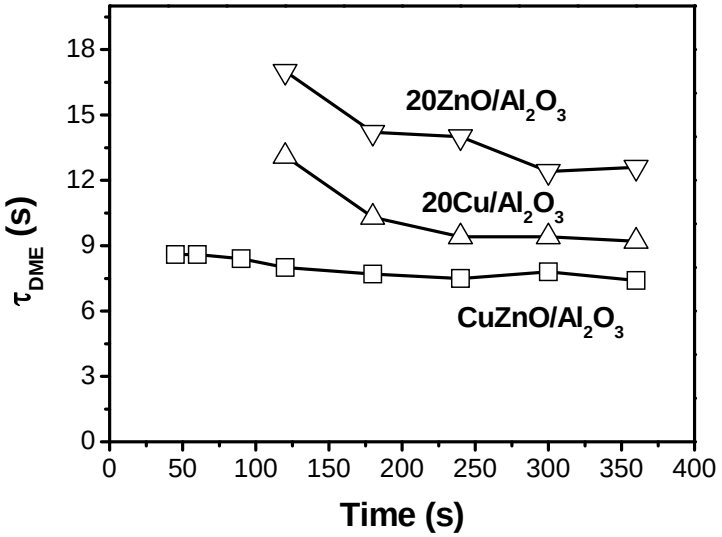

Figure 5.8 Surface reaction residence times for DME (τ_{DME}) vs. TOS.

5.4 Discussion

5.4.1 Correction for readsorption effects and meaning of the surface reaction parameters

SSITKA is a powerful technique to determine average surface reaction parameters under reaction conditions. However, readsorption can have a significant effect on the values of surface residence times measured for some oxygenates, such as MeOH and acetaldehyde, as reported elsewhere [40, 48-51]. This is due to the strong readsorption ability of these oxygenates in the catalyst bed and the resulting chromatographic effect. By performing CO hydrogenation with different total flow rates, the impact of readsorption is able to be ascertained. It is clear as shown in Figure 5.9 that τ_{MeOH} increases linearly with increasing space time in the catalyst bed. The results clearly show

that interparticle readsorption contributed significantly to the values of the surface reaction residence times as previous noted by our group [49, 51-52]. Therefore, the readsorption effect cannot be ignored and must be taken into account before any full interpretation of SSITKA data. By extrapolating τ_{MeOH} to 0 space time, a more accurate estimation of MeOH residence time during synthesis can be obtained (τ^0_{MeOH}) [40, 48-50]. However, this corrected value, τ^0_{MeOH}, may still be a slight overestimation of the real reaction residence time due to possible readsorption occurring on sites within pores, which is much more difficult to eliminate. Readsorption is a requirement for DME formation (from MeOH synthesis) but can also affect the surface residence time for DME [40, 48-49, 52]. Thus, $\tau_{DME'}$ and $\tau_{DME''}$ were also corrected by a similar method as performed for MeOH (not shown). A final overall corrected value for DME, τ^0_{DME}, can be calculated using a similar equation as before: $\tau^0_{DME} = 1/3*\tau^0_{DME'} + 2/3*\tau^0_{DME''}$. A more accurate estimation of the concentration of active surface intermediates, N^0_i, can be calculated using the corrected surface residence time, τ^0_i. It should be noted that τ_{MeOH} only needs to be corrected for reversible MeOH readsorption, but not for DME formation.

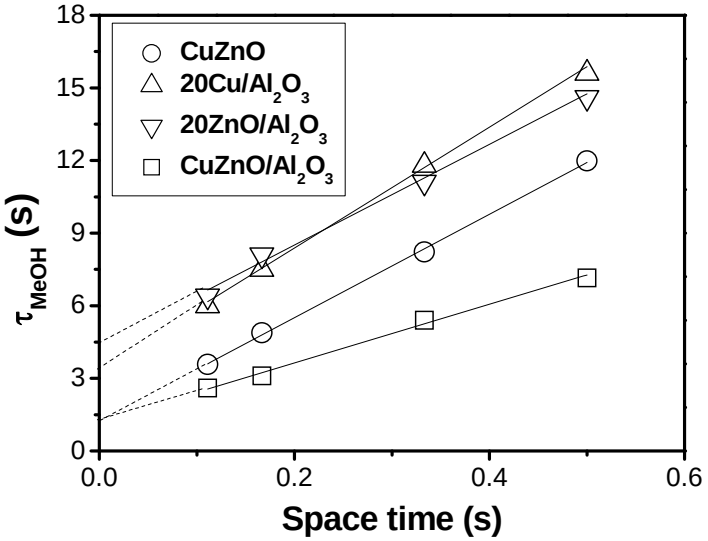

Figure 5.9 τ_{MeOH} vs. space time during MeOH synthesis at steady state.

Figure 5.10 shows a scheme for the comparison of the formation of MeOH and DME on CuZnO and CuZnO/Al_2O_3 surfaces. It can be seen from Figure 5.10 (a) that reactants ($CO + H_2$) react on the active sites on the surface of CuZnO, and then desorb as MeOH molecules. Figure 5.10 (b), however, shows that the products of MeOH and DME are formed in more complex ways for CuZnO/Al_2O_3: (1) CO and H_2 react first on the active sites on CuZnO and produce MeOH as in Figure 5.10 (a); (2) some of the MeOH formed by (1) readsorbs on surface sites of Al_2O_3, then desorbs as MeOH without further reaction occurring; and (3) some of the MeOH formed by (1) readsorbs on surface acid sites of Al_2O_3 reacting to form DME which subsequently desorbs. Obviously, readsorption of MeOH and DME molecules can occur multiple times which is the reason for the need to correct the data to account for this.

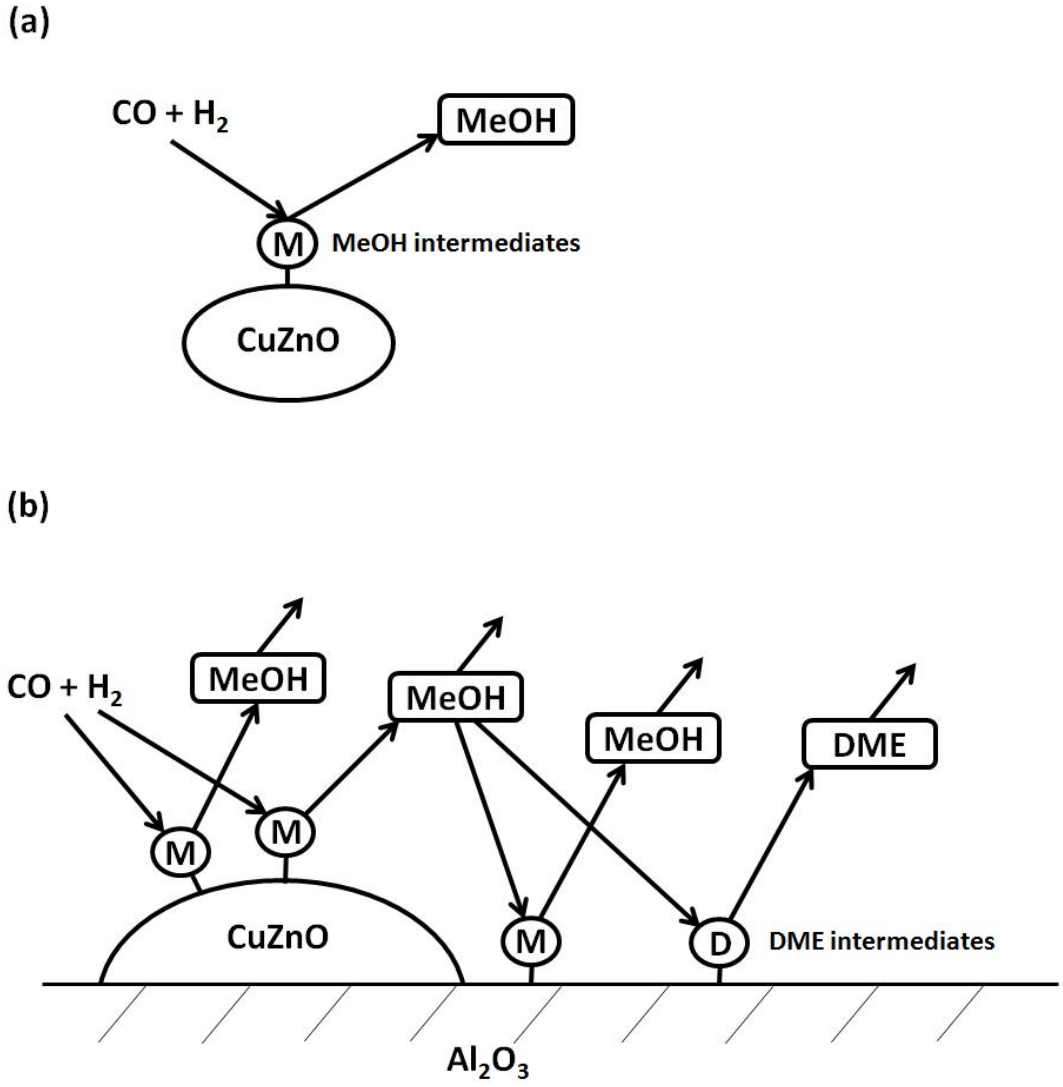

Figure 5.10 Schemes for the formation of MeOH and DME on (a) CuZnO and (b) $CuZnO/Al_2O_3$.

N^0_{MeOH} for CuZnO is calculated according to an equation similar to that given in the previous section because no DME formed:

$$N^0_{MeOH} = \tau^0_{MeOH} * R_{MeOH}$$

The equation to calculate N^0_{MeOH} for all catalysts containing Al_2O_3 and able to produce DME, however, must be modified because both MeOH and DME derive from MeOH intermediates, so that the total rate of MeOH synthesis is the sum of rates for MeOH and DME.

$$N^0_{MeOH} = \tau^0_{MeOH} * (R_{MeOH} + R_{DME})$$

Since DME is formed by the readsorption of MeOH formed on the acid sites of Al_2O_3, the corrected average surface reaction residence time for the formation of DME from MeOH actually consists only of the difference between the corrected average surface residence times measured for DME and MeOH. As mentioned in the previous section, DME intermediates can be separated into two types according to the number(s) of ^{12}C on the product. At any given time (and in particular at the time of the isotopic switch), two kinds of situations exist on the acid sites of Al_2O_3 surface making DME: (1) some sites are occupied by 2-C intermediates (essentially as DME) and give rise to DME", (2) some other sites have only 1-C DME precursor intermediates (essentially as MeOH) and then give rise to DME'. It would be nice if $N^0_{DME"}$ and $N^0_{DME'}$ could be determined separately. However, the steady-state reaction rate for DME (R_{DME}) was a combination of $R_{DME'}$ and $R_{DME"}$. $R_{DME'}$ and $R_{DME"}$, which varied with time during the isotopic transient, were difficult to separate due to limitations of the equipment and varied with time during the transient (i.e., were never constant). However, a relative

good approximation of overall N^0_{DME} can be determined by the following equation:

$$N^0_{DME} = 0.5*R_{DME}*(\tau^0_{DME} - \tau^0_{MeOH})$$

$$= 0.5*R_{DME}*[(1/3*\tau^0_{DME'} + 2/3*\tau^0_{DME''}) - \tau^0_{MeOH}] \text{ (units: μmol DME/g-cat.)}$$

The factor of 0.5 is used for N^0_{DME} since R_{DME} was calculated on a carbon atom basis but DME involves 2 carbon atoms. N^0_{DME} also underestimates slightly the number of occupied sites since it does not take into account that some sites have only a 1-C precursor on them. Moreover, there may be some potentially active sites on the Al_2O_3 which are not occupied (vacant sites) at the time of switch.

In summary, N^0_{MeOH} and N^0_{DME} represent the concentration of active intermediates on the catalyst surface for MeOH and DME, respectively, at steady-state. This is closely related to the number of active sites with reaction at steady-state. The total number of sites would also include ones not occupied (vacant) at any given time, ones occupied by readsorbing products without further reaction, and deactivated sites.

The intrinsic activity is typically determined by dividing the rate for a specific product by the number of exposed surface sites based on chemisorption results (TOF_{chem}). However, TOF_{chem} does not represent a true intrinsic activity since the surface atoms/sites measured by chemisorption are not usually identical to the active surface sites for reaction and some active sites may have deactivated during the approach to steady-state [39]. A more accurate way to determine the true intrinsic activity for the active sites is from the reciprocal of τ_i (or τ^0_i in this case) obtained by SSITKA measurements (TOF_{ITK}). This is equal to R_i/N^0_i, which is rate of "i" formation divided by the number of active surface intermediates of "i" (related closely to the number of active sites). This number

has also been considered as a pseudo-first-order constant rate k_i in previous studies [40, 49]. Table 5.4 contains the corrected values of τ_{MeOH} (τ^0_{MeOH}), $\tau_{DME'}$ ($\tau^0_{DME'}$), $\tau_{DME''}$ ($\tau^0_{DME''}$), N_{MeOH} (N^0_{MeOH}), and the resulting overall τ_{DME} (τ^0_{DME}), N_{DME} (N^0_{DME}) and TOF^0_{ITK} for the various catalysts. A better understanding of the main issues addressed by this paper can be reached by interpreting the corrected values of the surface reaction parameters from SSITKA in combination with the characterization and reaction results.

Table 5.4 Corrected steady-state surface reaction parameters for MeOH synthesis on the various catalysts[a].

Catalysts	τ^0_{MeOH} (s)	TOF^0_{ITK}[b] for MeOH (s^{-1})	N^0_{MeOH}[c] (μmol MeOH/g-cat.)	N^0_{MeOH}[c] (Cu basis) (μmol MeOH/g-Cu)	N^0_{MeOH}[c] (ZnO basis) (μmol MeOH/g-ZnO)	$\tau^0_{DME'}$ (s)	$\tau^0_{DME''}$ (s)	τ^0_{DME} (s)[d]	TOF^0_{ITK}[b,f] for DME (s^{-1})	N^0_{DME}[c] (μmol DME/g-cat.)
CuZnO	1.2	0.83	0.14	0.21	0.42	-	-	-	-	-
$CuZnO/Al_2O_3$	1.2	0.83	0.15	1.13	2.24	7.6	4.6	5.6	0.23	0.125
$20Cu/Al_2O_3$	3.4	0.29	0.08	0.40	-	8.8	6.4	7.2	0.26	0.023
$20ZnO/Al_2O_3$	4.3	0.23	0.21	-	1.05	9.8	8.6	9.0	0.21	0.052

[a] τ^0_{MeOH}, $\tau^0_{DME'}$ and $\tau^0_{DME''}$ are the corrected values for τ_{MeOH}, $\tau_{DME'}$ and $\tau_{DME''}$, respectively. Corrected residence times (τ^0_{MeOH}, $\tau^0_{DME'}$ and $\tau^0_{DME''}$) were obtained by extrapolating τ_{MeOH}, $\tau_{DME'}$ or $\tau_{DME''}$ to 0 s of space time.

[b] $TOF^0_{ITK,i} = 1/\tau^0_i$.

[c] For CuZnO: $N^0_{MeOH} = \tau^0_{MeOH} * R_{MeOH}$; For other catalysts: $N^0_{MeOH} = \tau^0_{MeOH} * (R_{MeOH} + R_{DME})$, $N^0_{DME} = 0.5*R_{DME}*(\tau^0_{DME} - \tau^0_{MeOH})$.

[d] $\tau^0_{DME} = 1/3* \tau^0_{DME'} + 2/3* \tau^0_{DME''}$.

[f] TOF^0_{ITK} for DME $= 1/(\tau^0_{DME} - \tau^0_{MeOH})$.

5.4.2 Impact of the Al_2O_3 support on CuZnO

A support may provide not only a good dispersion of the active components but also a modification of the interactions between the main components and promoters [53]. It is known that the nature of the support can change the activity and selectivity of CuZnO for CO/CO_2 hydrogenation [36, 53-55]. Sun et al. [54] found that the addition of Al_2O_3 to CuZnO binary catalysts led to smaller crystallites and made Cu and ZnO an amorphous-like structure, which resulted during CO_2 hydrogenation in a higher CO_2 conversion and a higher yield of MeOH. Shishido et al. [36] proposed that the addition of Al_2O_3 species inhibited the aggregation of Cu in a CuZnO system based on BET results and Cu metal surface area. In this investigation it was found that $CuZnO/Al_2O_3$ had a much higher BET surface area and pore volume than that of CuZnO, in agreement with reported results that the surface area for $CuZnO/Al_2O_3$ catalysts is mostly due to Al_2O_3 [42]. It is noteworthy that XRD patterns of the catalysts before reduction (Figure 5.2) were dominated by the presence of copper oxide. The distinct diffraction lines in non-reduced CuZnO and $CuZnO/Al_2O_3$ were mostly assignable to CuO. Along with the high dispersion/amorphous ZnO patterns, these results suggest that ZnO species/structure served as spacers between Cu particles in the reduced catalysts, preventing Cu from sintering. A similar observation has also been made by Kasatkin et al. [56] based on their TEM results.

Since the active sites for CO hydrogenation are located on CuZnO and not the support, expression of rate on a CuZnO weight basis would be useful for a better understanding of the catalytic performance of the various CuZnO based catalysts. Table

5.5 shows a comparison of reaction rates on this basis for both CuZnO and CuZnO/Al_2O_3. It can be seen in Table 5.5 that CuZnO/Al_2O_3 exhibited a 5.6 times higher overall activity compared to CuZnO. MeOH was the only product for both catalysts initially (data not shown). However, with TOS, the selectivity on CuZnO/Al_2O_3 became 52.3% MeOH and 44.9% DME at steady state (see Table 5.2). Because of being a secondary reaction, the selectivity for DME is a strong function of the amount of catalyst present and residence time of MeOH in the catalyst bed.

Table 5.5 A comparison of the steady-state catalytic properties and surface reaction parameters for CuZnO and for CuZnO/Al_2O_3 based on the amount of CuZnO.

Catalyst	Total rate for CO hydrogenation (μmol C/g-CuZnO/s)	Rate of specific products (μmol C/g-CuZnO/s)		N^0_{MeOH} (μmol MeOH/g-CuZnO)	N^0_{DME} (μmol DME/g-CuZnO)
		MeOH	DME		
CuZnO	0.113	0.113	-	0.14	-
CuZnO/Al_2O_3	0.630	0.330	0.279	0.75	0.63

In a previous study, this relationship was confirmed by plotting the rate of formation for DME vs. total P_{MeOH} on Pd supported catalysts [40]. Total P_{MeOH} is defined as the total partial pressure of MeOH produced in the reactor and is equal to P_{MeOH} exiting the reactor plus an equivalent partial pressure of MeOH which was converted to DME (total $P_{MeOH} = P_{MeOH} + 2*P_{DME}$). Figure 5.11 gives a plot of the rate of DME formation for catalysts which produced DME as a function of total P_{MeOH}. It can be easily seen from Fig. 11 that there exists a linear dependency between the two variables. This is not surprising since the rate of DME formation should be primarily a function of MeOH concentration (i.e., total P_{MeOH} in the reactor) and the amounts of Al_2O_3 used for all the

catalysts were identical, barring some major poisoning or blockage of the Al_2O_3 acid sites by the Cu or ZnO - which does not seem to have occurred. It was noteworthy that the typical amounts of surface acid sites on γ-Al_2O_3 [57], which is a function of calcination temperature, are three orders of magnitude higher than the measured numbers of acidic sites occupied by DME in this study due to the small partial pressure of MeOH formed at the differential conversion conditions used. Therefore, any blockage or poisoning effects of the Al_2O_3 surface could be ignored.

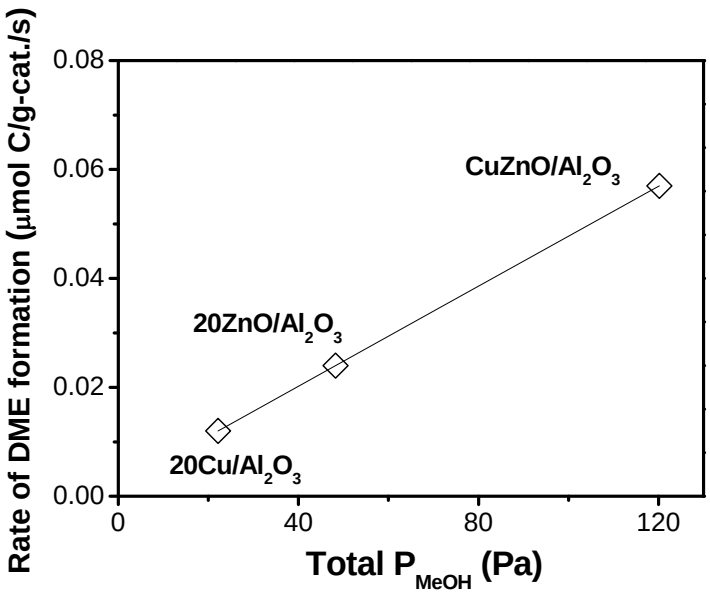

Figure 5.11 Rate of DME formation vs. equivalent P_{MeOH} at exit (equivalent P_{MeOH} = $P_{MeOH} + 2*P_{DME}$).

It should be noted from Table 5.4 that τ^0_{MeOH} was the same for both CuZnO and $CuZnO/Al_2O_3$ at steady-state, indicating that the intrinsic activity of MeOH formation was not affected by the Al_2O_3 support. The calculated values of TOF^0_{ITK} based on τ^0_{MeOH} and τ^0_{DME} are shown in Table 5.4. TOF^0_{ITK}s for MeOH on both CuZnO and $CuZnO/Al_2O_3$ increased during the induction period (data not shown) and reached the same value ultimately. Surface concentrations of intermediates were also estimated on a per gram CuZnO basis (see Table 5). N^0_{MeOH} was 5.4 times higher for $CuZnO/Al_2O_3$ than that for CuZnO. Combined with the same τ^0_{MeOH} values obtained for both catalysts, the results indicate that the observed difference in reaction rates for MeOH formation on Al_2O_3 -supported vs. unsupported CuZnO was mostly due to the difference in the surface concentration of intermediates (i.e., sites), supporting the claim of higher dispersion of CuZnO on Al_2O_3 [36, 42]. This observation also implies that there may be only one type of site for the formation of MeOH on both CuZnO and $CuZnO/Al_2O_3$.

A smaller TOF^0_{ITK} for DME compared to MeOH was as expected due to DME being produced from the readsorption and secondary reaction of MeOH. Even though the formation of DME from MeOH is much faster than MeOH synthesis if the partial pressures of their reactants are similar [48], in this case the partial pressure of MeOH (reactant for DME formation) was low relative to the partial pressure of CO and H_2 (reactants for MeOH synthesis). The DME formation rate can be concluded to be limited by the MeOH formation rate in this case.

5.4.3 Impact of the components

The roles of the components, Cu or ZnO, in CuZnO-based catalysts have been

widely studied. Usually CuZnO-based catalysts have been studied either in comparison with Cu/CuO or with ZnO single component catalysts [27, 29, 58-59]. There exists, to the best to our knowledge, no explicit report so far which includes and compares experiments for a systematic series of Cu, ZnO and CuZnO catalysts. In this study, however, the components of Cu and ZnO were examined and compared together with CuZnO-based catalysts by CO hydrogenation and SSITKA results for a deeper understanding of the effects of individual components at the site level. It is noteworthy that Al_2O_3-supported Cu, ZnO and CuZnO (Cu/Al_2O_3, ZnO/Al_2O_3, $CuZnO/Al_2O_3$) were used in this study rather than unsupported components because Al_2O_3-supported catalysts lead to better dispersions comparing to unsupported ones and, therefore, higher activities for CO hydrogenation. Use of unsupported Cu and ZnO having poor activities for CO hydrogenation could be due to low dispersions and would result in inaccurate interpretation of the data.

As can be seen in Table 5.2, the reaction activities varied significantly for the various catalysts. The reaction results for 13.3 wt% Cu/Al_2O_3 and 6.7 wt% ZnO/Al_2O_3 are shown for the purpose of comparing with $CuZnO/Al_2O_3$, which contained 13.3 wt% Cu and 6.7 wt% ZnO. However, higher loadings (20 wt%) of the Al_2O_3-supported Cu and ZnO catalysts were used for the main comparisons in this study in order to increase the overall activity, which resulted in less error in estimating surface parameters. Comparing high (20 wt%) vs. low (6.7 or 13.3 wt%) loadings of ZnO and Cu catalysts, respectively, even though the reaction rates were higher for the higher loadings, as expected. The product selectivities, however, were essentially the same for ($20Cu/Al_2O_3$ and

13.3Cu/Al_2O_3) and (20ZnO/Al_2O_3 and 6.7ZnO/Al_2O_3). These results suggest that different loadings did not change the intrinsic properties of either Cu/Al_2O_3 or ZnO/Al_2O_3.

It should be noted that 20Cu/Al_2O_3 and 20ZnO/Al_2O_3 can be used for comparison with CuZnO/Al_2O_3 only for intrinsic properties, such as surface residence time (τ^0_i) or turnover frequency (TOF^0_{ITK}), because these properties are only related to the sites and are not affected by the number of sites or the amount of catalytic material. The most ideal comparisons of extrinsic properties (i.e., rates of reaction or surface concentrations of intermediates) on CuZnO/Al_2O_3, Cu/Al_2O_3 and ZnO/Al_2O_3 would be made using the same metal and metal oxide surface areas and particle sizes. However, due to the difficulty of obtaining and fixing those kinds of properties for these particular supported catalysts, alternative methods had to be applied by: (1) using Cu/Al_2O_3 and ZnO/Al_2O_3 with corresponding metal loadings with CuZnO/Al_2O_3 (13.3Cu/Al_2O_3 and 6.7ZnO/Al_2O_3), or (2) normalizing the original parameters to the same metal (Cu) or metal oxide (ZnO) weight basis. Such alternative methods provide a reasonable comparison of these parameters.

The reaction rates for these catalysts were in the order of CuZnO/Al_2O_3 > 13.3Cu/Al_2O_3 > 6.7ZnO/Al_2O_3, with the range being from 0.113-0.025 μmol C/g-cat/s (within a factor of 5). This is somewhat surprising since the combination of Cu and ZnO has been proposed to exhibit significantly higher activity than the Cu or ZnO species by themselves when using similar surface metal areas [10]. A possible explanation is that the usage of a support may result in a better dispersion for Cu (especially) and ZnO which may effectively prevent the Cu or ZnO particles from aggregation or sintering.

The products of $13.3Cu/Al_2O_3$ for MeOH synthesis conditions were mainly CH_4 with roughly 30% of products being MeOH and DME at steady-state. The activity and selectivity results are in line with what d'Alnoncourt et al. [60] found for MeOH synthesis: the presence of ZnO in Cu catalysts resulted in an increase in MeOH formation activity, along with a decrease in the heat of adsorption of CO.

The synergy of Cu and ZnO for MeOH formation can be observed at a site level by comparing TOF^0_{ITK} for MeOH (Table 5.4). For comparison of this site intrinsic property, the results for $20Cu/Al_2O_3$ and $20ZnO/Al_2O_3$ will be used due to their higher activities. TOF^0_{ITK} for MeOH followed an order of $CuZnO/Al_2O_3 >> 20Cu/Al_2O_3 > 20ZnO/Al_2O_3$, but the differences were within a factor of 4. It can be seen from Table 5.4 that $CuZnO/Al_2O_3$ also exhibited a higher N^0_{MeOH} than $20ZnO/Al_2O_3$ or $20Cu/Al_2O_3$ using a Cu or ZnO weight basis. $20ZnO/Al_2O_3$ exhibited a lower MeOH formation rate than $CuZnO/Al_2O_3$ both because of its lower intrinsic reaction activity (TOF^0_{ITK}) and its fewer number of sites. The low reaction rate on $20Cu/Al_2O_3$ was also caused by both a low intrinsic activity and a low value of N^0_{MeOH}, related to number of available active sites. The observed low activity for $20Cu/Al_2O_3$ is in agreement with reports in the literature concerning the low activity of Cu-based catalysts for CO hydrogenation [9, 27, 31, 61].

It should be noted that the differences (τ^0_{MeOH}-τ^0_{DME}) were within experimental error for catalysts producing DME, which suggested that the surface site residence times for DME production were very similar (see also TOF^0_{ITK} for DME in Table 5.4). This should be expected since DME formed only on the Al_2O_3 and the residence time for making DME (τ^0_{DME}-τ^0_{MeOH}) should not be affected by the catalytic species (Cu and ZnO)

for MeOH synthesis. As mentioned in the previous section, the DME formation rates were limited by the formation of MeOH as evidenced by the linear relationships for the reaction rates of DME formation and for N^0_{DME} with total P_{MeOH} (see Figures 11 and 12). Therefore, further interpretation of the surface reaction parameters for DME synthesis has no value for these conditions.

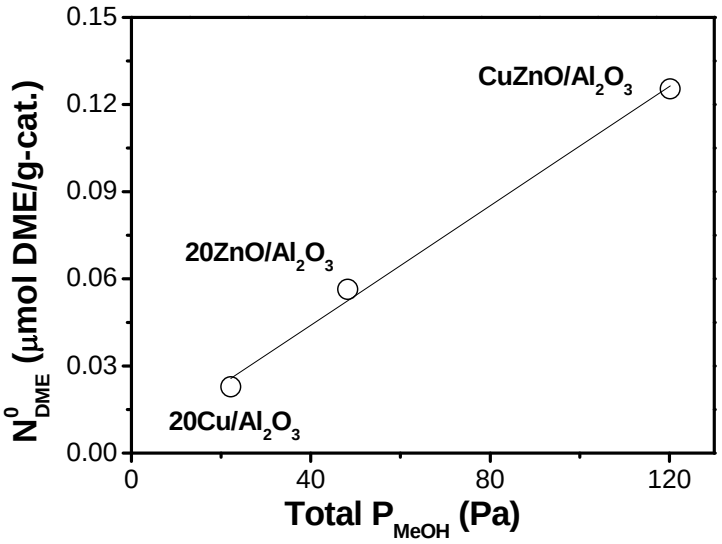

Figure 5.12 N^0_{DME} vs. equivalent P_{MeOH} at exit (equivalent $P_{MeOH} = P_{MeOH} + 2*P_{DME}$).

5.5 Conclusions

Even though the effects of different supports and components on CuZnO-based catalysts for MeOH synthesis have received a great deal of attention in the past, this study has explored for the first time at the reaction site level the impact of the components and a Al_2O_3-support on CuZnO-based catalysts. Using SSITKA, surface kinetic parameters

were able to be determined, providing a better understanding of support and component effects. Based on BET and XRD analysis for CuZnO, 20Cu/Al_2O_3 and 20ZnO/Al_2O_3 and CuZnO/Al_2O_3, it was found that the different combinations of Cu and ZnO components or the addition of the Al_2O_3 support resulted in markedly different surface areas and structures.

CO hydrogenation results indicated that the overall reaction activity of CuZnO-based catalysts were higher than catalysts with only Cu or ZnO components but not orders of magnitude higher, indicating some synergy between Cu and ZnO species. DME is a secondary reaction product from the dehydration of MeOH and was produced only on the acidic sites of Al_2O_3 when it was present as a support. Based on the dependency of the rate of DME formation and the corresponding partial pressure of MeOH, the rates of DME formation was found to be limited primarily by the amount of MeOH formed on the Cu and ZnO components.

The original SSITKA surface reaction parameters, τ_i and N_i, obtained from SSITKA were corrected for readsorption effects to τ^0_i and N^0_i. τ^0_{MeOH} (corrected average surface reaction residence time for MeOH formation) was essentially the same for both CuZnO and CuZnO/Al_2O_3, indicating that the Al_2O_3 support does not change the nature of active sites for the production of MeOH on CuZnO. Higher intrinsic "site" activities ($TOF^0_{ITK} = 1/ \tau^0_{MeOH}$) for MeOH on CuZnO-based catalysts than those on Cu/Al_2O_3 or ZnO/Al_2O_3 also clearly indicated the synergy of Cu and ZnO. The higher activity observed for CuZnO/Al_2O_3 was due to both a higher intrinsic "site" activity (because of CuZnO) and a larger concentration of active surface intermediates (and sites). A linear dependency of

the surface concentration of DME intermediates (N^0_{DME}) with the amount of MeOH produced was a further indication of DME formation being limited by MeOH synthesis.

Our results can be summarized as follows:

(1) The reaction rates for MeOH formation on CuZnO and CuZnO/Al_2O_3 were nearly identical on a per gram catalyst basis; however, on a per gram CuZnO basis, CuZnO/Al_2O_3 had a much higher rate. This difference was due to the higher concentration of active surface intermediates/sites, almost certainly reflecting an increased dispersion of the supported CuZnO. The identical "site" activities seen for these 2 catalysts suggest that the sites, however, were identical for making MeOH. Thus, the only roles that the Al_2O_3 appeared to play was in increasing CuZnO dispersion and providing acid sites for the conversion of MeOH to DME.

(2) Using a support, higher dispersions of Cu and ZnO were possible (for Cu/Al_2O_3 and ZnO/Al_2O_3 catalysts) resulting in better comparisons to the CuZnO catalysts. Cu/Al_2O_3 and ZnO/Al_2O_3 exhibited lower MeOH formation rates compared to CuZnO/Al_2O_3 because of their lower intrinsic activities and lower surface concentrations of intermediates. Based on overall rates as well as the surface reaction parameters measured, it would appear, however, that, while there is some synergy between Cu and ZnO in producing MeOH on CuZnO catalysts, this synergy does not result in an order-of-magnitude increase in the site activity or active site concentration.

(3) Cu/Al_2O_3 was capable of producing significant hydrocarbon selectivity, but $CuZnO/Al_2O_3$ and ZnO/Al_2O_3 were not. This seems to imply that the presence of ZnO inhibits the hydrocarbon formation ability of Cu.

5.6 Acknowledgements

We acknowledge financial support from the US Department of Energy (Award No. DE-PS26-06NT43024).

5.7 References

[1] S. Pradhana, A.S. Reddya, R.N. Devia, S. Chilukuri, Catal. Today 141 (2009) 72.

[2] S. Sá, H. Silva, L. Brandãoa, J.M. Sousa, A. Mendes, Appl. Catal. B-Environ. 99 (2010) 43.

[3] J.P. Breen, J.R.H. Ross, Catal. Today 51 (1999) 521.

[4] B.A. Peppley, J.C. Amphlett, L.M. Kearns, R.F. Mann, Appl. Catal. A-Gen. 179 (1999) 31.

[5] D.B. Clarke, A.T. Bell, J. Catal. 154 (1995) 314.

[6] Y. Amenomiya, Appl. Catal. 30 (1987) 57.

[7] G. Ghiotti, F. Boccuzzi, Catal. Rev. 29 (1987) 151.

[8] P.J.A. Tijm, F.J. Waller, D.M. Brown, Appl. Catal. A-Gen. 221 (2001) 275.

[9] R. Burch, S.E. Golunski, J. Chem. Soc. Faraday Trans. 86 (1990) 2683.

[10] R.G. Herman, K. Klier, G.W. Simmons, B.P. Finn, J.B. Bulko, T.P. Kobylinski, J. Catal. 56 (1979) 407.

[11] T. Fujitani, M. Saito, Y. Kanai, T. Kakumoto, T. Watanabe, J. Nakamura, T. Uchijima, Catal. Lett. 25 (1994) 271.

[12] R. Burch, R.J. Chappell, Appl. Catal. 45 (1988) 131.

[13] Y. Kanai, T. Watanabe, T. Fujitani, T. Uchijima, J. Nakamura, Catal. Lett. 38 (1996) 157.

[14] Y. Fu, T. Hong, J. Chen, A. Auroux, J. Shen, Thermochim. Acta 434 (2005) 22.

[15] D. Mao, W. Yang, J. Xia, B. Zhang, G. Lu, J. Mol. Catal. A-Chem. 250 (2006) 138.

[16] D. Mao, W. Yang, J. Xia, B. Zhang, Q. Song, Q. Chen, J. Catal. 230 (2005) 140.

[17] K. Klier, Adv. Catal. 31 (1982) 243.

[18] K.C. Waugh, Catal. Today 15 (1992) 51.

[19] V. Ponec, Surf. Sci. 272 (1992) 111.

[20] Y. Kanai, T. Watanabe, T. Fujitani, M. Saito, J. Nakamura, T. Uchijima, Catal. Lett. 27 (1994) 67.

[21] J.R. Monnier, M.J. Hanrahan, G. Apai, J. Catal. 92 (1985) 119.

[22] G.C. Chinchen, K.C. Waugh, D.A. Whan, Appl. Catal. 30 (1987) 333.

[23] J. Yoshihara, C.T. Campbell, J. Catal. 161 (1996) 776.

[24] W.X. Pan, R. Cao, D.L. Roberts, G.L. Griffin, J. Catal. 114 (1988) 440.

[25] R. Burch, S.E. Golunski, M.S. Spencer, Catal. Lett. 5 (1990) 55.

[26] C.V. Ovesen, B.S. Clausen, J. Schiøtz, P. Stoltze, H. Topsøe, J.K. Nørskov, J. Catal. 168 (1997) 133.

[27] Y. Choi, K. Futagami, T. Fujitani, J. Nakamura, Appl. Catal. A-Gen. 208 (2001) 163.

[28] J.-D. Grunwaldt, A.M. Molenbroek, N.-Y. Topsøe, H. Topsøe, B.S. Clausen, J. Catal. 194 (2000) 452.

[29] N.-Y. Topsøe, H. Topsøe, Top. Catal. 8 (1999) 267.

[30] B.S. Clausen, J. Schiøtz, L. Gråbæk, C.V. Ovesen, K.W. Jacobsen, J.K. Nørskov, H.

Topsøe, Top. Catal. 1 (1994) 367.

[31] T. Fujitani, J. Nakamura, Appl. Catal. A-Gen. 191 (2000) 111.

[32] M.S. Spencer, Catal. Lett. 50 (1998) 37.

[33] J. Słoczyn´ski, R. Grabowski, P. Olszewski, A. Kozłowska, J. Stoch, M. Lachowska, J. Skrzypek, Appl. Catal. A-Gen. 310 (2006) 127.

[34] C. Yang, Z. Ma, N. Zhao, W. Wei, T. Hu, Y. Sun, Catal. Today 115 (2006).

[35] L. Wang, W. Ding, Y. Liu, W. Fang, Y. Yang, J. Nat. Gas Chem. 19 (2010) 487.

[36] T. Shishido, Y. Yamamoto, H. Morioka, K. Takaki, K. Takehira, Appl. Catal. A-Gen. 263 (2004) 249.

[37] P.C.K. Vesborg, I. Chorkendorff, I. Knudsen, O. Balmes, J. Nerlov, A.M. Molenbroek, B.S. Clausen, S. Helveg, J. Catal. 262 (2009) 65.

[38] S.L. Shannon, J.G. Goodwin, Jr., Chem. Rev. 95 (1995) 677.

[39] J.G. Goodwin, Jr., S. Kim, W.D. Rhodes, In: Catalysis, J.J. Spivey, Ed.; The Royal Society of Chemistry: Cambridge, U.K., 2004; Vol. 17, Chapter 8.

[40] S.H. Ali, J.G. Goodwin, Jr., J. Catal. 176 (1998) 3.

[41] M.N. Barroso, M.F. Gomez, J.A. Gamboa, L.A. Arrúa, M.C. Abello, J. Phys. Chem. Solids 67 (2006) 1583.

[42] S.D. Jones, L.M. Neal, H.E. Hagelin-Weaver, Appl. Catal. B-Environ. 84 (2008) 631.

[43] B.R. Strohmeier, D.E. Levden, R.S. Field, D.M. Hercules, J. Catal. 94 (1985) 514.

[44] F. Meyer, R. Hempelmann, S. Mathur, M. Veith, J. Mater. Chem. 9 (1999) 1755.

[45] J.S. Lee, K.H. Lee, S.Y. Lee, Y.G. Kim, J. Catal. 144 (1993) 414.

[46] G. Meitzner, E. Iglesia, Catal. Today 53 (1999) 433.

[47] T. Matsushima, J.M. White, J. Catal. 44 (1976) 183.

[48] S.H. Ali, J.G. Goodwin, Jr., J. Catal. 171 (1997) 333.

[49] S.H. Ali, J.G. Goodwin, Jr., J. Catal. 170 (1997) 265.

[50] S.H. Ali, J.G. Goodwin, Jr., J. Catal. 171 (1997) 339.

[51] J. Gao, X. Mo, J.G. Goodwin, Jr., J. Catal. 275 (2010) 211.

[52] S. Vada, J.G. Goodwin, Jr., J. Phys. Chem. 99 (1995) 9479.

[53] X.-M. Liu, G.Q. Lu, Z.-F. Yan, J. Beltramini, Ind. Eng. Chem. Res. 42 (2003) 6518.

[54] Q. Sun, Y.-L. Zhang, H.-Y. Chen, J.-F. Deng, D. Wu, S.-Y. Chen, J. Catal. 167 (1997) 92.

[55] X. Guo, D. Mao, G. Lu, S. Wang, G. Wu, J. Catal. 271 (2010) 178.

[56] I. Kasatkin, P. Kurr, B. Kniep, A. Trunschke, R. Schlögl, Angew. Chem. Int. Edit. 46 (2007).

[57] J.R. Anderson, In: Structure of Metallic Catalysis, Academic Press: London, U.K., 1975; Chapter 2.

[58] Z. Hu, J. Dong, S. Chen, S. Peng, J. Colloid Interf. Sci. 194 (1997) 332.

[59] C.V. Ovesen, B.S. Clausen, B.S. Hammershøi, G. Steffensen, T. Askgaard, I. Chorkendorff, J.K. Nørskov, P.B. Rasmussen, P. Stoltze, P. Taylor, J. Catal. 158 (1996) 170.

[60] R.N. d'Alnoncourt, M. Kurtz, H. Wilmer, E. Löffler, V. Hagen, J. Shen, M. Muhler, J. Catal. 220 (2003) 249.

[61] N.-Y. Topsøe, H. Topsøe, J. Mol. Catal. A-Chem. 141 (1999) 95.

CHAPTER SIX

THE SYNTHESIS OF HYDROCARBONS AND OXYGENATES DURING CO HYDROGENATION ON COCUZNO CATALYSTS: ANALYSIS AT THE SITE LEVEL USING MULTIPRODUCT SSITKA

This paper addresses the effect of component interaction in CoCuZnO catalysts on oxygenate synthesis during CO hydrogenation. Formation of the various products was investigated for the first time using in-situ multiproduct SSITKA. CO hydrogenation was carried out in a fixed-bed differential reactor at 250^{o}C and 1.8 atm. SSITKA results showed that Cu can decrease the activity for all products probably due to Cu blockage of the Co surface. ZnO appears to serve as a support for Co and may increase somewhat the intrinsic activities for higher oxygenates. However, the effects for Cu and ZnO with Co were not additive. The Co-Cu-ZnO combination resulted in a synergy that greatly increased selectivities for higher oxygenates by significantly decreasing the ability for hydrocarbon formation. Interestingly, the rate of synthesis for C_2 oxygenates on Co/CuZnO was identical to that on Co/Al_2O_3 - but without the high production rate of hydrocarbons.

6.1 Introduction

Higher oxygenates, especially alcohols, synthesized from syngas have been widely touted as an attractive alternative source of liquid transportation fuels. Also, because of environmental reasons, use of low molecular weight alcohols as octane enhancers for automotive fuels is now widespread [1-2]. The use of ethanol (EtOH) as an alternative fuel in automobiles has been proposed since it exhibits the same quantity of chemical energy as that of regular gasoline but with less emission of greenhouse gases as well as other pollutants [3]. In addition to the environment benefits as an alternative fuel to gasoline, EtOH has also the potential to be considered as a transportation fuel and the source of hydrogen for fuel cell applications [4-5]. The research and development of EtOH synthesis from syngas, therefore, has received much attention [6].

There are five typical classes of catalysts offering ways to prepare alcohols from syngas: (1) Rh-based catalysts [7-9]; (2) Mo-based catalysts [10-13]; (3) modified Fisher-Tropsch synthesis catalysts [14-15]; (4) modified methanol (MeOH) synthesis catalysts (by doping with alkali metal) [16-20] and (5) Co-Cu catalysts, which is a combination of (3) and (4) [21-28]. Rh-based catalysts have been found to be the most efficient catalysts for the synthesis of C_{2+} oxygenates at mild conditions of low temperature and pressure [7-8]. However, the industrial application of Rh-based catalysts is limited due to Rh's low activity and the high cost. CuZnO-based catalysts and supported Co catalysts (especially Co/Al_2O_3) are typical choices for MeOH synthesis and Fischer–Tropsch synthesis (FTS), respectively. Co-Cu catalysts were heavily researched by *Institute Français du Petrole* (IFP) in the 1980s and were considered to be potentially high

performance catalysts due to their high selectivity, ca. 70-80%, for higher oxygenate synthesis [27-29]. The elemental composition of choice for IFP Co-Cu catalysts included Cu, Co, Zn, Al, and alkali promoters. Proposed reaction conditions varied but the total pressure and reaction temperature were usually between 20-250 bar and 150-400^{o}C, respectively (preferably between 50-150 bars and 220-350^{o}C) [27]. For fixed operating conditions, the higher alcohol ($C_{2+}OH$) yield increased with the Co/Cu ratio [21]. A mechanism for the synthesis of alcohols on the series of CoCu-based catalysts was proposed by Kiennemann et al. [30], involving the interaction of formyl and formate intermediates for the synthesis of MeOH and carbene intermediates for chain growth and formation of higher alcohols.

Unfortunately, the preparation of IFP catalysts does not appear to be easily scaled up for industrial application because of a high tendency to uncontrolled decomposition of the glassy intermediate [21] and/or the difficulty of reproducible preparations because of the complexity of the preparation process. Research on Co-Cu catalysts has not been pursued significantly and knowledge about the mechanism and the effect of the different elemental components in the catalyst on catalytic performance is still limited, even though no suitable commercial higher oxygenate catalyst has yet been found.

This study is a follow-up investigation to that reported in ref. [31] by our group. The objective for ref. [31] was to probe the interactions of different components in model Co/CuZnO catalysts deduced from the IFP patents. CuZnO is a commercial MeOH synthesis catalyst, while Co is a well known and active FTS catalyst. Cu and ZnO catalyst as components in a higher oxygenate synthesis catalyst have received a great deal

of attention [1, 32-37]. The reaction results given in ref. [31] confirm that only the combination of all three components (Co, Cu and ZnO) leads to a relatively high selectivity for C_{2+} oxygenates. Steady-state isotopic transient kinetic analysis (SSITKA) was also carried out at methanation conditions to investigate the effects of the various catalyst components on CO hydrogenation activity. SSITKA is a powerful technique that provides in-situ surface kinetic information for a reaction on a heterogeneous catalyst under actual reaction conditions. SSITKA permits the estimation of the surface reaction residence times, concentrations of active intermediates, and intrinsic site activities and can help in the delineation of the surface reaction mechanism. This technique was first developed by Happel, Bennett, Biloen and Bell [38-41] in late 1970s and 1980s. In the previous study [31], the presence of ZnO and/or Cu in Co/CuZnO were found to cover/block significant numbers of active sites on Co for CO hydrogenation resulting in the significantly lower activity of the Co/CuZnO combination.

The main focus of this study was to better understand the relationships between different products at the site level. In this study, multiproduct SSITKA was utilized to further investigate the catalysts studied in ref. [31] by measuring the surface reaction parameters leading to various hydrocarbon and oxygenate products.

6.2 Experimental

6.2.1 Catalyst preparation

The catalysts used in this study were the same as used in ref. [31]. Their preparation is summarized here. Cobalt nitrate hexahydrate (Aldrich, synthetic), Copper nitrate

trihydrate (Alfa Aesar, 99.5%), and Zinc nitrate hexahydrate (Alfa Aesar, 99.998%) were used without further purification. CuZnO, CoCu and CoZnO were prepared by a precipitation method. The metal loading ratios were determined based on the optimum ratios for alcohol synthesis proposed by Arena et al. [42] and Slaa et al. [36]. Taking CuZnO as an example, the desired amounts of copper and zinc nitrate solution were mixed to produce 6 g of CuZnO catalyst. The mixture was precipitated using Na_2CO_3 solution (Na_2CO_3: H_2O = 1: 3 in volume) at room temperature. The resulting mixture was left in a fume hood overnight. The mixture was then filtered, washed for 6 times with 1 L of hot (ca. 100^oC) deionized water, dried at 120^oC for 12 h and then calcined in air at 350^oC for 4 h. CoCu and CoZnO were prepared by a similar procedure. Co/CuZnO was prepared by impregnation to incipient wetness of the prepared CuZnO using an aqueous solution of cobalt nitrate hexahydrate (1.5 mL cobalt nitrate solution/ 1 g CuZnO). The incipient wetness impregnation method was used for the combination of Co with CuZnO rather than precipitation based on a preliminary comparison of catalysts prepared by the two different methods. The results showed that Co/CuZnO prepared by impregnation exhibited higher alcohol selectivities comparing to the catalyst with the same composition but prepared by the co-precipitation method. After mixing, the solution was dried at 120^oC for 12 h before being calcined in air at 350^oC for 4 h (ramp rate to 350^oC of 10^oC/min). Co/γ-Al_2O_3 (Alfa-Aesar, γ-phase, 99.98%) with 10 wt% Co was also prepared by the incipient wetness impregnation method for comparison purposes, the preparation procedure is described in detail elsewhere [43].

6.2.2 Catalyst characterization

Although XRD was carried out in our previous study for the investigation of structure and crystallite size for the calcined catalysts, the actual oxidation state and crystallinity for Cu-containing Co catalysts after reduction were not clear. XRD was performed in this study to identify the phases and crystallinity of Cu-containing Co catalysts (CoCu and Co/CuZnO) after reduction. The reduced form of Co is well known to give the active sites for Fischer-Tropsch synthesis [44]; thus, it is necessary to activate Co catalysts by reduction prior to reaction. However, the oxidation potential of highly dispersed reduced cobalt metal exposed to air and the high exothermicity of this oxidation would cause the degradation of a reduced Co catalysts exposed to air by sintering and would be a potential fire hazard [45]. Therefore, passivation of the surface is necessary to prevent rapid oxidation upon exposure to air. Therefore, reduction followed by passivation was carried out prior to XRD measurements. The catalysts were reduced in-situ in a differential fixed bed reactor at 300^{o}C in H_2 (30 mL/min) for 1 h using a ramp rate of 5^{o}C/min. Following the reduction, the catalysts were flushed by inert gas (He, 30mL/min) as the temperature decreased to room temperature, and then passivated with 2% O_2/Ar (4 mL/min) for 1 h at room temperature. X-ray diffraction patterns for the catalysts after pretreatment were collected in a Scintag XDS 2000 θ/θ powder X-ray diffractometer (XRD) using Cu Kα1/Kα2 (λ=1.540592 Å and 1.544390Å, respectively) radiation and a step size of 0.03^{o} in the 2θ range of 5-70^{o}.

6.2.3 CO hydrogenation

The reaction system setup is shown in Figure 6.1. CO hydrogenation was carried out in a differential fixed-bed reactor with a maximum conversion below 10% in order to minimize concentration and temperature gradients. A catalyst sample (0.05 g for CoZnO and Co/Al_2O_3; 0.3 g for other catalysts) with 3 g of an inert powder (α-alumina) were mixed and used to avoid channeling effects and hot spots. The samples were then loaded between quartz wool plugs in the middle of the reactor and the temperature was observed by a thermocouple positioned close to the catalyst bed. The reaction lines and the sampling valves were kept at ca. 200°C by wrapping with heating tape to avoid condensation of oxygenate and higher hydrocarbon products. A Varian 3380 GC equipped with a flame ionization detector (FID) and a thermal conductivity detector (TCD) was used to analyze the effluent samples on-line. A Restek RT-QPLOT column (I.D. 0.53 mm and length 30 m) connecting to an FID was capable of separating and detecting C_1-C_7 hydrocarbons and oxygenates, while a Restek HayeSep® Q column (I.D. 3.18 mm and length 1.83 m) connecting to a TCD was used for the separation and detection of CO and other inorganic gases.

Prior to the reaction, the catalyst was reduced in-situ at 300°C with a ramp rate of 5°C/min under 30 mL/min of H_2 for 1h at 1atm, and then cooled down to the reaction temperature of 250°C. After reduction, the reaction started as the gas flow was switched to a CO-H_2-He mixture (95%CO + 5%Ar: 9 mL/min; H_2: 18 mL/min; He: 3 mL/min) at a constant pressure of 1.8 atm. A H_2/CO ratio of 2:1 was applied for a preferable condition of EtOH production [7, 46]. Although the selectivities of oxygenates may be greater at

more suitable conditions (e.g., lower reaction temperature and higher pressure), current reaction conditions were chosen in order to maximize the formation of C_1-C_2 products, especially C_{2+} oxygenates, for the purpose of easily detection by MS [7]. The conditions of reaction used for the catalysts in this study were also found (data not shown) to result in no mass or heat transfer effects on the reaction kinetics measured. The reaction reached a pseudo-steady state after 15 h TOS (time-on-stream). The identification and calibration of the products were achieved using standard gases [alkanes (C_1-C_7), alkenes (C_2-C_7) and oxygenates (MeOH, EtOH, 1-propanol, 1-butanol, acetaldehyde and acetone), Scott Specialty Gases]. The selectivity (C atom%) for a specific product was calculated based on carbon efficiency using the formula $n_iC_i/\Sigma n_iC_i$, where n_i and C_i represent the carbon number and molar concentration of the *i*th product, respectively.

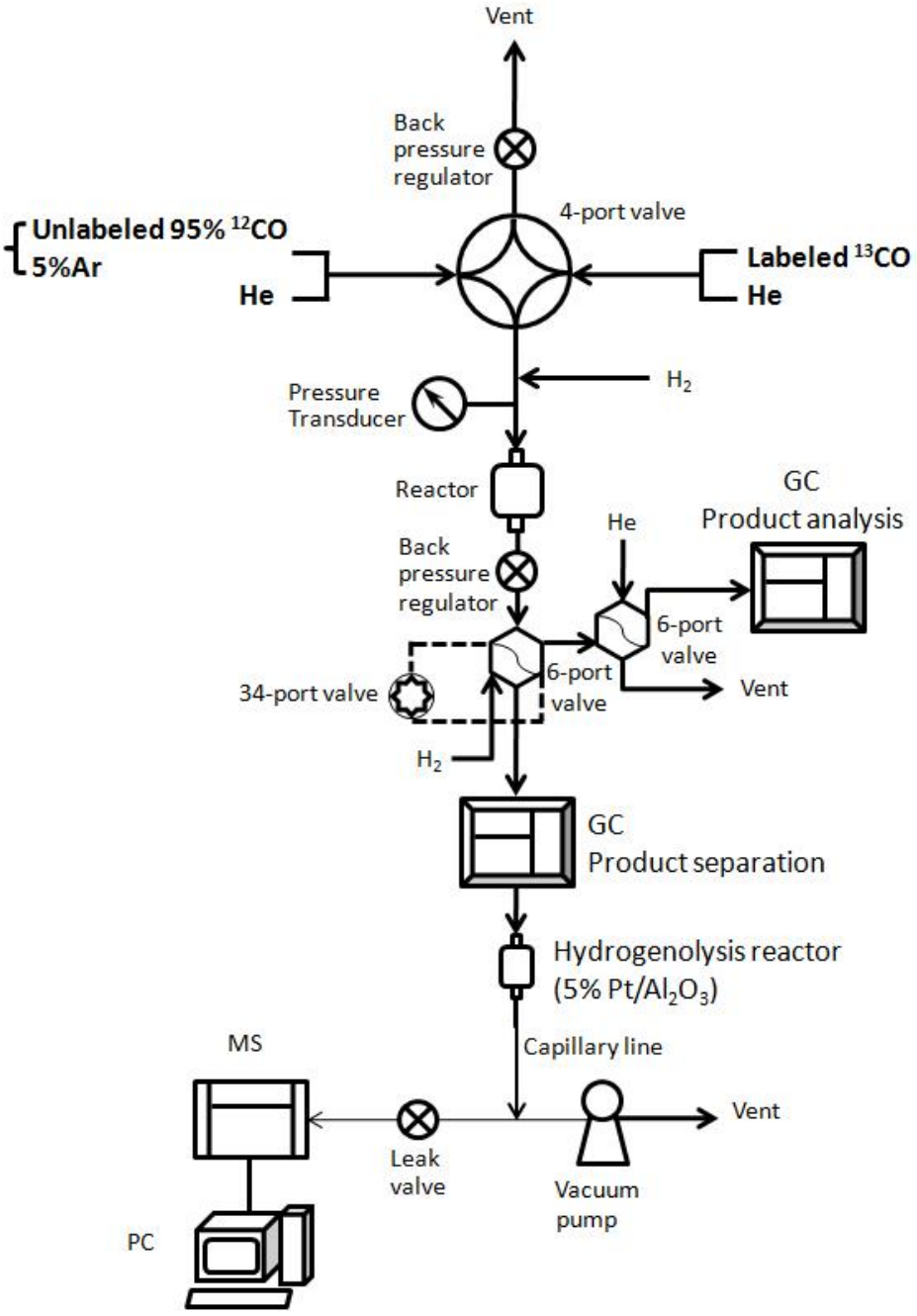

Figure 6.1 The reaction system for multiproduct SSITKA.

6.2.4 SSITKA

Surface reaction measurements were carried out after reaction steady-state was reached. During SSITKA measurements (Figure 6.1), a switch between 95% ^{12}CO + 5% Ar (National Specialty Gases) and ^{13}CO (Isotec, 99%) was made using a Valco 2-position valve with an electric actuator without disturbing any other reaction conditions. That is, the reaction total flow rate and the total pressure for the two gas feed streams were maintained at constant values during the switch. Two back pressure regulators in the reaction system were used to minimize any pressure disturbance during the switch. The gas-phase holdup time was determined by using 5% Ar in the unlabelled ^{12}CO stream as an inert tracer.

Direct isotopic analysis by mass spectroscopy (MS, Pfeiffer Vacuum) was difficult due to fragmentation and overlapping of the heavier hydrocarbons/oxygenates. To avoid this, products heavier than CH_4 were converted to CH_4 prior to MS analysis. Thus, a Valco 34-port auto-sampling valve was employed to collect 16 effluent samples during the 5-min-period of the isotopic transients after a switch. The collected effluent samples were injected into and separated by a GC equipped with an RT-QPLOT column. Thirty cc/min of H_2 was used as the carrier gas and as a source of H_2 for the subsequent hydrogenolysis. After separation, the products were fed into a hydrogenolysis/hydrogenation reactor containing 5 g of Pt/Al_2O_3 held at 400^oC to convert hydrocarbons and oxygenates to CH_4. The resulting CH_4 was subsequently injected into the MS equipped with a high-speed data acquisition system for analysis. The isotopic

concentration detected by MS could be applied for further interpretation to the specific products collected in the sample loops of the 34-port valve.

Figure 6.2 shows a typical set of normalized isotopic transients of CH_4, C_2H_n, MeOH, AcH and EtOH obtained by switching from ^{12}CO to ^{13}CO for Co/CuZnO at steady-state. Surface reaction parameters for the intermediates of CH_4, C_2H_n, MeOH, AcH and EtOH were determined from the isotopic transient curves for the specific species by SSITKA data analysis software. The areas between the normalized transients of the corresponding species and the inert tracer Ar are equal to the average surface residence times (τ_i) of the reactive species. The concentration of active surface intermediates for a specific product can be determined by $N_i = Rate_i * \tau_i$ [47-48]. A major improvement of this methodology (multiproduct SSITKA) is that surface reaction parameters can be determined for the various products, without the common MS analysis problem caused by fragmentation or overlapping of different products.

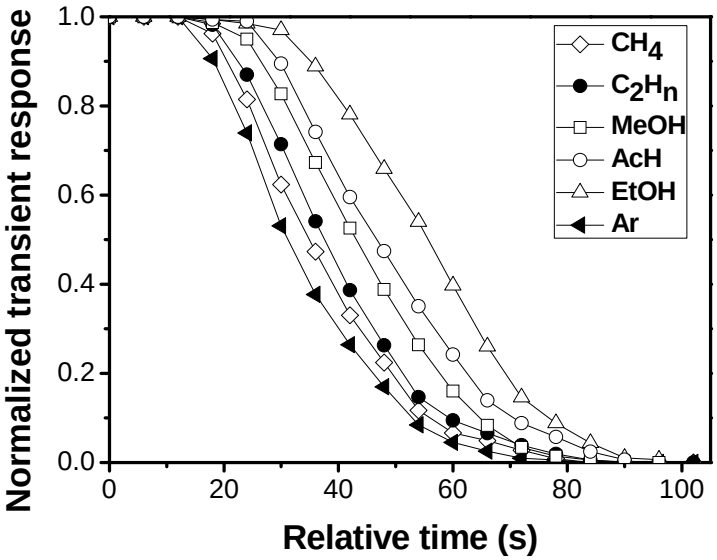

Figure 6.2 Typical normalized SSITKA transient responses for ^{12}C in CH_4, C_2H_n, MeOH, AcH, EtOH and for Ar, following a $^{12}CO//^{13}CO$ switch during steady-state for CO hydrogenation on Co/CuZnO.

6.3 Results

6.3.1 Catalyst preparation

The basic characterizations such as BET surface area, pore volume, average pore size and elemental analysis were carried out and performed earlier [31] but the results are given here in Table 6.1 for completeness. Table 6.1 also shows the preparation method and composition for the various catalysts. CoZnO showed a significantly higher BET surface area than the copper containing catalysts since Cu/CuO provides very limited surface area [49]. Co/Al_2O_3 exhibited a similar BET surface area and pore volume to that of CoZnO. The average pore sizes, however, were pretty similar for all catalysts.

Table 6.1 Composition, preparation method, BET surface area, pore volume and average pore size of the catalysts studied (from [31]).

Catalyst	Co (wt%)[a]	Molar ratio[a]	Preparation method[b]	BET surface area (m^2/g)[d]	Pore volume (cm^3/g)[e]	Average pore size (nm)[e]
Co/Al_2O_3	10	-	impregnation	102.0	0.60	25.8
CuZnO	-	Cu:Zn = 2.5:1	co-precipitation	29.8	0.13	30.5
CoZnO	30.4	Co:Zn = 1.1:1	co-precipitation	96.4	0.57	29.7
CoCu	18.8	Co:Cu = 1.0:2.5	co-precipitation	43.9	0.26	25.6
Co/CuZnO	16.5	Co:Cu:Zn = 1.1:2.5:1	Impregnation co-precipitation[c]	21.1	0.12	22.1

[a] Based on elemental analysis.
[b] All catalysts were calcined at 350°C in static air after preparation.
[c] CuZnO was first prepared by co-precipitation followed by calcination at 350°C. Then, Co was added to CuZnO by the impregnation method, followed by calcination at 350°C.
[d] Max error = ± 5%
[e] Max error = ± 10%

Figure 6.3 shows XRD patterns for the reduced and passivated catalysts contained Co and Cu (CoCu and Co/CuZnO). XRD characterization for the as-prepared calcined catalysts is given in our previous study [31]. However, the structure and crystallite sizes for Co and Cu after reduction may be more meaningful for understanding these catalysts. As can be seen, the peaks corresponding to metallic Cu (ICDD 040836) were prominent for both catalysts. The metallic Cu peaks presented for both catalysts could be attributed to face-centered cubic Cu [50-51]. Cu oxide structures, in both Cu_2O (ICDD 030892) and CuO (ICDD 741021) forms, could be identified for Co/CuZnO, but the peak intensity was much stronger for CuO than that for Cu_2O. No discernable Co-related peaks could be observed for CoCu, which may indicate that Co is X-ray amorphous (i.e., highly dispersed) for this catalyst. It is known that Co and Cu metals do not alloy [50-52].

Co/CuZnO, however, exhibited distinguishable diffraction peaks for Co_3O_4 (ICDD 421467). It should be noted that the species of Cu_2O, CoO and Co_3O_4 all display a diffraction peak at about 36.5°, resulting in difficulty in identifying the XRD patterns for these individual compounds at this location [53]. The possibility of the presence of a Cu-Co oxide spinel structure could not be ruled out due to a distinct shoulder peak at about 44° [54]. However, it is difficult to identify Cu-Co oxide spinel by other diffraction peaks due to the overlap of these diffraction peaks with Cu_2O, CoO and Co_3O_4 at about 32° and 37°. A weak peak which can be attributed to ZnO (ICDD 890511) could be observed for Co/CuZnO. A significant difference for the XRD results of as-prepared and reduced passivated Co-Cu containing catalysts is the presence of metallic Cu, which is consistent with what has been reported by Llorca et al. [52], i.e., that metallic copper aggregates exist with highly dispersed cobalt as inferred from their XRD, TEM and XPS results. The results are also in line with our previous TPR results that reduction of Cu oxide occurs at a relatively low temperature (< 250°C) [31]. The average crystallite size can be estimated by applying the Scherrer equation. Reduced Co/CuZnO had an average crystallite size of 13.2 nm for Co_3O_4. This value is pretty much the same as the value (14.6nm) obtained for the calcined Co/CuZnO [31].

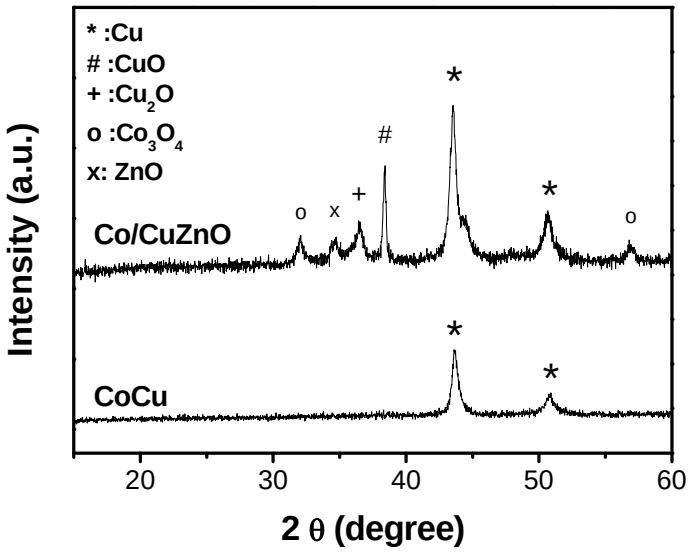

Figure 6.3 Power XRD patterns for the reduced and passivated CoCu and Co/CuZnO catalysts.

6.3.2 CO hydrogenation

Table 6.2 summarizes the results for CO hydrogenation at 250^{o}C and 1.8 atm. The steady-state rates were measured after 15 h TOS. Activities are compared on both a per catalyst weight basis and per cobalt weight basis. It can be seen that CoZnO exhibited the highest reaction rate among all the catalysts on a "per catalyst weight" basis. However, Co/Al_2O_3 showed a higher activity than CoZnO on a "per Co weight" basis. All Cu-containing catalysts exhibited significantly lower reaction rates (1-2 orders of magnitude) than Co/Al_2O_3 and CoZnO. The catalytic activity for all catalysts in this study followed the same trend (CoZnO > Co/Al_2O_3 > CoCu > CuZnO ~ Co/CuZnO) as found in our previous study [31].

With respect to the product selectivity, it can be seen from Table 6.2 that Co/Al_2O_3, CoZnO and CoCu exhibited similar results. Most products for the three catalysts were hydrocarbons but with somewhat different distributions. The total oxygenate selectivities for the three catalysts were all lower than 5%. CuZnO produced mainly MeOH (99.3%) as expected. The low activity and high MeOH selectivity is typical for CuZnO. Co/CuZnO catalyst exhibited a product distribution completely different from the other catalysts. The selectivity for oxygenates was nearly 60%, including 30.1% C_2 oxygenates (EtOH and ACH). The results are similar to what has been found previously for alkali promoted or unpromoted Co/CuZnO catalysts with selectivities of 30-70 % for alcohols and 30-50% for EtOH [2, 55-56]. Thus, only the combination of Co, Cu and ZnO resulted in a high selectivity for C_{2+} oxygenates.

Table 6.2 Catalytic properties of the various catalysts for CO hydrogenation at steady-state[a].

Catalyst	Rate[b] (μmol C/g-cat/s)	Rate (Co basis)[b] (μmol C/g-Co/s)	Selectivity[c] (C-atom %)					
			CH_4	$C_{2+}HC$[d]	MeOH	AcH[e]	EtOH	Other C_{2+} oxy.[f]
Co/Al_2O_3	6.90	69.0	47.1	51.3	1.0	-	0.4	0.2
CuZnO	0.08	-	0.7	-	99.3	-	-	-
CoZnO	8.97	29.5	37.4	59.6	0.7	0.6	1.0	0.7
CoCu	0.20	1.06	25.4	70	1.2	0.7	2.0	0.7
Co/CuZnO	0.10	0.61	16.4	23	18.2	4.2	25.9	12.3

[a] Catalyst: 0.3 g; Inert : 3 g α-alumina; Reduction at 300°C; Reaction conditions: T = 250°C, P = 1.8 atm; Flow rate = 30mL/min (H_2:CO:He =18:9:3); Data were taken at TOS = 15 h.
[b] Max. error = ± 5% of all the values measured.
[c] Molar selectivity = carbon efficiency = $n_iC_i / \sum n_iC_i$.
[d] Hydrocarbons with 2 or more carbons.
[e] AcH refers to acetaldehyde.
[f] Oxygenates with 2 or more carbons.

6.3.3 SSITKA

Multiproduct SSITKA measurements permitted the determination of how different combinations of Co, Cu and ZnO species affect the surface reaction parameters, including the surface reaction residence times (τ_i) and surface concentrations of intermediates (N_i) for the different products. The methods used to estimate the surface reaction parameters have been reported in detail elsewhere [7, 48, 57]. Table 6.3 shows the surface reaction residence times (τ_i) for different products on the various catalysts studied. Space time had little or no effect on the τ_i's for the hydrocarbons. However, the average surface reaction residence times of MeOH, AcH (acetaldehyde) and EtOH changed with different space times (not shown). This is due to the significant readsorption of these products in the catalyst bed and the resulting chromatographic effect, as reported in previous papers from our group [7, 58-59]. Figure 6.4 shows how the average residence times of MeOH, AcH and EtOH for Co/CuZnO linearly increased with increasing space time. Similar phenomena were observed for all catalysts in this study which produced these oxygenates. Readsorption effects, therefore, have to be taken into consideration before any further interpretation of SSITKA data. More accurate estimation of τ_i (τ^0_i) can be obtained by correcting for readsorption by extrapolating the value of τ_i to 0 space time. The corrected values of τ_i (τ^0_i), N_i (N^0_i) and TOF_{ITK} (TOF^0_{ITK}) are shown in Table 6.3 (see footnotes to Table 6.3 for how N^0_i and $TOF^0_{ITK,I}$ were calculated). The corrected values for reversibly adsorbing CO and hydrocarbons were identical with the values measured due to minimal readsorption. Later discussion will focus only on the corrected surface reaction

parameters rather than the uncorrected ones because the former reflect the synthesis and are not complicated by readsorption effects.

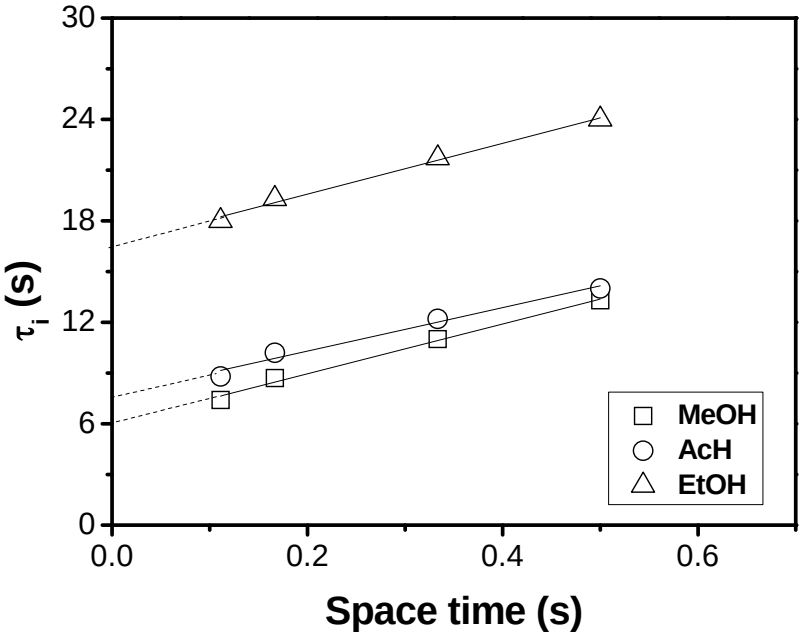

Figure 6.4 τ_{MeOH}, τ_{AcH} and τ_{EtOH} vs. space time during steady-state for CO hydrogenation on Co/CuZnO.

TOF^0_{ITK}, which is the reciprocal of τ^0_i, is a reasonable estimate of site turnover frequency. It is equal to R_i/N^0_i with units of s^{-1} [48]. It can be seen from Table 6.3 that the intrinsic activities for each individual product for all catalysts followed the same trend: $TOF^0_{CH4} > TOF^0_{C2Hn} > TOF^0_{MeOH} > TOF^0_{AcH} > TOF^0_{EtOH}$. However, the differences between the TOF^0_i's were significant, both among products and among catalysts. CH_4 and C_2H_n had relatively larger TOF^0_{ITK}, which is not surprising for catalysts producing mostly hydrocarbons, such as Co/Al_2O_3, CoZnO and CoCu. However, CuZnO and

Co/CuZnO, which produced primarily oxygenates, showed similar values for TOF^0_{CH4} and TOF^0_{C2Hn} as found for the catalysts producing mainly hydrocarbons. The TOF^0_i's for CH_4 and C_2H_n measured for the catalysts in this study were relatively greater than those reported for Rh-based catalysts [7], which may indicate a better capability for hydrocarbon production on these catalysts. As to the intrinsic activities for oxygenates, the TOF^0_i for MeOH was slightly larger for CuZnO (0.24 s^{-1}) than for the other catalysts. The TOF^0_{AcH}'s were very similar for CoZnO and Co/CuZnO, while CoCu exhibited a smaller one. TOF^0_{EtOH}'s were much lower than those of other products, which was ca. 0.05 s^{-1} for all catalysts except CoZnO (0.12 s^{-1}).

The corrected surface concentrations of intermediates (N^0_i) are also shown in Table 6.3. This is the number of active intermediates on the surface and can be regarded as an approximation of the number of active sites producing a particular product i. Although τ^0_i's for a specific product were similar to a large degree, N^0_i's changed dramatically from catalyst to catalyst. With respect to the formation of C_1-products (CH_4 and MeOH), N^0_{CH4} for Co/Al_2O_3 and CoZnO were about two orders of magnitude greater than those for other catalysts, not surprising since they were also the most active in making hydrocarbons. N^0_{MeOH} for the different catalysts followed the trend of Co/Al_2O_3 ~ CoZnO ~ CuZnO > Co/CuZnO > CoCu. It should be noted that although Co/Al_2O_3 and CoZnO had very small selectivities for MeOH, the surface concentrations of MeOH intermediates were comparable to that for CuZnO, which primarily produced only MeOH. C_{2+} products included C_2H_n, AcH and EtOH in this study. Similar to N^0_{CH4}, N^0_{C2Hn}'s for Co/Al_2O_3 and CoZnO exhibited values two orders of magnitude higher than for other

catalysts. It should be noted that N^0_{CH4}'s were less than N^0_{C2Hn}'s for all catalysts except CuZnO. The difference between N^0_{CH4} and N^0_{C2Hn} was larger for CoZnO than for Co/Al_2O_3, indicating the higher potential of chain growth for hydrocarbons on CoZnO (see selectivities in Table 6.2). N^0_{AcH} and N^0_{EtOH} followed the same order for catalysts which could produce both AcH and EtOH: CoZnO > Co/CuZnO > CoCu. N^0_{AcH} for CoZnO was more than one order of magnitude greater than for the other two catalysts. Although N^0_{EtOH} had the same trend as N^0_{AcH} for the three catalysts, the differences between the values were not identical. The value of N^0_{EtOH} for CoZnO was almost twice and one order of magnitude larger than those for Co/CuZnO and CoCu, respectively.

Table 6.3 Uncorrected and corrected surface reaction parameters for CO hydrogenation on the various catalysts measured by SSITKA[a].

Product[i] (or reactant)	Rate[b] (μmol C/g/s)	Selectivity[c] (C-atom %)	τ_i[d] (s)	τ^0_i[e] (s)	TOF^0_{ITK}[f] (s^{-1})	N^0_i (μmol/g-cat.)
Co/Al_2O_3						
CO	44.6	-	1.5	1.5	-	67.0
CH_4	3.25	47.1	2.1	2.1	0.48	6.82
C_2H_n[h]	3.54	51.3	3.3	3.3	0.30	11.7
MeOH	0.07	1.0	6.2	4.6	0.21	0.32
AcH	-	-	-	-	-	-
EtOH	0.03	0.4	19.7	17.4	0.06	0.48
CuZnO						
CO	7.4	-	2.2	2.2	-	16.4
CH_4	0.0005	0.7	3.6	3.6	0.28	0.001
C_2H_n[h]	-	-	-	-	-	-
MeOH	0.076	99.3	6.4	4.1	0.24	0.31
AcH	-	-	-	-	-	-
EtOH	-	-	-	-	-	-
CoZnO						
CO	44.6	-	1.2	1.2	-	53.6
CH_4	3.35	37.4	1.5	1.5	0.67	5.03
C_2H_n[h]	5.35	59.6	3.6	3.6	0.28	19.1
MeOH	0.06	0.7	6.2	4.9	0.20	0.31
AcH	0.05	0.6	7.2	6.1	0.16	0.33
EtOH	0.09	1.0	9.4	8.0	0.12	0.72
CoCu						
CO	7.4	-	1.6	1.6	-	11.9
CH_4	0.051	25.4	2.0	2.0	0.50	0.10
C_2H_n[h]	0.140	70.0	3.4	3.4	0.29	0.48
MeOH	0.002	1.2	9.6	6.9	0.14	0.02
AcH	0.001	0.7	12.3	9.9	0.10	0.01
EtOH	0.004	2.0	23.6	20.2	0.05	0.08
Co/CuZnO						
CO	7.4	-	2.4	2.4	-	17.9
CH_4	0.016	16.4	3.5	3.5	0.29	0.06
C_2H_n[h]	0.023	23.0	5.0	5.0	0.20	0.12
MeOH	0.018	18.2	8.7	6.0	0.17	0.11
AcH	0.004	4.2	10.2	7.7	0.13	0.03
EtOH	0.026	25.9	19.3	16.6	0.06	0.42

[a] Co/Al_2O_3 and Co/ZnO: 0.05g, other catalysts: 0.3 g; Inert : 3 g α-alumina; Reduction at 300°C; Reaction conditions: T = 250°C, P = 1.8 atm; Flow rate = 30mL/min (H_2:CO:He =18:9:3); Data were taken at TOS = 15 h. All reactions were carried out at differential conversions with % CO conversion < 5%.
[b] At Steady-state rate.
[c] Molar selectivity = carbon efficiency = $n_iC_i / \sum n_iC_i$.
[d] Uncorrected surface residence time of intermediates.
[e] Corrected surface residence time of intermediates.
[f] $TOF^0_{ITK,\,i} = 1/\tau^0_i$.
[g] $N_i = Rate_i * \tau_i$.
[h] Hydrocarbons with 2 carbons.
[i] Experimental errors of all the results for CH_4 and C_2H_n are ± 10%; experimental errors of all the results for MeOH, AcH and EtOH are ±15%;

6.4 Discussion

There have been very few studies focusing on the mechanism of chain growth and formation of higher oxygenates on CoCuZnO-based catalysts, due in part to the complexities associated with multi-component catalysts and higher oxygenate synthesis. More insight into reaction at the site level, however, was obtained by this study using CO hydrogenation on different systematic combinations of the Co, Cu and ZnO components (CoCu, CoZnO and Co/CuZnO).

Before discussion of the various CoCuZnO-based catalysts, the results for CuZnO and Co/Al_2O_3 will be discussed first. As seen in Table 6.3, a low activity of CuZnO for CH_4 was observed and was reflected a low surface concentration of active CH_4 intermediates (N^0_{CH4}), or CH_4 formation sites. CuZnO had a three orders of magnitude higher concentration of MeOH intermediates than CH_4 ones - the source of its high MeOH selectivity and its CO hydrogenation activity. This activity was still two orders of magnitude lower than the overall activity of Co/Al_2O_3. However, CuZnO has been shown to exhibit a higher intrinsic activity and a higher amount of active surface intermediates for MeOH synthesis when compared to other Cu- or ZnO- based catalysts, even Cu- or ZnO-based catalysts supported on Al_2O_3 and expected to have much better active catalyst dispersions [60]. The result for CuZnO is an indication of the synergy between Cu and ZnO species to form active sites for MeOH synthesis. However, it should be noted that the TOF^0_{ITK}'s for CH_4 and MeOH were similar on CuZnO. However, CuZnO makes little CH_4 because of having few CH_4 formation sites (active surface intermediates).

Most products of CO hydrogenation on Co/Al_2O_3 at the reaction conditions used in this study were hydrocarbons, as expected (Tables 6.2 and 6.3). The total selectivity for oxygenates was less than 2%. TOF^0_{ITK} for MeOH and EtOH were approximately 50% and 10%, respectively, of that for CH_4, indicating that the rates of formation of MeOH and EtOH on the sites were slower than that for CH_4. Because of that and more importantly the greater (order of magnitude) concentration of CH_4 active intermediates, the selectivity for CH_4 was 50 times and two orders of magnitude greater than that for MeOH and EtOH, respectively. Similar observations were also found for higher hydrocarbons. Even though most products made by Co/Al_2O_3 were hydrocarbons, it is noteworthy that its ability to produce MeOH, based on site activity (TOF^0_{ITK}) for MeOH and concentration of active MeOH intermediates (N^0_{MeOH}) was comparable as to that of CuZnO. Thus, Co/Al_2O_3 was technically as good a MeOH synthesis catalyst in terms of rate as CuZnO under these reaction conditions. This ability is just not usually noted due to the greater activity of Co/Al_2O_3 for the synthesis of hydrocarbons which results in a low selectivity for MeOH. The TOF^0_{ITK} for EtOH was the lowest for all the products made by Co/Al_2O_3.

Table 6.2 shows that the combinations of CoCu and Co/CuZnO (Cu-containing Co catalysts) exhibited very low activities relative for Co/Al_2O_3, but the combination of CoZnO led to a very high activity for CO hydrogenation. In addition, their product distributions were significantly different from each other. Although CoCu and CoZnO both produced primarily hydrocarbons (> 95%), CoCu produced slightly larger and smaller fractions of C_{2+} hydrocarbons and CH_4, respectively, than CoZnO did. Both

CoZnO and CoCu had less than 5% selectivities for the formation of oxygenates. Co/CuZnO, however, produced about 60% oxygenates with 30.1% C_{2+} oxygenates (EtOH and ACH).

The low activities for the Cu-containing catalysts are perhaps somewhat surprising on one hand since Cu has been widely suggested to provide the main active sites for MeOH synthesis [61-62] and for higher oxygenate synthesis [63-64]. Cu is also a well known reduction promoter for Fe-based FTS catalysts [65] and also decreases the temperature required for Co reduction [31]. Several studies have found that the activity for CO hydrogenation did not change much with the addition of Cu to Co while the selectivity altered significantly [21, 66]. Our XRD profiles showed that Co-species were X-ray amorphous and likely highly dispersed in the CoCu catalyst even without a refractory oxide support. Therefore, the low activity of CoCu could be possibly due to factors other than Co dispersion. Several factors have been proposed [31, 64, 67] that may explain this seeming contradiction between the present study and some others. The most important could be the effective blockage of potentially FTS active sites on the Co surface by Cu as well as Cu aggregation due to high loadings of Cu (> 20% in the Cu-containing catalysts in this study). Other factors, such as different preparation methods or different compositions, especially the presence of alkali species [21, 66], may also play a role.

By comparing the multiproduct SSITKA results for Co/Al_2O_3 and CoCu, it can be seen that the intrinsic activities (TOF^0_{ITK}) in making hydrocarbons and higher oxygenates were very close (within experimental error) for the two catalysts, except that CoCu had a

better ability to produce AcH. The tremendous difference in reaction rates for the two catalysts (Co/Al_2O_3 >> CoCu) was due to the large difference in the concentration of active surface intermediates (N^0_i) for both hydrocarbons and higher oxygenates.

It would appear that the presence of ZnO (in CoZnO) may have somewhat enhanced the site activities (TOF^0_{ITK}) for making CH_4 and higher oxygenates (compared to Co/Al_2O_3). The increased rates for higher oxygenate formation (relative to Co/Al_2O_3) was due to both higher intrinsic activities (TOF^0_{ITK}) and greater surface concentrations of active sites (N^0_i). The formation rates for higher hydrocarbons were also relatively higher for CoZnO than Co/Al_2O_3 because of having more intermediates/active sites. It would appear that ZnO acted as a support for Co, permitting a reasonable Co dispersion and leading to the presence of a higher concentration of hydrocarbon and oxygenate producing sites on a per g catalyst basis. Similar observations about ZnO have also been made previously for Cu-based catalysts [60, 68].

Co/CuZnO exhibited a very low activity for CO hydrogenation, like CoCu. Comparing Co/Al_2O_3 and Co/CuZnO, while the concentrations of intermediates/sites (N^0_i) for C_{2+} oxygenates were essentially the same for both catalysts, the concentrations of intermediates/sites for hydrocarbons were reduced by two orders of magnitude. It was this loss of sites for hydrocarbons, not a loss of activity by the sites, that appears to have caused the shift in selectivity towards higher oxygenates (and also MeOH) when CuZnO was combined with Co. Intriguingly, the rate of oxygenate synthesis on Co/CuZnO is similar to that on Co/Al_2O_3. However, this fact is not usually noticed since the rates are so low relative to that for hydrocarbons on Co/Al_2O_3. The possible synergy of Co, Cu

and ZnO appear to decrease hydrocarbon formation relative to oxygenate formation. The dramatic decrease for surface concentration of hydrocarbons is probably not just due to blockage by Cu of Co since it is hard to argue that somehow Cu or CuZnO would only block hydrocarbon formation without also blocking sites for oxygenate formation. It should be noted that N^0_{CO}, the coverage of reversibly adsorbing CO during reaction as determined by SSITKA, was about 4 times greater for Co/Al_2O_3 than Co/CuZnO, indicating further the lower dispersion of Co (less exposed Co surface atoms) for the latter catalyst. CO coverage of Co during reaction as determined by SSITKA has been shown to be very representative and similar to typical chemisorption measurements for Co catalysts used to determine Co dispersion [69].

Figure 6.5 shows a simplified schematic of the proposed mechanism for the formation of hydrocarbons and oxygenates for CO hydrogenation on Co/CuZnO [30]. CO possibly adsorbs on two different types of sites and reacts with adsorbed hydrogen to produce MeOH or hydrocarbons and higher oxygenates, respectively [as shown in Fig. 5, paths (I) and (II)]. The significant increase in selectivity for MeOH formation on Co/CuZnO comparing to Co/Al_2O_3 could be due to the synergy of Cu and ZnO species (CuZnO), which has been confirmed to produce mostly MeOH, as shown in Figure 6.5, path (I). In Co/CuZnO, 83 wt% of the catalyst was CuZnO in the identical proportions as in the CuZnO catalyst. However, some CO must adsorb on Co sites and produce hydrocarbons. The hydrocarbon intermediates must be able to further react to form C_{2+} oxygenates by insertion of a CH_xO-species from the synergy between Co, Cu and ZnO species, as shown in Figure 6.5 (II). In addition, the lower TOF^0_{ITK}'s for C_{2+} oxygenates

than hydrocarbons could be another indication that higher oxygenates are formed from hydrocarbon intermediates.

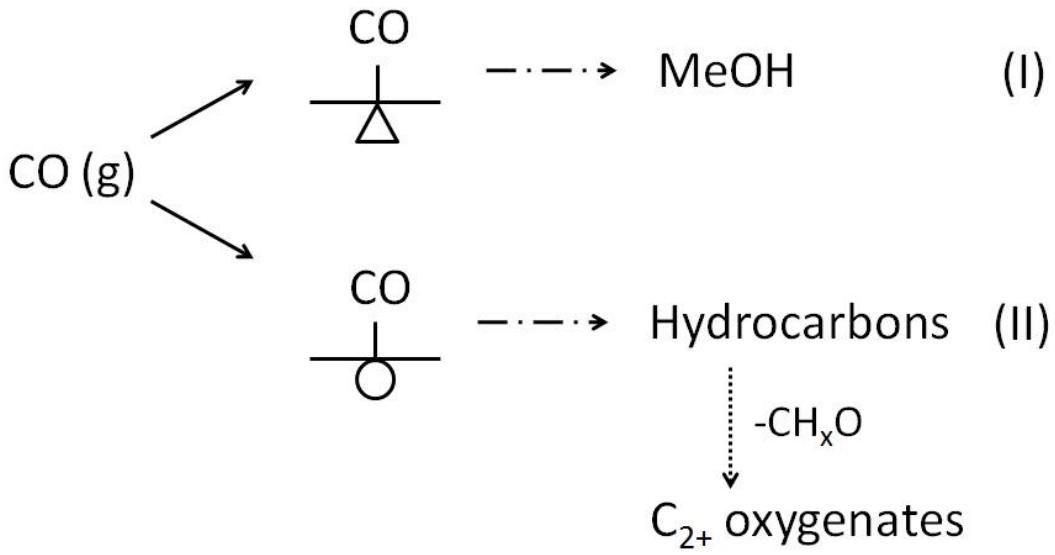

Figure 6.5 A simplified schematic of the proposed mechanism [30] for CO hydrogenation on a Co/CuZnO catalyst.

Although CoCu, CoZnO and Co/CuZnO had very different product distributions, their TOF^0_{ITK}'s for specific products were reasonably similar (the differences are less than 50% with some being within experimental error). TOF^0_{ITK}'s for CH_4 followed a trend of CoZnO > CoCu > Co/CuZnO, which was the same as that found for SSITKA at methanation conditions [31]. These results show that ZnO possibly increased the site activity for CH_4 formation compared to Al_2O_3-supported Co, but Cu did not.

In summary, the effects Cu and ZnO have on a Co catalyst were observed in this study. The addition of Cu decreased the overall activity, which may be mainly due to the blockage by Cu of the Co surface, resulting in small values of N^0_i for CoCu and Co/CuZnO. The presence of ZnO appeared to increase the site activities for C_{2+}

oxygenates, which was reflected by increasing TOF^0_{ITK}'s. However, ZnO also appeared to serve to help maintain Co dispersion leading to large values of N^0_i as well. The combination of Co, Cu and ZnO seemed to combine some of the effects from both Cu and ZnO, such as the decrease of the hydrocarbon formation and the maintenance of the ability for oxygenate formation. However, the effects of Cu and ZnO on Co were not additive, which could be due to the occurrence of new synergies between the three components Co-Cu-ZnO.

6.5 Conclusions

The relationships between the hydrocarbon and oxygenate products during CO hydrogenation on CoCuZnO-based catalysts were investigated for the first time at a site level using multiproduct SSITKA. By comparing the SSITKA results for the various catalysts, several conclusions can be made about the combination of Co with Cu and/or ZnO:

(1) Cu alone acts to decrease activity of Co for all products, probably by blockage of the Co surface. Cu does not affect the intrinsic activities for either hydrocarbon or oxygenate formation based on the TOF^0_{ITK}'s.

(2) ZnO alone acts as a support (dispersion agent), keeping Co highly dispersed and very active for hydrocarbon synthesis. It appears to also possibly increase the site activities for C_{2+} oxygenates.

(3) The combination of Cu and ZnO with Co appears to be able to maintain the oxygenate synthesis ability of highly dispersed Co (such as for Co/Al_2O_3) while

simultaneously decreasing its ability to make hydrocarbons by loss of hydrocarbon synthesis sites.

Previous studies [21, 30] proposed that the combination of Co with CuZnO could effectively increase the selectivities for higher oxygenates due to the C_1-oxygenate sites ($-CH_xO$) contributed by CuZnO. Higher alcohols were hypothesized to be formed through the reaction of a hydrocarbon species and a C_1-oxygente entity. The results from this study, however, indicate that Co (in the form of Co/Al_2O_3) already makes oxygenates including higher oxygenates. This fact tends to be overlooked due to the high hydrocarbon activity of Co/Al_2O_3. In combination with CuZnO, the hydrocarbon activity is so diminished that this oxygenate formation ability become significant not in terms of high activity but rather in terms of high selectivity. Although in absolute terms, the rate of formation of C_{2+} oxygenates was identical on Co/Al_2O_3 and Co/CuZnO, it is hard to argue the partial blockage by Cu of the Co surface decreases the hydrocarbon formation rate by two orders of magnitude without affecting C_{2+} oxygenate synthesis. Thus, synergy between Co-Cu-ZnO cannot be ruled out and perhaps takes a form that in essence decreases hydrocarbon desorption before/without $–CH_xO$ insertion. However, it is interesting that the formation rate of C_{2+} oxygenates on Co/Al_2O_3 is as good as on Co/CuZnO - just not as selective.

6.6 Acknowledgements

The authors acknowledge financial support from the U.S. Department of Energy (Award No. DE-PS26-06NT43024).

6.7 References

[1] J.C. Slaa, G.J.M. Weierink, J.G. van Ommen, J.R.H. Ross, Catal. Today 12 (1992) 481.

[2] V. Mahdavi, M.H. Peyrovi, M. Islami, J.Y. Mehr, Appl. Catal., A-Gen. 281 (2005) 259.

[3] A.E. Farrell, R.J. Plevin, B.T. Turner, A.D. Jones, M. O'Hare, D.M. Kammen, Science 311 (2006) 506.

[4] S. Velu, N. Satoh, C.S. Gopinath, K. Suzuki, Catal. Lett. 82 (2002) 145.

[5] D.A. Deluga, J.R. Salge, L.D. Schmidt, X.E. Verykios, Science 303 (2004) 993.

[6] V. Subramani, S.K. Gangwal, Energ. Fuel 22 (2008) 814.

[7] J. Gao, X. Mo, J.G. Goodwin, Jr., J. Catal. 275 (2010) 211.

[8] H. Ngo, Y.Y. Liu, K. Murata, Reac. Kinet. Mech. Catal. 102 (2011) 425.

[9] M.A. Haider, M.R. Gogate, R.J. Davis, J. Catal. 261 (2009) 9.

[10] H.C. Woo, K.Y. Park, Y.G. Kim, I.S. Nam, J.S. Chung, J.S. Lee, Appl. Catal. 75 (1991) 267.

[11] A. Muramatsu, T. Tatsumi, H. Tominaga, J. Phys. Chem. 96 (1992) 1334.

[12] G.-Z. Bian, L. Fan, Y.-L. Fu, K. Fujimoto, Appl. Catal., A-Gen. 170 (1998) 255.

[13] Z. Li, Y. Fu, J. Bao, M. Jiang, T. duo Hu, T. Liu, Y.-n. Xie, Appl. Catal. A-Gen. 220 (2001) 21.

[14] N. Zhao, R. Xu, W. Wei, Y. Sun, React. Kinet. Catal. L. 75 (2002) 297.

[15] M. Xiang, D. Li, H. Xiao, J. Zhang, H. Qi, W. Li, B. Zhong, Y. Sun, Fuel 87 (2008) 599.

[16] G. Natta, U. Colombo., I. Pasquon, in: Catalysis (P.H. Emmet, Ed), vol. V, Chap. 3, Reinhold, New York. (1957) 131.

[17] K.J. Smith, R.B. Anderson, Can. J. Chem. Eng. 61 (1983) 40.

[18] E. Tronconi, L. Lietti, P. Forzatti, I. Pasquon, Appl. Catal., 47 (1989) 317.

[19] L. Lietti, E. Tronconi, P. Forzatti, Appl. Catal., 70 (1991) 73.

[20] A.-M. Hilmen, M. Xu, M.J.L. Gines, E. Iglesia, Appl. Catal., A-Gen 169 (1998) 355.

[21] P. Courty, D. Durand, E. Freund, A. Sugier, J. Mol. Catal. 17 (1982) 241.

[22] P. Chaummette, P. Courty, D. Durand, P. Grandvallet, C. Travers, British Patent 2 158 30 (1984).

[23] W.X. Pan, R. Cao, G.L. Griffin, J. Catal. 114 (1988) 447.

[24] J.I. Di Cosimo, A.J. Marchi, C.R. Apesteguia, J. Catal. 134 (1992) 594.

[25] J.E. Baker, R. Burch, S.E. Golunski, Appl. Catal. 53 (1989) 279.

[26] J.E. Baker, R. Burch, S.J. Hibble, P.K. Loader, Appl. Catal. 65 (1990) 281.

[27] A. Sugier, E. Freund, US Patent 4 122 110 (1978).

[28] A. Sugier, E. Freund, US Patent 4 291 126 (1979).

[29] P. Courty, P. Chaummette, D. Durand, C. Verdon, US Patent 4 780 481 (1988).

[30] A. Kiennemann, C. Diagne, J.P. Hindermann, P. Chaumette, P. Court, Appl. Catal., 53 (1989) 197.

[31] X. Mo, Y.-T. Tsai, J. Gao, D. Mao, J.G. Goodwin, Jr., submitted to J. Catal. (2011).

[32] D.J. Elliott, F. Pennella, J. Catal. 114 (1988) 90.

[33] J.G. Nunan, R.G. Herman, K. Klier, J. Catal. 116 (1989) 222.

[34] J.G. Nunan, C.E. Bogdan, K. Klier, K.J. Smith, C.-W. Young, R.G. Herman, J. Catal.

113 (1988) 410.

[35] J.G. Nunan, C.E. Bogdan, K. Klier, K.J. Smith, C.-W. Young, R.G. Herman, J. Catal. 116 (1989) 195.

[36] J.C. Slaa, J.G. van Ommen, J.R.H. Ross, Catal. Today 15 (1992) 129.

[37] V. Mahdavia, M.H. Peyrovia, M. Islamib, J.Y. Mehr, Appl. Catal., A-Gen 281 (2005) 259.

[38] J. Happel, Chem. Eng. Sci. 33 (1978) 1567.

[39] C.O. Bennett, ACS Symp. Ser. 178 (1982) 1.

[40] P. Biloen, J. Mol. Catal. 21 (1983) 17.

[41] M. Depontes, G.H. Yokomizo, A.T. Bell, J. Catal. 104 (1987) 147.

[42] F. Arena, K. Barbera, G. Italiano, G. Bonura, L. Spadaro, F. Frusteri, J. Catal. 249 (2007) 185.

[43] Y.-T. Tsai, X. Mo, A. Campos, J.G. Goodwin, Jr., J.J. Spivey, Appl. Catal. A-Gen. 396 (2011) 91.

[44] B. Ernst, A. Bensaddik, L. Hilaire, P. Chaumette, A. Kiennemann, Catal. Today 39 (1998) 329.

[45] S. Hammache, J.G. Goodwin, Jr., R. Oukaci, Catal. Today 71 (2002) 361.

[46] A. Egbebi, J.J. Spivey, Catal. Commun. 9 (2008) 2308.

[47] S.L. Shannon, J.G. Goodwin, Jr., Chem. Rev. 95 (1995) 677.

[48] J.G. Goodwin, Jr., S. Kim, W.D. Rhodes, In: Catalysis, J.J. Spivey, Ed.; The Royal Society of Chemistry: Cambridge, U.K., 2004; Vol. 17, Chapter 8.

[49] S. Fujita, M. Usui, H. Ito, N. Takezawa, J. Catal. 157 (1995) 403.

[50] N.D. Subramanian, G. Balaji, C.S.S.R. Kumar, J.J. Spivey, Catal. Today 147 (2009) 100.

[51] Z.Q. Yang, C.Y. You, L.L. He, J. Alloys Compd 423 (2006) 128.

[52] J. Llorca, N. Homs, O. Rossell, M. Seco, J.-L.G. Fierro, P. Ramírez de la Piscina, J. Mol. Catal. A-Chem. 149 (1999) 225.

[53] D. Barreca, C. Massignan, Chem. Mater. 13 (2001) 588.

[54] H. Xu, W. Chu, L. Shi, S. Deng, H. Zhang, React. Kinet. Catal. Lett. 97 (2009) 243.

[55] X. Xu, E.B.M. Doesburg, J.J.F. Scholten, Catal. Today 2 (1987) 125.

[56] P. Chaumette, P. Courty, D. Durand, P. Grandvallet, C. Travers, GB Patent 2,158,730 (1985).

[57] N. Lohitharn, J.G. Goodwin, Jr., Catal. Commun. 10 (2009) 758.

[58] S.H. Ali, J.G. Goodwin, Jr., J. Catal. 171 (1997) 333.

[59] S.H. Ali, J.G. Goodwin, Jr., J. Catal. 171 (1997) 339.

[60] Y.-T. Tsai, X. Mo, J.G. Goodwin, Jr., J. Catal. submitted for publication (2011).

[61] L.-S. Kau, K.O. Hodgson, E.I. Solomon, J. Am. Chem. Soc. 111 (1989) 7103.

[62] B.S. Clausen, G. Steffensen, B. Fabius, J. Villadsen, R. Feidenhans'l, H. Topsøe, J. Catal. 132 (1991) 524.

[63] A.-M. Hilmen, M. Xu, M.J.L. Gines, E. Iglesia, Appl. Catal. A-Gen. 169 (1998) 355.

[64] R. Tavares Figueiredo, M. López Granados, J.L.G. Fierro, L. Vigas, P. Ramírez de la Piscina, N. Homs, Appl. Catal. A-Gen. 170 (1998) 145.

[65] C.-H. Zhang, Y. Yang, B.-T. Teng, T.-Z. Li, H.-Y. Zheng, H.-W. Xiang, Y.-W. Li, J. Catal. 237 (2006) 405.

[66] S. Deng, W. Chu, H. Xu, L. Shi, L. Huang, J. Nat. Gas Chem. 17 (2008) 369.

[67] X. Dong, X.-L. Liang, H.-Y. Li, G.-D. Lin, P. Zhang, H.-B. Zhang, Catal. Today 147 (2009) 158.

[68] I. Kasatkin, P. Kurr, B. Kniep, A. Trunschke, R. Schlögl, Angew. Chem. Int. Edit. 46 (2007) 7324.

[69] Y.-T. Tsai, J.G. Goodwin, Jr., J. Catal. 281 (2011) 128.

CHAPTER SEVEN

SUMMARY

Ethanol is a potential alternative fuel and one of the practical solutions of the environmental crisis in the future. Although Rh-based catalysts were well-known as the most selective ethanol synthesis catalysts, their industrial applications were limited to the high cost and the low activity. The object of this study was to develop effective catalysts for ethanol synthesis with lower cost. Co and CuZnO catalysts have been proposed to be the widely-known Fischer-Tropsch Synthesis (FTS) and methanol synthesis catalysts. The efforts have been made to probe the role that Co and CuZnO-based catalysts played in CO hydrogenation. The combinations of different components including Co, Cu and/or ZnO have also been investigated for CO hydrogenation. Otherwise, a systematic comparison was made for chemisorption close to ambient vs. under reaction conditions for Group VIII metal catalysts in this study.

A study of investigating the catalytic performance for CO hydrogenation on the solid base, hydrotalcite (HT), Co-based catalysts was conducted. 10 wt% Co-based catalysts were prepared using incipient wetness impregnation method. Except for HT, pre-calcined HT (CHT), Al_2O_3 and MgO were used as supports for comparison purposes. These catalysts were characterized by BET surface area and porosity analysis, XRD, TEM/STEM/EDX, TPR and H_2 chemisorption. The catalytic activities and selectivities for these Co catalysts were evaluated using a fixed-bed reactor at 230^{o}C, 1.8 atm, and $H_2/CO = 2$. The results showed that Co/HT exhibited the highest steady-state reaction rates comparing to other Co catalysts. The effects of different reduction temperatures

(300-600^{o}C) for Co/HT were also investigated. It has been found that the reaction rate for Co/HT was highest at a reduction temperature of 500^{o}C. The product distribution for Co/HT obeyed an Anderson–Schulz–Flory distribution and the chain growth probability (α) did not change significantly by the different reduction temperatures for Co/HT. Combining the characterization and reaction results, the catalytic performance of Co catalysts during CO hydrogenation were related to the thermal stability properties of hydrotalcite, BET surface area, particle size of Co, the interaction between Co and the support, and the reducibility of Co. HT is a promising support for Co catalysts for FTS based on our results. The reactivity of Co/HT for FTS was comparable with Co/Al_2O_3, a well-known FTS catalyst, without adding any reduction promoter.

A systematic comparison of the relationship of H_2 or CO chemisorption measurements at close ambient temperature (25-100^{o}C) vs. under CO hydrogenation conditions by steady-state isotopic transient kinetic analysis (SSITKA) was made for a wide variety of Group VIII metal catalysts (Co, Fe, Ru, Pt and Rh). The comparisons were made by using the ratios of N_T^*/N_{chem} (amount of chemisorption by SSITKA vs. by static chemisorptions) for the various metal catalysts. The ratio of N_T^*/N_{chem} should be close to unity if there exists full coverage of the metal surface at both static chemisorption and reaction temperatures. However, the value of N_T^*/N_{chem} could be affected by H_2 spillover, carbon deposition, formation of metal carbides, SMSI or other mechanisms causing active site blockage. The ratio of N_T^*/N_{chem} was found to be almost always close to unity for Co catalysts with a wide variety of supports and promoters. However, larger N_T^*/N_{chem} ratios were typical for Ru catalysts supported on SiO_2 without

promoters (V promotion on Rh/SiO_2 resulted in the H_2 chemisorption suppression). Values much smaller than unity can be observed for both Fe and Pt catalysts. Apparently, Co is the best candidate for using chemisorption measured at reaction temperature by SSITKA. SSITKA can be applied as a complementary technique to static chemisorption, XRD line broadening, and TEM for estimating metal dispersion and metal particle size.

CuZnO-based catalysts for MeOH synthesis have received a great deal of attention in the past for their high MeOH selectivity. This study, however, explored for the first time at a site level the impact of components and a Al_2O_3 support on CuZnO-based catalysts. The catalytic properties of the catalysts for CO hydrogenation were investigated using a differential fixed bed reactor at 250°C and 1.8 atm, and a ratio of $H_2/CO = 8$. Surface kinetic parameters were able to be determined by SSITKA results. SSITKA measurements were carried out at the same conditions as CO hydrogenation. CO hydrogenation results suggested that the overall reaction activity of CuZnO-based catalysts were higher than catalysts with only Cu or ZnO components, indicating some synergy between Cu and ZnO species, but not orders of magnitude higher. DME is a secondary reaction product from the dehydration of MeOH and produced only on the acidic sites on the surface of Al_2O_3 when it was presented as a support. The rates of DME formation had a linear dependency with the corresponding partial pressure of MeOH and were found to be limited mainly by the concentration of produced MeOH. Surface reaction parameters should be corrected for readsorption effects for MeOH and DME. It was found from the SSITKA results that: (1) The difference in reaction rates for CuZnO and $CuZnO/Al_2O_3$ was due to the better dispersion of CuZnO. The same values

of residence time in making MeOH for the two catalysts suggested that the only function of Al_2O_3 was to increase the CuZnO dispersion and provide acidic sites for DME production; (2) Supported Cu and ZnO catalysts (Cu/Al_2O_3 and ZnO/Al_2O_3 catalysts) exhibited lower MeOH formation rates compared to $CuZnO/Al_2O_3$ due to both their lower intrinsic activities and lower surface concentrations of intermediates, indicating some synergy between Cu and ZnO, but the synergy does not result in an order-of-magnitude increase in site activity; (3) $CuZnO/Al_2O_3$ and ZnO/Al_2O_3 did not produce hydrocarbons at steady-state, but Co/Al_2O_3 did. This seems to imply that the presence of ZnO inhibits the hydrocarbon formation ability of Cu.

The relationships between the hydrocarbon and oxygenate products during CO hydrogenation on CoCuZnO-based catalaysts were investigated for the first time at a site level by SSITKA. Several conclusions about the role Cu and ZnO played in Co catalysts could be made: (1) Cu might block the surface of Co and resulted in the decrease in activity for all products; (2) The presence of ZnO might possibly increase somewhat the site activities for both hydrocarbon and C_{2+} oxygenates. ZnO appeared to act as a support to maintain Co highly dispersed and active for hydrocarbon and higher oxygenate production; (3) The addition of Cu and ZnO into Co was be able to maintain the oxygenate synthesis ability while decreasing the ability of making hydrocarbons. Although previous studies showed that the combination of Co with CuZnO could effectively increase the selectivities for higher oxygenates, our results showed that Co (in the form of Co/Al_2O_3) already has the ability to make oxygenates, including higher oxygenates. This fact tends to be neglected due to the extremely high hydrocarbon

acidity. However, it is hard to argue at this time the blockage by Cu of the Co surface decreases the hydrocarbon formation rate by two orders of magnitude without affecting C_{2+} oxygenate synthesis. The new synergy between Co, Cu and ZnO cannot be ruled out and probably takes a form that in essence decreases hydrocarbon desorption before or withour $–CH_xO$ insertion.

APPENDICES

APPENDIX A

The TOS activities and selectivities for CO hydrogenation on $20Cu/Al_2O_3$ and $20ZnO/Al_2O_3$

Table A-1: The TOS results for CO hydrogenation on $20Cu/Al_2O_3$[a,b].

Time (min)	Total rate (umol/g/s)	CH_4 selectivity (%)	CH_4 rate (μmol/g/s)	MeOH selectivity (%)	MeOH rate (μmol/g/s)	DME selectivity(%)	DME rate (μmol/g/s)
5	-	-	-	-	-	-	-
25	-	-	-	-	-	-	-
45	0.013	100	0.013	0	0.000	0	0.000
60	0.018	100	0.018	0	0.000	0	0.000
90	0.025	100	0.025	0	0.000	0	0.000
120	0.035	89.7	0.031	3.4	0.001	6.9	0.002
150	0.043	86.3	0.037	6.6	0.003	7.7	0.003
180	0.051	83.3	0.042	7.8	0.004	8.9	0.005
210	0.059	76.4	0.045	10.9	0.006	12.7	0.007
240	0.065	73.1	0.048	12.2	0.008	14.7	0.010
300	0.07	69.5	0.049	14.2	0.010	16.3	0.011
360	0.07	68.4	0.048	14	0.010	17.5	0.012

[a] Catalyst: 1g, inert (α-Al_2O_3): 2g. Reaction was carried out at 250°C; P_T = 1.8 atm, flow rate = 30 mL/min (H_2: He: CO = 8:1:1.). All reactions were carried out at differential conversions with % CO conversion < 5%. Max. error = ±5%.

[b] Carbon selectivity = $n_iC_i/\Sigma n_iC_i$.

Table A-2 The TOS results for CO hydrogenation on $20ZnO/Al_2O_3$[a,b].

Time (min)	Total rate (μmol/g/s)	CH_4 selectivity (%)	CH_4 rate (μmol/g/s)	MeOH selectivity (%)	MeOH rate (μmol/g/s)	DME selectivity(%)	DME rate (μmol/g/s)
5	-	-	-	-	-	-	
25	-	-	-	-	-	-	
45	-	-	-	-	-	-	
60	0.007	33	0.002	67.2	0.005	0	0
90	0.01	27.8	0.003	72.2	0.007	0	0
120	0.018	13	0.002	55.2	0.010	31.8	0.006
150	0.025	9.2	0.002	55.4	0.014	35.4	0.009
180	0.032	0	0.000	56.1	0.018	43.9	0.014
210	0.039	0	0.000	53	0.021	47	0.018
240	0.046	0	0.000	51.7	0.024	48.3	0.022
300	0.045	0	0.000	49.4	0.022	50.6	0.023
360	0.048	0	0.000	49.6	0.024	50.4	0.024

[a] Catalyst: 1g, inert (α-Al_2O_3): 2g. Reaction was carried out at 250°C; P_T = 1.8 atm, flow rate = 30 mL/min (H_2: He: CO = 8:1:1.). All reactions were carried out at differential conversions with % CO conversion < 5%. Max. error = ±5%.

[b] Carbon selectivity = $n_iC_i/\Sigma n_iC_i$.

APPENDIX B

SSITKA methanation results for the various K^+-doped Pt/C catalysts

[As published in Journal of Catalysis, 280 (2011) 89-95]

Table B-1 Initial reaction rates and SSITKA results for CO hydrogenation on K^+-doped Pt/C catalysts.

Catalyst	R_M[a] (10^{-3}μmol/g/s)	τ_{CO}[b] (s)	N_{CO}[c] (μmol/g)	τ_M[b] (s)	N_M[d] (μmol/g)	$1/\tau_M$ (s^{-1})	E_{app} (kcal/mol)
00K/Pt	74	2.4	30	5.0	0.37	0.20	26.3
20K/Pt	64	2.3	29	4.8	0.31	0.21	28.5
40K/Pt	55	2.4	30	4.8	0.25	0.20	27.9
80K/Pt	47	2.5	32	4.8	0.20	0.21	28.2

[a] Rate of CH4 formation: Error = ±2 * 10^{-3} μmol/g cat-s.
[b] Average surface residence time of rev. ads. CO: Error = ±0.2 s.
[c] Surface concentration of rev. ads. CO: Error = ±5%.
[d] Surface concentration of carbon-containing intermediates leading to CH_4: Error = ±4%.